

ABSTRACT

Title of Document: METHANE DYNAMICS IN MARINE SYSTEMS

Lauren Miranda Gelesh, Master of Science, 2015

Directed By: Assistant Professor, Dr. Laura Lapham,
Chemistry Department

Laboratory and field experiments were performed to investigate methane (CH_4) in marine systems. Laboratory experiments explored the impact of aerobic CH_4 oxidizing bacteria on the dissolution process of CH_4 hydrate. The pure culture, *Methylomicrobium album*, grew at high pressure (34 atm), but not at low temperature (15°C). Hydrate was formed in media containing culture, but was not stable to perform dissolution experiments. The culture used was found to be unsuitable for hydrate dissolution experiments. Field experiments were performed in the Chesapeake Bay estuary, where CH_4 concentrations were measured in bottom water and sediment pore-water. Results showed that bottom water CH_4 concentrations increased to $40\mu\text{M}$ in mid-July, which coincided with decreasing oxygen concentrations and decreasing CH_4 concentrations, which coincided with increasing oxygen concentrations in the fall. These observations supported the hypothesis that estuarine emissions of CH_4 are being enhanced by seasonal hypoxia and that estuarine CH_4 emissions may be currently underestimated.

METHANE DYNAMICS IN MARINE SYSTEMS

By

Lauren Miranda Gelesh

Thesis submitted to the Faculty of the Graduate School of the
University of Maryland, College Park, in partial fulfillment
of the requirements for the degree of
Master of Science
2015

Advisory Committee:
Assistant Professor Laura Lapham, Chair
Research Associate Professor Andrew Heyes
Assistant Professor Michael Gonsior
Assistant Professor Karen Lloyd

© Copyright by
Lauren Miranda Gelesh
2015

Acknowledgements

Foremost, I would like to thank my advisor, Dr. Laura Lapham, for the opportunity, the support, and the guidance along the road at the Chesapeake Biological Laboratory. Your enthusiastic energy, eternal optimism, and gentle touch made my graduate school experience enjoyable and enriching. I would also like to thank my committee members for their guidance and contributions to help me develop my thesis and myself as a scientist.

I would also like to thank the Lapham Lab: Kathleen and Cedric. Thank you, Kathleen, for all of your assistance with lab work and advice on my project. Thank you for staying late to grind coppers and answering countless questions that saved me many a trips up to Laura's office. Thank you, Cedric, for your gas chromatograph tune-ups and espresso shots that helped me to keep chugging along.

Thank you to the analytical services lab and to the IRMS lab. A special thanks to Dana Biasatti for instruction and assistance. And thank you to Dr. Bill Boicourt for collaborating with me and providing me the opportunity to acquire a unique and exciting dataset. Also, thanks, to Dr. Malcolm Scully for granting me access to sensor your data. And thank you to Captain Michael Hulme, and the crew of the R.V. Rachel Carson for a number of successful and safe cruises. And thank you also to the Captain and crew of the R.V. Sharp. Thank you Hillary Lane for assisting me with my pH calculation.

And thank you to the CBL community for your support. Thank you to Cheryl for bearing the brunt of and listening so devotedly to my many Brindy stories. I would like to thank my office mates, Caroline, YuanYuan, MengJie, Emily, Hannah, and Jess for their support and advice throughout my graduate school experience. Thanks Elaine for all of your support and coffee. And thank you to the Graduate Education Committee and the University of Maryland Jacob K. Goldhaber Award for providing funding for travel to Galveston, Texas. Also thanks to the Petroleum Research Fund and the Doctoral New Investigator award for funding my project.

Thank you to my family for your unwavering support and genuine interest in my adventures in science. And thanks to the Southern Maryland tennis community for the cathartic tennis that helped me to burn away the stress and make it to the finish line.

Most of all, thank you to my husband Ryan Hook for all of your support and advice along my path to a Master of Science degree. And thank you Brindy for always making me laugh at the end of every day, no matter how long you had to wait.

Table of Contents

Acknowledgements.....	ii
Table of Contents.....	iii
List of Tables.....	v
List of Figures.....	vi
Chapter 1: Methane Deep in the Ocean and High in the Sky.....	1
1.1 Introduction.....	1
1.2 Methane in the Carbon Cycle.....	1
1.2.1 Methane in the Atmosphere.....	1
1.2.2 Global Budget.....	3
1.3 Methane in Marine Systems.....	4
1.4 Approaches used in Methane Biogeochemistry.....	6
1.5 Focus of this Thesis.....	7
Chapter 2: The Impact of the Aerobic Methane Oxidizing Bacteria <i>Methylomicrobium album</i> on Gas Hydrate Stability in Laboratory Experiments.....	9
2.1 Abstract.....	9
2.1.1 Keywords.....	10
2.1.2 Abbreviations.....	10
2.2 Introduction.....	10
2.2.1 Approach.....	13
2.3 Materials and Methods.....	16
2.3.1 Pressure Chamber Experiments.....	16
2.3.2 Culturing Techniques.....	18
2.3.3 Analytical.....	20
2.3.4 Culture Vial Experiments.....	22
2.3.5 Bottom Water Enrichment.....	26
2.4 Results.....	27
2.4.1 Culture Growth at Optimal Conditions.....	27
2.4.2 The Addition of Copper to the Growth Media.....	29
2.4.3 The Impact of Cold Temperature on Culture Growth.....	31
2.4.4 Pressure Chamber I: Culture Growth at High Pressure and Low Temperature.....	34
2.4.5 Pressure Chamber II: Culture Growth at High Pressure and Variable Temperature.....	35
2.4.6 Pressure Chamber III: Culture Growth at High Pressure and Decreasing Temperature.....	37
2.4.7 Pressure Chamber IV: Forming Hydrate in the Presence of the Culture... 39	
2.3.8 Bottom Water Enrichment.....	40
2.5 Discussion.....	40
2.6 Next Steps.....	41
2.7 Conclusion.....	41
Chapter 3: Methane in the Chesapeake Bay.....	43
3.1 Abstract.....	43

3.1.1	Keywords	44
3.1.2	Abbreviations	44
3.2	Introduction	44
3.2.1	Testing HEMF in the Chesapeake Bay	49
3.3	Methods	51
3.3.1	OsmoSampler Deployment on Landers	51
3.3.2	Landers	52
3.3.3	Lander Deployment	53
3.3.4	Lander Recovery	54
3.3.5	OsmoSampler Time Stamp	54
3.3.6	Sub-sampling Procedure of Coils and Analytical Methods	56
3.4	Results	59
3.4.1	Verification of OsmoSamplers	59
3.4.2	Bottom Water (BW) Chemistry	60
3.4.3	Pore-water (PW)	62
3.4.4	Dissolved Organic Carbon	64
3.5	Discussion	65
3.5.1	Proof of Concept: Using OsmoSamplers in a Shallow Water Estuary	65
3.5.2	Bottom Water Methane Concentrations Increase with Hypoxia	66
3.5.3	Temporal Observations Provided by Continuous Sampling	67
3.5.4	Method Development for Dissolved Organic Carbon Analysis	72
3.5.5	Implications of Chesapeake Bay Methane Flux	73
3.6	Conclusion	75
Chapter 4:	Conclusion	77
4.1	Understanding the Impacts	77
4.1.1	The Chesapeake Bay	77
4.1.2	Aerobic Methane Oxidizing Bacteria	77
4.2	Next Steps	79
4.2.1	Validating HEMF	79
4.2.2	Hydrate Dissolution Experiments: A New Bug or Just Do it?	79
4.3	Conclusions	80
Appendices	81
Appendix A:	Sterilization Procedures	81
Appendix B:	Generating Seed Stock	82
Appendix C:	Calculations	84
Appendix D:	Cavity Ring Down Spectroscopy	85
Appendix E:	DAPI Staining	86
Appendix F:	Solid Phase Extraction	87
Appendix G:	Chamber Experiment Details	88
Appendix H:	Bottom Water Enrichment	90
Appendix I:	Culture Vial Headspace Analysis	91
Appendix J:	Chesapeake Bay Supplemental	93
Bibliography	105

List of Tables

Table 2.1. The recipe for the Nitrate Minimal Salts Culture Media provided by ATCC for *M. album* culture is shown.

Table 2.2. The details for each method of GC analysis are shown in the table.

Table 2.3. An experimental outline of culture work performed in culture vials and the pressure chamber is shown below.

Table 2.4. Results of experiments performed in culture vials and the pressure chamber are shown below. Methane oxidation rates were derived from the slope values of linear regressions fitted to the treatment concentrations of % CH₄.

Table 3.1. Chesapeake Bay data and calculations that were used to calculate CH₄ flux and pH increase related to methanogenesis and methane oxidation.

Table J.1. Chesapeake Bay OsmoSampler deployment and sample data.

Table J.2. Chesapeake Bay OsmoSampler pore-water data.

Table J.3. Chesapeake Bay OsmoSampler bottom water data.

Table J.4. Chesapeake Bay sensor data.

List of Figures

Figure 2.1. A generalized structure of gas hydrate is shown in which molecules of gas are enclosed in a cage of water molecules. Reprinted from Maslin et al., 2010, copyright 2010, with permission from the Royal Society.

Figure 2.2. A Gulf of Mexico solubility curve and temperature plot are shown with a water column (white) and sediment (grey), with the sediment water interface (SWI) indicated with a line. The Hydrate Stability Zone (HSZ) is shown in the right box below the dashed line and to the right of the solid line, indicating methane solubility, derived from the results of a thermodynamic model (Duan and Mao, 2006). The temperature diagram in the left box shows the water column (white) and the sediment (grey) temperatures. Reprinted from Lapham et al., 2010, Copyright 2010, with permission from Elsevier.

Figure 2.3. The expected results of the hydrate dissolution experiment with an aerobic methane oxidizing bacteria culture are shown. The predicted impacts of culture on dissolution (dashed line) are compared to dissolution occurring in the absence of culture (solid line). A plot of methane concentrations over time shows the possible impact of the culture on the hydrate dissolution rate (A). The horizontal dotted line (A) represents the concentration of methane at saturation. As methane is consumed by aerobic oxidation of methane, hydrate dissolution rates are increased and aqueous methane increases more rapidly to saturation. A plot of $\delta^{13}\text{C-CH}_4$ over time shows the possible impact of the culture on the stable isotopes of CH_4 -carbon (B). Aerobic oxidation of methane will also deplete the light carbon isotopes of methane, generating less negative values of $\delta^{13}\text{C-CH}_4$.

Figure 2.4. The biochemical pathway of methane oxidation is shown where methane is converted to carbon dioxide with the enzymes performing each step to the right. Formaldehyde can either be assimilated into cellular material or converted to carbon dioxide (Hanson and Hanson, 1996).

Figure 2.5. Parr pressure chamber (600mL volume) used for hydrate experiments.

Figure 2.6. A culture schematic of the [A.] original pure culture obtained from ATCC (passage 0), the expanded [B.] seed stock (passage 1), the [C.] working culture used for experiments at atmospheric pressure (passage 2), and the working culture used for [D.] pressure chamber experiments (passage 3).

Figure 2.7. The results of the Culture Vial I experiment at optimal conditions of 30⁰C and 1 atm are shown. Percent CH_4 (A) and Oxygen (B) headspace measurements and stable isotope measurements of $\delta^{13}\text{C-CH}_4$ (‰) (C) are shown from the second passage. Error bars in C show standard error on duplicate measurements.

Figure 2.8. The results of the Culture Vial I experiment at optimal conditions of 30°C and 1 atm are shown. Percent CH₄ (A) and oxygen (B) headspace measurements and stable isotope measurements of δ¹³C-CH₄ (‰) (C) are shown from the third passage. Error bars in C show standard error on duplicate measurements.

Figure 2.9. The spectrophotometry results of the Culture Vial II experiment with A) regular media and B) increased copper media at 30°C and 1 atm.

Figure 2.10. The headspace methane results from the Culture Vial II experiment with regular media and increased copper media are shown. Percent methane headspace measurements were made of culture grown in regular media (A.) and copper media (B.) at 30°C and 1 atm.

Figure 2.11. The headspace oxygen from the Culture Vial II experiment with regular media and increased copper media are shown. Percent oxygen headspace measurements were made of culture grown in regular media (A.) and copper media (B.) at 30°C and 1 atm.

Figure 2.12. The spectrophotometry results of the Culture Vial III temperature experiment are shown. Growth curve of spectrophotometry measurements at 405 nm for the experiment at 30°C (A.), 10°C (B.), and 1°C (C.) and 1 atm.

Figure 2.13. The headspace methane results of the Culture Vial III temperature experiment are shown. Percent methane headspace measurements for the experiment at 30°C (A.), 10°C (B.), and 1°C (C.) and 1 atm.

Figure 2.14. The headspace oxygen results of the Culture Vial III temperature experiment are shown. Percent oxygen headspace measurements for the experiment at 30°C (A.), 10°C (B.), and 1°C (C.) and 1 atm.

Figure 2.15. The Pressure Chamber I experiment was carried out at 1°C at 39 atm. Methane and oxygen measurements of headspace and media containing culture from the pressure chamber are shown.

Figure 2.16. The Pressure Chamber I experiment was carried out at 1°C at 39 atm. Spectrophotometry measurements at 405 nm of media containing culture from the pressure chamber experiment I at 1°C at 39 atm.

Figure 2.17. The Pressure Chamber II experiment was carried out at variable temperatures and at 34 atm. Spectrophotometry measurements at 405nm of media containing culture from the pressure chamber experiment II at 15°C at 34 atm. After 46 days, the temperature was increased to 30°C, indicated by the vertical line.

Figure 2.18. The Pressure Chamber II experiment was carried out at variable temperatures and at 34 atm. Methane and oxygen measurements of headspace gas concentrations and media methane concentrations containing culture from the

pressure chamber at 15°C at 34 atm. After 46 days, the temperature was increased to 30°C, indicated by the vertical line.

Figure 2.19. The Pressure Chamber II experiment was carried out at variable temperatures and at 34 atm. Stable isotope analysis measurements of $\delta^{13}\text{C-CH}_4$ from headspace are shown of the pressure chamber at 15°C at 34 atm. After 46 days, the temperature was increased to 30°C, indicated by the vertical line. Error bars show standard error on duplicate measurements.

Figure 2.20. The Pressure Chamber III experiment was carried out at variable temperatures and at 34 atm. The variable temperatures over time (A) and spectrophotometry measurements at 405 nm of culture (B) are shown.

Figure 2.21. The Pressure Chamber III experiment was carried out at variable temperatures and at 34 atm. Methane measurements of headspace and media containing culture from the pressure chamber experiment are shown.

Figure 2.22. The Pressure Chamber III experiment was carried out at variable temperatures and at 34 atm. Stable isotope measurements of $\delta^{13}\text{C-CH}_4$ of headspace and media methane for pressure chamber are shown. Error bars show standard error on duplicate measurements. Analysis of media methane-carbon was conducted on the last two samples.

Figure 2.23. A gas hydrate phase diagram is shown. The Pressure Chamber Experiments I-IV are plotted on the diagram based on the pressure and temperature conditions at which the experiments were conducted.

Figure 2.24. An enrichment was performed using bottom water from the Gulf of Mexico. Spectrophotometric measurements of OD_{405} are shown.

Figure 3.1. A conceptual model of Hypoxia Enhanced Methane Flux (HEMF).

Figure 3.2. Map of Chesapeake Bay with CH_4 gas shown in grey (Hill, 1992). The benthic lander discussed in this project was deployed at a Mid-Bay sampling site indicated with a black star (38.28196N, -76.23317', water depth 30 m). The white dot, within the black star, indicates the third lander site, located 0.5 km from the site of the first and second lander that was used for temperature data in place of the data lost on the second lander. The white star indicates the location of a sediment core collected in Reeburgh (1969).

Figure 3.3. A: Osmo-pump and copper sample coil that make up the OsmoSampler. B: First Deployment Lander. C: Second Deployment Lander. D: Rhizone filter.

Figure 3.4. A: Osmotic Pump. B: Sample Coil. C: Coil sectioning. D: Extraction of 0.5 m samples not using gastight extraction. E: Gastight extraction of 4.5 m samples.

Figure 3.5. Salinity from CTD measurements as well as osmo-coil salinity measurements collected over the course of two three-month deployments, indicated by the dark line.

Figure 3.6. Bottom water O₂ and CH₄ concentrations collected over the course of two three-month deployments, separated by the dark line.

Figure 3.7. Pore-water measurements of CH₄ and SO₄ concentrations collected over the course of two three-month deployments, indicated by the dark line, are shown. The pore-water was collected from sediment depth 0 to 30 cm.

Figure 3.8. Pore-water CO₂ and SO₄ concentrations collected over the course of two three-month deployments, indicated by the dark line. The SO₄ data is from Figure 3.7. The pore-water was collected from sediment depth 0 to 30 cm.

Figure 3.9. Pore-water CH₄ concentrations (mM) and δ¹³C-CH₄ (‰) values collected over the course of two three-month deployments, indicated by the dark line. The CH₄ data is from Figure 3.7.

Figure 3.10. Bottom water and pore-water samples were pooled to create a sample representing high CH₄ conditions and a sample for low CH₄ conditions for each water type during each deployment, resulting in 8 samples total (Table J.1). A: Bottom water DOC (mg/L). B: Pore-water DOC (mg/L). Blanks measured were 0.9 ± 0.1 mg L⁻¹ DOC (standard deviation, n = 4).

Figure 3.11. Bottom water O₂ and CH₄ concentrations are shown (Data from figure 3.6) with the decrease in O₂ occurring with the increase in CH₄ highlighted by the shaded box.

Figure 3.12. Bottom water O₂ and CH₄ concentrations are shown (Data from figure 3.6) with the increase in O₂ occurring with the decrease in CH₄ highlighted by the shaded box.

Figure 3.13. Bottom water O₂ and CH₄ concentrations are shown (Data from figure 3.6) with the wind events highlighted by the shaded boxes.

Figure 3.14. Pore-water SO₄ and CH₄ concentrations are shown (Data from figure 3.7) with the decreases in SO₄ and increases in CH₄ highlighted by the shaded boxes.

Figure 3.15. Pore-water CH₄ concentrations and stable isotopic ratios of CH₄ carbon are shown (Data from figure 3.9) with the methanogenic periods highlighted by the shaded box and the oxidation periods shown by the darker shaded box.

Figure D.1. Measurements of stable isotopes from Delta V Isotope Ratio Mass Spectrometer (IRMS) and Cavity Ring-Down Spectroscopy (CRDS) of δ¹³C-CH₄

for pressure chamber experiment II. Error bars show standard error on duplicate measurements.

Figure J.1. Dispersion gradients for methane and sulfate along the copper sample tubing axis.

Chapter 1: Methane Deep in the Ocean and High in the Sky

1.1 Introduction

The research performed in this thesis investigated methane (CH_4) dynamics in marine systems. In this chapter, the role of CH_4 in the carbon cycle is discussed, specifically in the atmosphere and the hydrosphere, as well as microbial interactions and analytical techniques that can be applied to CH_4 dynamics. Shallow systems, such as estuaries, and deep marine systems that include methane hydrates, were investigated in this work and both are sources of atmospheric CH_4 . In the atmosphere, CH_4 is the most abundant hydrocarbon and can produce 20 times more radiative forcing than carbon dioxide over a 100 years' time period (Forster et al., 2007). Atmospheric CH_4 concentrations have been increasing in modern times and efforts to determine the mechanisms causing this increase are therefore of great importance.

1.2 Methane in the Carbon Cycle

Many elements are required for life, but carbon is the key to life as we know it. There are both organic and inorganic forms of carbon, which are part of the global carbon cycle. Carbon is transferred between the atmosphere, the hydrosphere, the terrestrial biosphere, and the lithosphere through fluxes controlled by physical, chemical, and biological processes. CH_4 , the most reduced form of carbon, can be produced and consumed by microorganisms in the hydrosphere and the terrestrial biosphere. CH_4 can also be released due to human activities as well as combusted to produce energy. CH_4 that is produced by natural and anthropogenic sources can be emitted to the atmosphere, where CH_4 plays an important role as a powerful greenhouse gas.

1.2.1 Methane in the Atmosphere

CH_4 concentrations in the atmosphere have a natural cycle associated with glacial (low atmospheric CH_4 concentrations) and interglacial (high atmospheric CH_4

concentrations) periods (Cicerone and Oremland, 1988). Concentrations of CH₄ obtained from ice core records indicate that variations on the order of 0.4 ppm have occurred over the last 160,000 years (Craig and Chou, 1982). However, in the last 200 years CH₄ concentrations have begun to rapidly increase from 750 ppb to 1.7 ppm (Cicerone and Oremland, 1988). Recent estimations of globally averaged atmospheric concentrations are over 1.8 ppm CH₄ (Nisbet et al., 2014). Reasons for this increase were hypothesized to be due to fossil fuel production and increasing agricultural sources such as CH₄ release from ruminant animals (Nisbet et al., 2014). Atmospheric CH₄ can also originate from natural sources such as wetlands and arctic permafrost. The amount of CH₄ released from these natural sources could also be impacted by climate change, possibly further increasing emissions of CH₄ to the atmosphere (Whiting and Chanton, 1993; Cao et al., 1998; Anisimov, 2007), forming a positive feedback mechanism, in that increasing concentrations of atmospheric CH₄ could lead to further increases in atmospheric CH₄.

In the atmosphere, CH₄ undergoes oxidation. As much as 85% of the CH₄ emitted to the atmosphere is oxidized in the troposphere (Dlugokencky et al., 1994). CH₄ molecules are initially oxidized by hydroxyl radicals (Cicerone and Oremland, 1988) shown in equation 1:



The final product of methane oxidation is CO₂ (Cicerone and Oremland, 1988). CH₄ directly impacts climate forcing through absorption in the infrared spectrum at 7.66 μm (Cicerone and Oremland, 1988). CH₄ is estimated to produce half of the climate forcing of CO₂, the most powerful contributor to the greenhouse gas effect (Hansen and Sato, 2001). The contribution of CH₄ to the greenhouse gas effect is thought to have increased by 30% since 1860 (Mitchell, 1989). Due to the increasingly important role of CH₄ in climate forcing and atmospheric chemistry, it is critical to understand both the cause and effect of increases in atmospheric CH₄.

To understand increasing atmospheric CH₄ concentrations, the National Oceanic and Atmospheric Administration (NOAA) has measured CH₄ in the

atmosphere, starting in the late 1970's. Seasonal cycles occur in the Northern and Southern hemispheres, with minima occurring during the warm summer months and maxima during the cool winter months (Dlugokencky et al., 1994). Due to the temperature dependence of CH₄ sources, sinks, and atmospheric transport, the annual CH₄ cycles of the Northern and Southern hemisphere are out of phase (Dlugokencky et al., 1994). Because the Northern hemisphere contributes ~75% of the CH₄ emissions to the atmosphere (Fung, 1991), the phase of the Northern hemisphere can be seen in the global mixing ratio. The time series indicates growth periods from the 1970's to 1999 and from 2007 to present. The growth periods are believed to correspond to increases in fossil fuel production during those periods (Dlugokencky et al., 1994; Nisbet et al., 2014). The decline of the growth rate during the period from 1999 to 2007 has been attributed to decreases in fossil fuel production (Dlugokencky, 2003; Nisbet et al., 2014) and a speculated reduction of gas losses from the Former Soviet Union (Reshetnikov et al., 2000). There are many factors, in addition to fossil fuel production, that effect global atmospheric CH₄ concentration and it is these sources and sinks that make up the global CH₄ budget.

1.2.2 Global Budget

Major sources of atmospheric CH₄ emissions include rice fields, wetlands, ruminant animals, natural gas production, and landfills. The largest natural source of CH₄ are tropical wetlands (Bousquet et al., 2011) while the largest anthropogenic source is from rice fields (Cicerone and Oremland, 1988). Advances in natural gas extraction and the subsequent growth in natural gas extraction through the process of hydraulic fracturing could represent an expanding source of anthropogenic CH₄. Estimates as high as 12% to as low as 0.42% of produced gases could be lost to the atmosphere (Karion et al., 2013)(Allen et al., 2013). Gas hydrates are a large reservoir of CH₄ and as such could represent a significant source of atmospheric CH₄. However the atmospheric flux from existing hydrates remains difficult to constrain. Overall, the global production of CH₄ from all sources is estimated to be 1188.3 Tg yr⁻¹, However, the emissions of CH₄ to the atmosphere are estimated to be only 500 Tg yr⁻¹. Over half of the 1188.3 Tg yr⁻¹ of CH₄ that is produced is estimated to be

consumed through microbial oxidation processes that occur in marine systems (Reeburgh, 2007).

1.3 Methane in Marine Systems

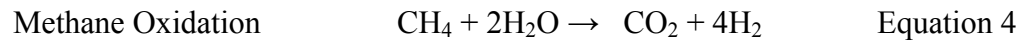
An enormous amount of CH₄ is produced via microbial transformation of organic matter and accumulated within marine sediments (Reeburgh, 2007). In marine environments, particulate organic carbon that reaches the sediments is partially transformed to dissolved organic carbon (DOC) and eventually respired to carbon dioxide (Burdige and Gardner, 1998) via a chain of energetically favorable, microbially-mediated processes (Froelich et al., 1979). The order of these processes is controlled by the free energy gained by each remineralization step. In sediments, these processes are limited by the redox conditions. As a result biogeochemical processes that dominate at the water sediment interface are different than ones in deeper sediments. In general aerobic respiration occurs near the surface of the sediment first, followed by the processes of denitrification, then manganese reduction, iron reduction, and sulfate reduction (Froelich et al., 1979). From thermodynamics methanogenesis, yielding only -0.30 kJ mol⁻¹ by the utilization of glucose, can only occur predominantly after or below sulfate reduction zones (Stumm and Morgan, 1996). The redox gradient in sediment provides a general understanding of the “geochemical condition” indicated by the dominant electron donor reaction, although the biogeochemical processes occurring in any zone is not limited to the dominant processes. Methanogens can produce CH₄ through the fermentation of acetate (Eq 2) or the reduction of carbon dioxide (Eq 3) (Whiticar, 1999).



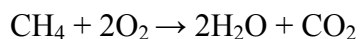
The pathway through which methanogenesis occurs is controlled by the availability of these competitive substrates. In fresh water systems, methanogenesis occurs predominantly through acetate fermentation, due to the availability of acetate

(Sugimoto and Wada, 1995). Acetate is typically unavailable to methanogens in marine water systems due to competitive microbial interactions. In saline waters, sulfate reducing bacteria outcompete methanogens, depleting acetate and hydrogen in the sulfate reducing sediment layer to concentrations too low for methane producing microorganisms (Lovley and Klug, 1986; Lovley and Goodwin, 1988). In marine systems, methanogenesis occurs through CO₂ reduction in sediments below the sulfate reduction zone, where sulfate is depleted and hydrogen is available (Hoehler et al., 1994; Hoehler et al., 1998). Microbial methanogenesis in both fresh and marine aquatic environments is an anaerobic process.

CH₄ can also be consumed by microorganisms through the process of methane oxidation. Methane oxidation can occur in both aerobic and anaerobic conditions. Anaerobic Oxidation of methane (AOM) occurs under strictly anoxic conditions, but the exact mechanism is not well understood (Valentine and Reeburgh, 2000). The process of AOM is thought to occur through a consortium of sulfate-reducing bacteria performing sulfate reduction (Eq 5) coupled to reverse methanogenesis (Eq 4) performed by methanogens, which yields the net reaction termed sulfate-dependent methane oxidation (SDMO) shown in equation 6 (Boetius et al., 2000):



AOM can also occur through iron and manganese reduction in marine systems (Beal et al., 2009) as well as nitrate reduction (Raghoebarsing et al., 2006), though sulfate-dependent AOM is considered the dominant mechanism of anaerobic oxidation of methane in marine systems (Reeburgh, 2007). CH₄ can also be oxidized aerobically, by aerobic methane oxidizing bacteria or methanotrophs in oxygenated environments (Eq 7):



Equation 7

Aerobic methane oxidation can occur in both oxygenated surface sediment layers, as well as in the water column. It is through these processes of aerobic and anaerobic methane oxidation that ~90% of all CH₄ formed in marine sediments is oxidized and CH₄ flux from marine sediments to overlying water is minimized (Reeburgh, 2007). In marine systems, the relationship between microbial methane oxidation and production determines if that environment is a source or sink of CH₄.

1.4 Approaches used in Methane Biogeochemistry

To investigate CH₄ dynamics in marine systems, the sources and the sinks of CH₄ must be identified. Therefore, it is essential to distinguish between the microbial processes of methanogenesis and methane oxidation and to identify the dominant process occurring in a given environment. The processes of methanogenesis and methane oxidation influence the stable isotopes of carbon contained in CH₄ and the impacts of specific processes, termed kinetic isotope effects, can be used to give scientists clues as to the source of CH₄ and the processes acting on CH₄.

The stable isotopes of carbon are ¹²C and ¹³C which have the same number of protons, but differ by one neutron, where the lighter ¹²C has 6 neutrons and the heavier ¹³C has 7 neutrons. The relative abundances of carbon stable isotopes are 98.90% ¹²C and 1.10% ¹³C for a ratio of ¹³C/¹²C ratio of 0.011122 (Faure and Mensing, 2009). Because ¹²C and ¹³C vary slightly in mass by one neutron, the behavior of the isotopes varies slightly in a given process or reaction. In an irreversible kinetic reaction, this difference in isotopic behavior results in a kinetic isotope effect, where the isotopic ratio of the source material varies from the isotopic ratio of the produced material. For example, aerobic oxidation of methane by microbes causes an isotopic fractionation as lighter CH₄ molecules, containing lighter ¹²C, are converted more readily to carbon dioxide and leaving the heavier isotope behind. As a result the original pool of carbon isotopes contained in the CH₄ becomes depleted in ¹²C and the carbon dioxide pool becomes enriched in the lighter

^{12}C (Whiticar, 1999). This change in the isotopic ratio can be measured on an isotope ratio mass spectrometer (Reeburgh, 2007) and the standard delta notation for reporting this ratio is with the following equation (Eq 8):

$$\delta^{13}\text{C} = \left[\frac{\left(\frac{^{13}\text{C}}{^{12}\text{C}}\right)_{\text{Sample}}}{\left(\frac{^{13}\text{C}}{^{12}\text{C}}\right)_{\text{Standard}}} - 1 \right] \times 10^3 (\text{‰}) \quad (8)$$

where the standard is Vienna Pee Dee Belemnite (VPDB). This standard is enriched slightly in ^{13}C and has a $^{13}\text{C}/^{12}\text{C}$ ratio of 0.011237. Results are reported in units of per mil (‰). The stable isotope ratio of carbon found in CH_4 , denoted as $\delta^{13}\text{C}-\text{CH}_4$, can be used to determine the processes controlling CH_4 dynamics in a given environment. Methanogenesis and methane oxidation are both associated with kinetic isotope effects. Methanogenesis produces lighter CH_4 , generating more negative $\delta^{13}\text{C}-\text{CH}_4$ values. In a methane oxidizing environment, the CH_4 becomes heavier, as the lighter ^{12}C in CH_4 is preferentially oxidized and the resulting $\delta^{13}\text{C}-\text{CH}_4$ value becomes less negative. Stable isotope analysis was applied in this work to investigations of CH_4 dynamics in laboratory experiments simulating deep sea conditions and field work in a shallow estuary.

1.5 Focus of this Thesis

CH_4 is a powerful greenhouse gas the concentration of which is increasing in the atmosphere due to human activity. It is therefore critical that we understand in detail which sources have led to this increase. Marine systems may be an underestimated source of atmospheric CH_4 . Two such systems in need of study are estuaries and gas hydrate containing cold seeps. The need for studying these two components of the marine system will be discussed in great detail in the following chapters. The work of this thesis focuses on accessing factors that control the release of methane from gas hydrates and estuaries. To do this, laboratory and field experiments were carried out. In Chapter II, the deep marine system was explored

through high pressure laboratory experiments using pressure chambers to simulate gas hydrate forming conditions. The experiments sought to address the research question: Does the activity of aerobic methane oxidizing bacteria enhance the rate of gas hydrate dissolution? In Chapter III, the shallow marine system was explored through field experiments measuring bottom and pore-water CH_4 of the Chesapeake Bay Estuary over two three-month deployments, capturing the development and resolution of seasonal hypoxia. The time series produced through this work addressed the research question: Does CH_4 increase in the bottom water when oxygen decreases during seasonal hypoxia? In the final chapter, Chapter IV, the results of these experiments are described as well as the contributions of the results to our understanding of CH_4 dynamics in marine systems. In addition, some possible next steps are discussed for the direction of future research.

Chapter 2: The Impact of the Aerobic Methane Oxidizing Bacteria *Methylobacterium album* on Gas Hydrate Stability in Laboratory Experiments

2.1 Abstract

Methane (CH₄) hydrate is a crystalline structure of water and CH₄ gas molecules that forms under conditions of high pressure and low temperature, and saturated gas. Hydrates are the largest reservoir of CH₄, a potent greenhouse gas, thus understanding factors that control hydrate stability is critical. One factor that has not been studied is the interaction between microbes and gas hydrate. In natural systems, hydrates outcrop the seafloor, and are exposed to oxygenated seawater that may contain natural communities of aerobic methane oxidizing bacteria (methanotrophs). It is hypothesized in this thesis that these methanotrophs may destabilize gas hydrates by consuming the hydrate-bound methane which would result in the dissolution of methane hydrate. To test this hypothesis, the methane oxidizing bacteria, *Methylobacterium album*, was cultured in a high pressure chamber at pressure and temperature conditions suitable for gas hydrate experiments. This culture was then monitored over time by measuring headspace and aqueous concentrations of methane and oxygen, the stable isotopes of CH₄ carbon, and its cell density. If the culture grew, concentrations of CH₄ and oxygen would decrease over time and the stable isotopes of CH₄ carbon would increase. The culture was also grown in glass vials at 1 atm under different temperature and growth conditions. For all experiments carried out in the vials, CH₄ concentrations did not decrease with time, regardless of temperature or copper concentrations. While the stable isotope analysis of CH₄ carbon showed some enrichment in ¹³C, this is somewhat contradictory to the finding that CH₄ concentrations did not change. In the pressure chamber, the culture grew slowly at high pressure (34-39 atm) and relatively high temperature (30°C), but growth was not observed at lower temperatures (1-20°C). Hydrate was formed in media (with cells), but the hydrate did not form as expected, it was “slushy” and decomposed easily. Overall, it was concluded that *M. Album* is not a suitable organism for these hydrate experiments. Future work should focus on

finding a microbe that is suited for the deep sea, hydrate conditions, and possibly the usage of a surfactant to stabilize hydrate for use in dissolution experiments.

2.1.1 Keywords

CH₄, stable isotopes, CH₄ Hydrate, Aerobic Methane Oxidizing Bacteria, *Methylobacterium Album*, Aerobic Methane Oxidation

2.1.2 Abbreviations

CH₄ = Methane

GC = Gas Chromatography

IRMS = Isotope Ratio Mass Spectrometry

CRDS = Cavity Ring Down Spectroscopy

SPE = Solid Phase Extraction

2.2 Introduction

Methane (CH₄) is a powerful greenhouse gas that is found in both land and ocean reservoirs (Reeburgh, 2007; Kirschke et al., 2013). In ocean sediments, CH₄ is produced through microbial methanogenesis, but can also be formed by the thermal breakdown of buried organic matter. CH₄ can be either dissolved, gaseous or bound in gas hydrates (Reeburgh, 2007). Gas hydrates are crystalline structures of gas molecules (in this case CH₄) encased in water molecules (Fig 2.1). Hydrates form in ocean sediments due to high pressure, low temperatures, and moderate salinities (i.e. seawater), where there is a source of saturated CH₄ (Sloan and Koh, 2007). While

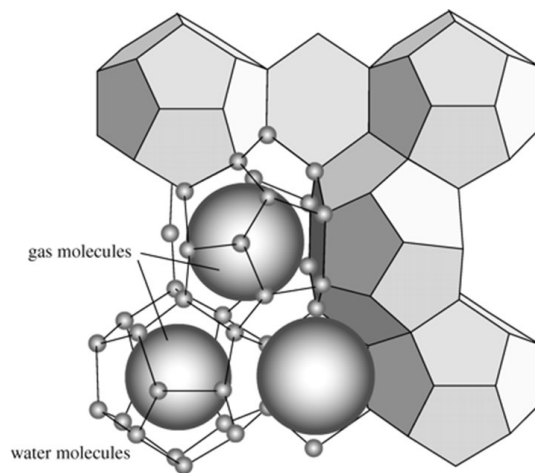


Figure 2.1. A generalized structure of gas hydrate is shown in which molecules of gas are enclosed in a cage of water molecules. Reprinted from Maslin et al., 2010, copyright 2010, with permission from the Royal Society.

most of the world's gas hydrate reserves are found in ocean sediments, hydrates are also found in arctic permafrost (Kvenvolden, 1988). The current global estimate of the amount of CH_4 contained in gas hydrates is approximately $1\text{-}5 \times 10^{15} \text{ m}^3$ (Milkov, 2004), which is double the energy bound in currently recoverable fossil fuels (Sloan and Koh, 2007). Because hydrates are a large reservoir of CH_4 , it is critical to understand the factors that control the stability of methane hydrates.

It is well known that pressure, temperature, CH_4 concentrations, and salinity control hydrate stability (Sloan and Koh, 2007). The stability conditions of gas hydrate are shown in Figure 2.2 in relation to a solubility curve of CH_4 , scaled to temperature and pressure (depth) in the water column and sediment. When these stability conditions are not met, gas hydrates will decompose via two distinct processes: dissolution and dissociation. Dissociation occurs when the pressure is too low, or temperatures are too high, and the hydrate dissociates into CH_4 gas and liquid

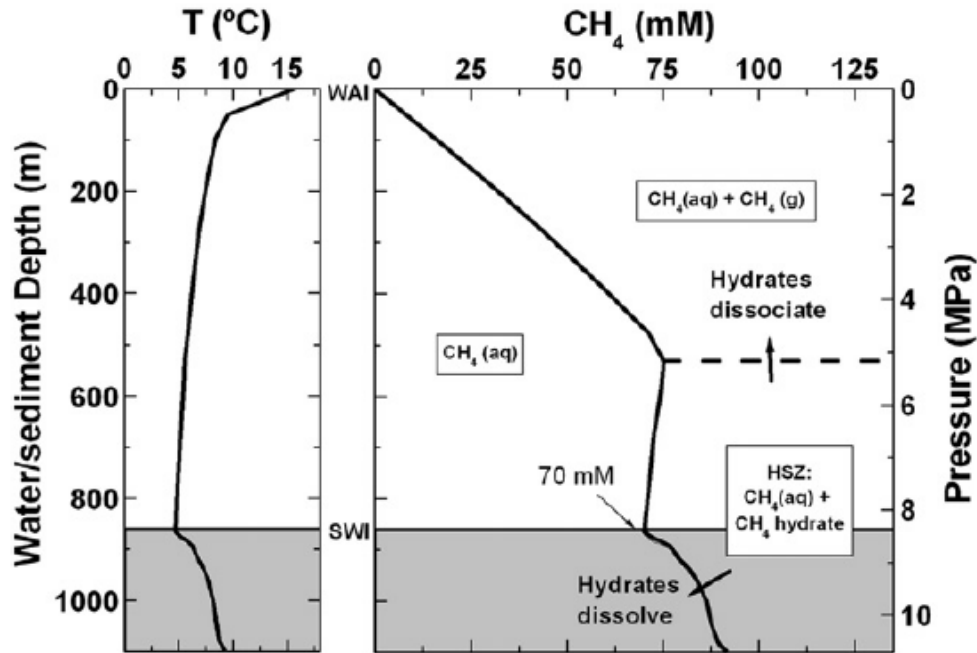
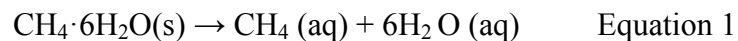


Figure 2.2. A Gulf of Mexico solubility curve and temperature plot are shown with a water column (white) and sediment (grey), with the sediment water interface (SWI) indicated with a line. The Hydrate Stability Zone (HSZ) is shown in the right box below the dashed line and to the right of the solid line, indicating methane solubility, derived from the results of a thermodynamic model (Duan and Mao, 2006). The temperature diagram in the left box shows the water column (white) and the sediment (grey) temperatures. Reprinted from Lapham et al., 2010, Copyright 2010, with permission from Elsevier.

water (Zhang and Xu, 2003). Dissociation is shown on Figure 2.2 with the horizontal dashed line. The water depth where this dissociation occurs (~500 m) is predictable based on thermodynamic calculations (Duan and Mao, 2006) and is relatively fast (within a few minutes). Dissociation can also be illustrated with a natural example: In an ocean setting, hydrates are more buoyant than seawater so if a piece of it were to break from the seafloor (shown in Figure 2.2 in grey), the hydrate would ascend through the water column (shown in Figure 2.2 in white) to the surface. As the hydrate is ascending, it will exit the hydrate stability zone at approximately 500 m water depth (shown in Figure 2.2 below the dashed line) and begin to dissociate into gas and water due to the lower hydrostatic pressure and warmer waters (Brewer et al., 2002). Dissolution, on the other hand, is a relatively slow process in which the kinetics are controlled by diffusion (Rehder et al., 2004). Dissolution occurs within the hydrate stability zone (below the dashed line in Figure 2.2), when the hydrate is exposed to an under-saturated external phase (Zhang and Xu, 2003), such as seawater low in CH₄ (to the left the solubility curve in Figure 2.2). Dissolution occurs via the following pathway:



where CH₄·6H₂O (s) represents solid CH₄ hydrate that decomposes into aqueous CH₄ and liquid water (H₂O).

Some studies have focused on understanding how microorganisms might affect gas hydrate stability (Sassen et al., 1999; Lanoil et al., 2001; Orcutt et al., 2004; Rogers et al., 2007). Orcutt et al. (2004) collected samples at the interface of gas hydrate and sediments and found significant rates of anaerobic methane oxidation coupled to sulfate reduction. While they did not measure rates of aerobic processes at the hydrate interface, the fact that these hydrates outcrop the seafloor into oxygenated seawater suggests that aerobic methane oxidation may also be occurring. In fact, in Japanese seeps, a genomic study found significant communities of aerobic methane oxidizers in bottom waters (Inagaki et al., 2004). Furthermore, aerobic methane oxidation rates of 3 to 1,000 nM d⁻¹ have been measured in marine bottom waters

dissolution rate was expected to be similar to previously measured values (Lapham et al., 2012) and exhibit no change in the ratio of stable isotopes of the CH₄ carbon (Lapham et al., 2012) (Fig 2.3a-b).

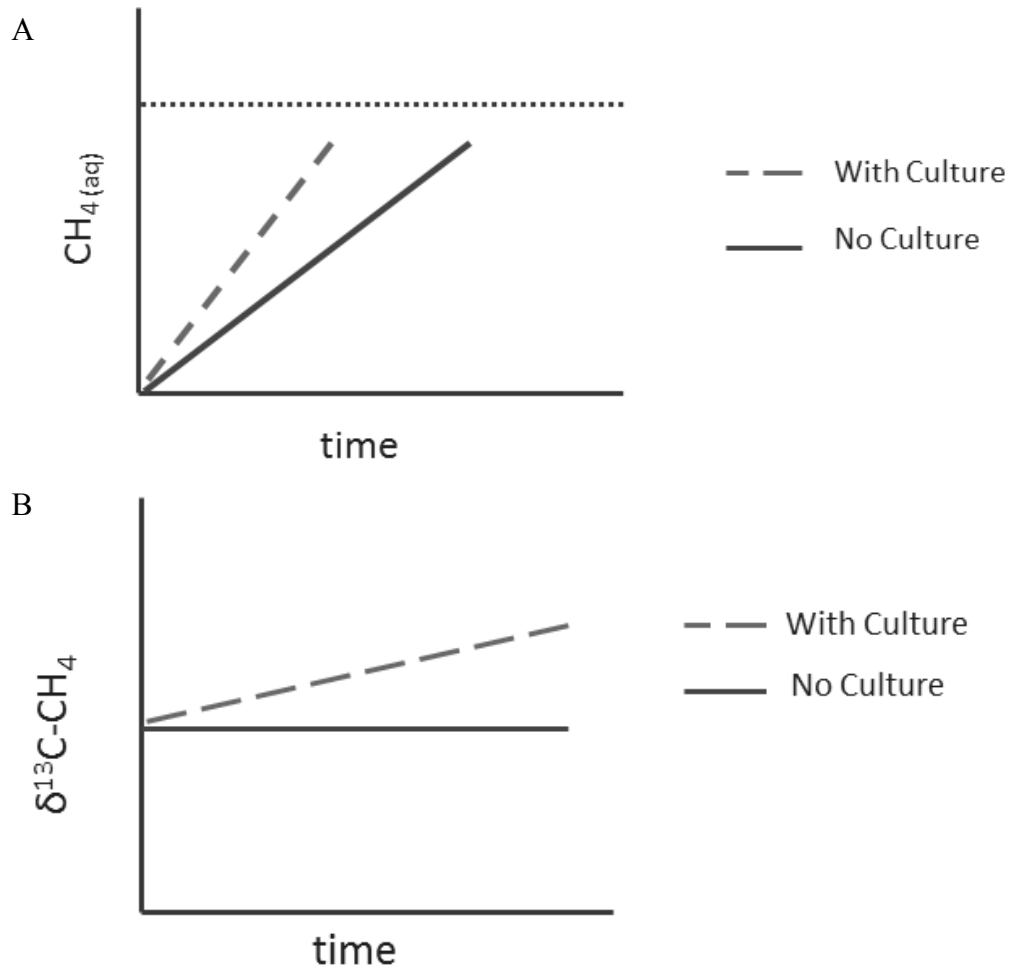


Figure 2.3. The expected results of the hydrate dissolution experiment with an aerobic methane oxidizing bacteria culture are shown. The predicted impacts of culture on dissolution (dashed line) are compared to dissolution occurring in the absence of culture (solid line). A plot of methane concentrations over time shows the possible impact of the culture on the hydrate dissolution rate (A). The horizontal dotted line (A) represents the concentration of methane at saturation. As methane is consumed by aerobic oxidation of methane, hydrate dissolution rates are increased and aqueous methane increases more rapidly to saturation. A plot of $\delta^{13}\text{C-CH}_4$ over time shows the possible impact of the culture on the stable isotopes of CH₄-carbon (B). Aerobic oxidation of methane will also deplete the light carbon isotopes of methane, generating less negative values of $\delta^{13}\text{C-CH}_4$.

To conduct these experiments, a methane oxidizing microbial culture was needed. Pure cultures of marine methanotrophs do not exist (Krause et al., 2014) and the literature on close relatives of seep methanotrophs in culture was sparse. However, there was one study that showed that the bacteria contained in bottom water near a CH₄ seep in Japan was closely related to the pure culture *Methylomicrobium album* (*M. album*) (Inagaki et al., 2004). For this reason, the pure culture *M. Album* was selected for this study.

M. album is a methanotroph from the class gammaproteobacter. The *Methylomicrobium* genus is comprised of gram-negative rods that are 0.5-1.0 µm wide and 1.5-2.5 µm long (Bowman et al., 1995). Aerobic methanotrophs, such as *M.*

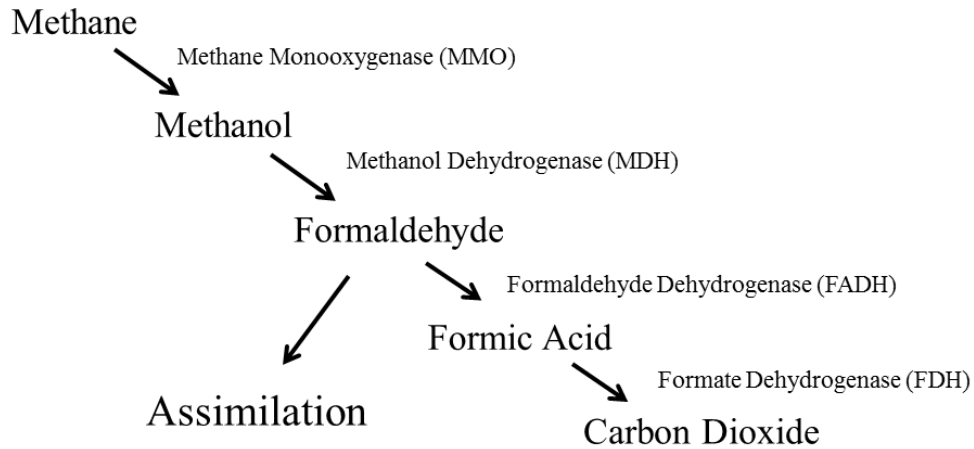


Figure 2.4. The biochemical pathway of methane oxidation is shown where methane is converted to carbon dioxide with the enzymes performing each step to the right. Formaldehyde can either be assimilated into cellular material or converted to carbon dioxide (Hanson and Hanson, 1996).

album, convert oxygen and CH₄ to carbon dioxide, via the net reaction shown in equation 3. However, this process occurs through a series of biochemical reactions (Fig 2.4). In the first step, CH₄ is converted to methanol using the enzyme methane monooxygenase (MMO) (Hanson and Hanson, 1996). The MMO enzyme occurs in two forms: the particulate or pMMO form and the soluble form or sMMO. The

pMMO form, expressed by *M. album*, requires copper for the utilization of aqueous CH₄ (Balasubramanian et al., 2010).

2.3 Materials and Methods

2.3.1 Pressure Chamber Experiments

A pressure chamber was used to perform the hydrate experiments. The chamber is a 600 mL stainless steel bench top chamber (Parr Co.) rated to 20.7 MPa and 225°C (Fig 2.5). The chamber was housed in an incubator to achieve stable temperatures. To ensure no gas leaks over time, the chamber was pressure tested with air up to 2.24 MPa, the maximum possible pressure used in these experiments. The chamber and all the fittings were considered gastight when the pressure was stable for at least 3 days. The chamber was sterilized before each experiment using a 10% bleach solution (described in detail in Appendix A).

The chamber was outfitted with several ports and gauges on both the top and the bottom. On the top, there was a pressure gauge (up to 20.7 MPa), two thermocouples (Type J) and two ports (Fig 2.5, Upper Left). The pressure gauge monitored the headspace pressure. The sensor of one thermocouple was placed in the upper portion on the inside of the chamber (to monitor temperature in the chamber headspace) while the other thermocouple sensor was placed in the bottom portion (to monitor the temperature of the liquid inside the chamber; Fig 2.5, Upper Right). One of the ports was used to fill the chamber with either liquid or gas via a dip tube on the inside. Liquids were introduced by using an Eldex high pressure pump with an adjustable flow rate that was set at 40 mL min⁻¹. Gases were introduced via high pressure regulators on the gas cylinders. The other port had a syringe adapter so that subsamples of the chamber headspace could be collected with a syringe (Fig 2.5, Upper Left).

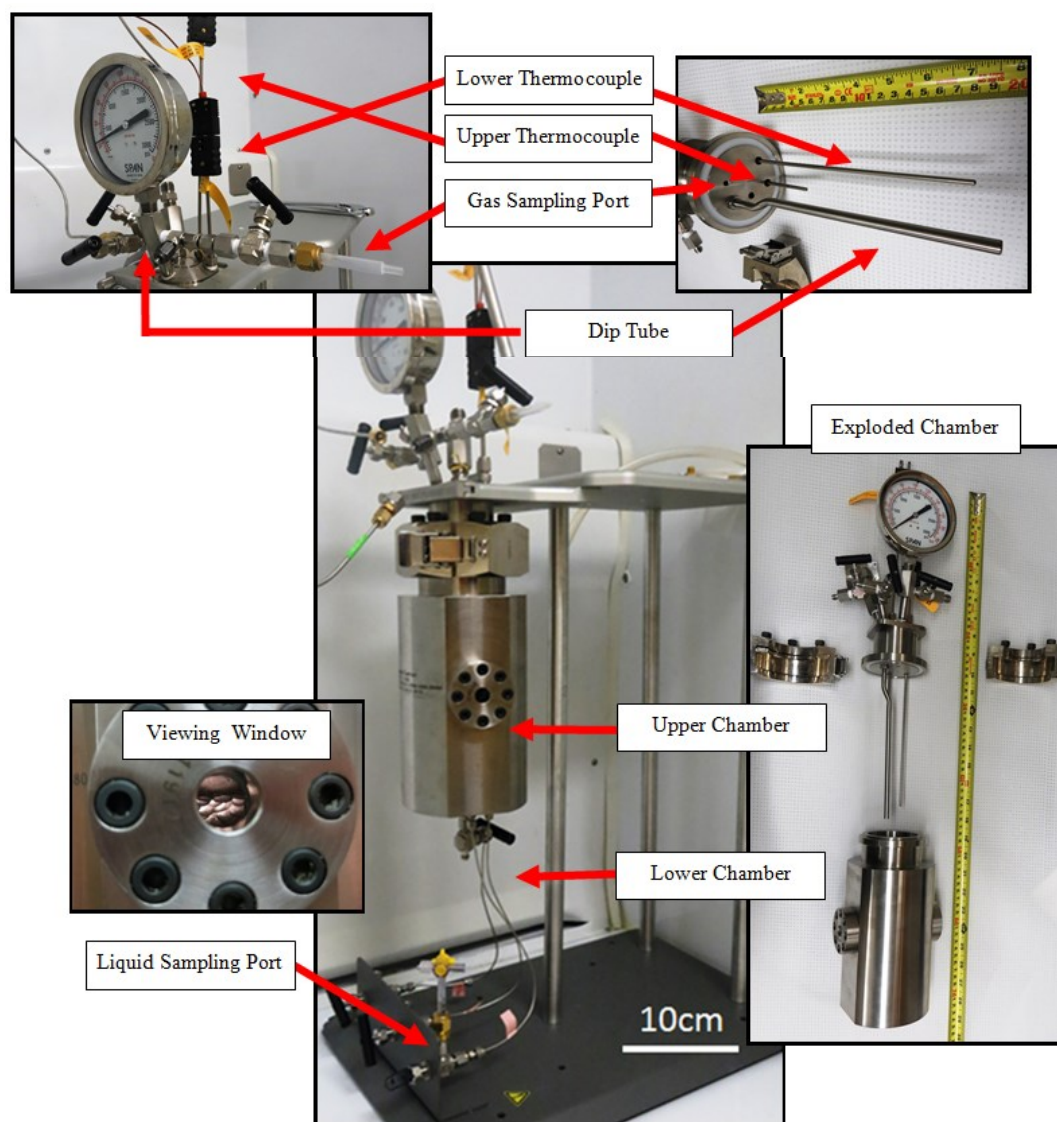


Figure 2.5. Parr pressure chamber (600mL volume) used for hydrate experiments.

On the bottom of the chamber, there were three sample ports and a waste valve that were connected to the lower part of the chamber. Only one of the sample ports was used for these experiments and was fitted with a syringe adapter to collect liquid samples (Fig 2.5, Center). To collect either a headspace or a liquid sample from the chamber, the ports were flushed with 1-3 mL of the gas or liquid and then ~1-3 mL of the sample was collected from the chamber.

2.3.2 Culturing Techniques

Obtaining the Culture. The pure culture isolate *M. album* was obtained from ATCC (Catalog Number 33003) for experimentation on 4 December 2012, stored for one week at -80°C, and then transferred to liquid nitrogen. A seed stock was prepared from the original culture and used as the working culture for glass vial and pressure chamber experiments (Fig 2.6) (described in detail in Appendix B).

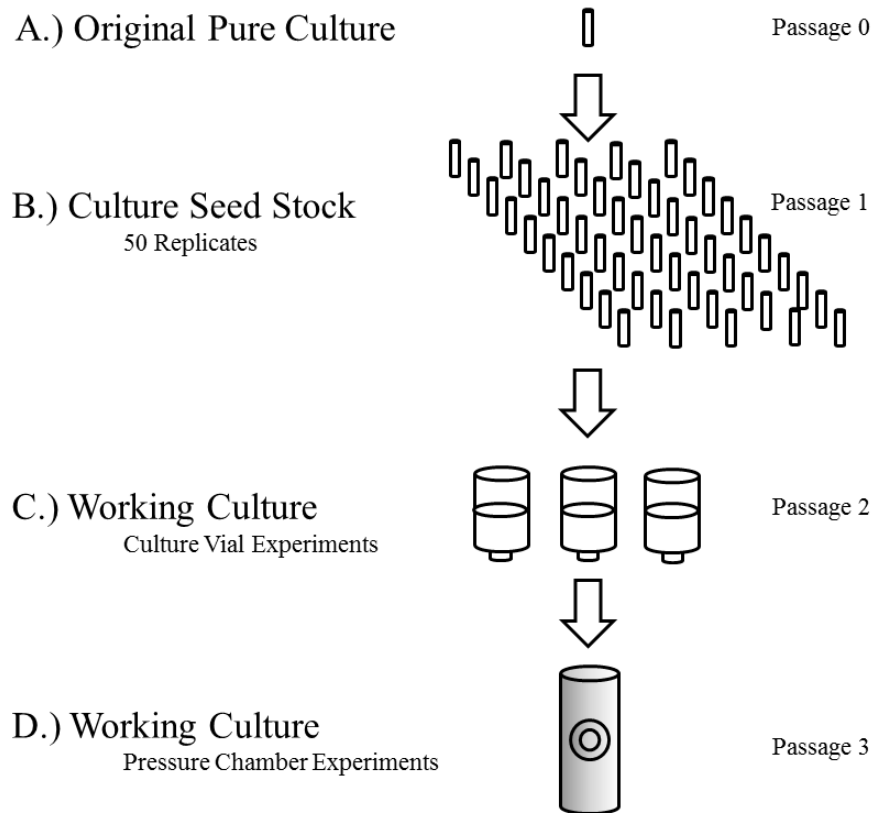


Figure 2.6. A culture schematic of the [A.] original pure culture obtained from ATCC (passage 0), the expanded [B.] seed stock (passage 1), the [C.] working culture used for experiments at atmospheric pressure (passage 2), and the working culture used for [D.] pressure chamber experiments (passage 3).

Materials needed for culturing work. All culture solutions contained liquid Nitrate Minimal Salts (NMS) growth media (Table 2.1) (Whittenbury et al., 1970). The liquid media was used in both glass serum vials and the stainless steel pressure chamber at a liquid to headspace ratio of approximately 1:1. The liquid

media was contained in glass serum vials with chloro-butyl rubber septa (14 mm

Table 2.1. The recipe for the Nitrate Minimal Salts Culture Media provided by ATCC for *M. album* culture is shown.

Nitrate Minimal Salts Media	Volume (mL)
Sodium-Potassium Phosphate Buffer, pH 7.10	6.5
<i>Sodium nitrate solution (20%) (Described Below)</i>	10.0
<i>L-F Salts Solution (Described Below)</i>	10.0
Distilled water	973.5
Total Volume	1500.0
<i>Sodium-Potassium Phosphate Buffer</i>	
KH₂PO₄	136.0 g
NaOH	28.8 g
Distilled water	1,000.0
<i>L-F Salts Solution</i>	
10% (w/v) MgSO₄·7H₂O solution	200.0
10% (w/v) CaCl₂·2H₂O solution	20.0
1% (w/v) ZnSO₄·7H₂O solution	4.9
1% (w/v) CuSO₄·5H₂O solution	0.2
1% (w/v) H₃BO₃ solution	0.6
1% (w/v) MnSO₄·H₂O solution	0.27
10% (w/v) FeSO₄ solution	10.0
Distilled water to	1,000.0

thick, 20 mm OD) fitted with aluminum collars to maintain a gaseous headspace and to prevent gas exchange. The septa were not pretreated, even though there is now some indication that butyl-rubber stoppers might be toxic to some methanotrophic cultures (Niemann, in review). The culture vials were autoclaved for sterilization (Detailed in Appendix A).

Treatment and Controls. Culture vial experiments were conducted using a treatment condition and two controls. The treatment contained the culture with a headspace gas mixture of 50% CH₄ and 50% air (~20% O₂ and no CH₄) to provide the environment needed to support methanotrophic growth. The abiotic

control sample also contained culture-free NMS media with a headspace gas mixture of 50% CH₄ and 50% air but was not inoculated to test if the culturing conditions were sterile. The biotic control was inoculated and contained a 100% air (no CH₄) headspace to provide a check that the organism being cultured required CH₄ for growth.

Subsampling glass vials. At each time point, liquid and gas subsamples were collected for analysis from the culture vials using a needle and sterile syringe. Before collecting the sample, an equal amount of either sterile media or gas (either 50% CH₄ or 100% air) was injected into the vials to compensate for the volume removed for the sub-sample. Since this procedure essentially diluted the signal at each time point, the final concentrations were corrected via methods described in Appendix C. Headspace samples taken for gas composition analysis remained in the 10 mL plastic syringes, but were analyzed within hours of collection. For stable isotope analysis, 1-2 mL headspace gas samples were added to 12.5 mL helium flushed glass serum vials that were sealed with butyl rubber septa. These vials were then stored upside down in a container of water at 4°C to minimize sample loss via diffusion through the septa. The samples were analyzed for isotopic composition within 6 months of collection (details below).

For the liquid samples, 1-2 mL of the sample was equilibrated with 2 mL of added helium in a 3 mL syringe by shaking the syringe for 2 minutes. An aliquot of the equilibrated headspace was then injected into a gas chromatograph to determine methane and oxygen concentrations (described below in detail).

2.3.3 Analytical

Cell Density. Cell densities were monitored as an indicator of culture growth using spectrophotometry. Approximately 1.5 mL liquid samples were collected from either the vials or the chamber and placed into cuvettes. The light scattering properties of the cells were measured by spectrophotometry at a wavelength of 405 nm (Dedysh and Dunfield, 2011) using a Thermo Scientific Genesys 10S UV-Vis spectrophotometer. The amount of scatter was used as an indicator of cell density. Sterilized NMS media was used as a blank.

Methane and oxygen concentrations. Headspace and media gas samples were measured for CH₄ and oxygen using gas chromatography (GC). Gas samples were either directly injected into the GC via a side port or a loop. The GC was a SRI 8610C equipped with HayeSep D and Mol Sieve columns, a Thermal Conductivity Detector (TCD), and a Flame Ionization Detector (FID). A standard was prepared by mixing 100% CH₄ and air at a ratio of 1:1 in a syringe. Certified CH₄ standards of 9,975 ppm CH₄, and 97.66 ppm CH₄ were also used. Several GC methods were developed to analyze these gas samples and are outlined in Table 2.2.

Table 2.2. The details for each method of GC analysis are shown in the table.

Method	Backflush (for CH ₄)	Backflush (for O ₂)	Measure O ₂ CH ₄ CO ₂
Details	Mol Sieve	No Mol Sieve	No Mol Sieve
Precision	1.98%	10.02%	6.89%
Temp (°C) FID/TCD	32 °C High/High	32 °C High/High	34 °C Med/High
Standards	9975 ppm CH ₄	1:1 CH ₄ and Air	10,500 ppm CH ₄ 1:1 CH ₄ and Air
Events	0.100 G ON 1.500 G OFF	0.050 G ON 0.600 G OFF	0.000 G ON 2.500 A ON 6.050 A OFF 0.600 G OFF
Sample Size	1 mL	3 mL	1 mL
Loop Size	NA (Direct Inject)	250 µL	NA (Direct Inject)
Analyte	CH ₄	O ₂	CH ₄ O ₂

Stable Carbon Isotope Analysis. To determine the $\delta^{13}\text{C}$ isotopic ratios of CH_4 ~1-3 mL aliquots of the gas samples were added to a helium-flushed 4.5 mL Exetainer® to reduce the concentration of the sample gas to ~3,000 ppm CH_4 , the ideal concentration for the isotope analysis. The Exetainers® were mounted into the Finnigan Gas Bench II Autosampler. The samples were analyzed using a Thermo Scientific Trace Gas Pre-Concentrator (containing a copper column at 1,000 °C to oxidize the CH_4 to CO_2) coupled to a Delta V Isotope Ratio Mass Spectrometer (IRMS). The IRMS was located in the Cooper lab at the Chesapeake Biological Laboratory. Calculations of $\delta^{13}\text{C}$ were normalized to the internal Vienna Pee Dee Belemnite standard. In addition, an external working CH_4 standard of 9,975 ppm CH_4 (helium balance) was used. The standard was calibrated by the Florida State University IRMS lab to be $37.4 \pm 0.085\%$. Stable isotope analyses were also performed using Cavity Ring Down Spectroscopy (CRDS) with a Picarro G2201-i Analyzer and a comparison of CRDS and IRMS results is described further in Appendix D.

The isotope value was also determined via IRMS for the two 100% methane cylinders used to prepare experiment headspaces. These values were used as the original isotope value for each experiment. The CH_4 contained within the cylinder used to prepare culture vial headspace had a $\delta^{13}\text{C}\text{-CH}_4$ value of $-38.5\% \pm 0.067$ and the cylinder used to prepare pressure chamber headspace contained CH_4 with a $\delta^{13}\text{C}\text{-CH}_4$ value of $-37.8\% \pm 0.088$.

2.3.4 Culture Vial Experiments

Three culture experiments were carried out in glass culture vials and four experiments in the pressure chamber. An outline of all experiments is shown in Table 2.3.

Culture Vial I, Initial Growth (30 °C at Atmospheric Pressure. The culture was passaged three times to become familiar with the growth of the culture at optimal conditions. A passage occurred when a small amount of turbid media (containing a dense concentration of cells) was transferred to fresh media in a new

culture vial. A passage was done to remove waste products and provide fresh nutrients for the cells. The first passage was monitored only visually and using light microscopy. The second and third passages were monitored every 2 to 5 days when gas samples were taken for GC and stable isotope analyses. Liquid samples were taken for spectrophotometric analysis.

Table 2.3. An experimental outline of culture work performed in culture vials and the pressure chamber are shown below.

Experiment	Containment	Days	Date	Temperature (°C)	Pressure (atm)	Analysis
Culture Vial I Initial Growth	Culture Vial 27 mL	53, 32, 20	1-18-13 to 3-12-13	30	1	GC Backflush Microscopy IRMS
Culture Vial II Copper	Culture Vial 27 mL	18	3-22-13 to 4-9-13	30	1	DAPI GC Backflush Measure O ₂ CH ₄ CO ₂ Spec
Culture Vial III Temperature	Culture Vial 27 mL	77	4-12-13 to 7-2-13	1, 10, 30	1	SPE-MS Measure O ₂ CH ₄ CO ₂ Spec
Pressure Chamber I	Pressure Chamber	39	4-16-13 to 5-24-13	1	39	Measure O ₂ CH ₄ CO ₂ Spec IRMS
Pressure Chamber II	Pressure Chamber	180	5-24-13 to 11-19-13	15 to 30	34	Measure O ₂ CH ₄ CO ₂ Spec IRMS Picarro
Pressure Chamber III	Pressure Chamber	170	11-19-13 to 5-7-14	30 to 5	34	Measure O ₂ CH ₄ CO ₂ Spec IRMS
Pressure Chamber IV	Pressure Chamber	41	5-8-14 To 6-17-14	10 to 1	41-94	Measure O ₂ CH ₄ CO ₂ Spec IRMS
Expansion (Final)	Culture Vial 120 mL	8	4-25-13 to 5-3-13	30	1	Spec
Enrichment	Culture Vial 120 mL	+400	6-13-13 to present	1, 15, 30	1, 2	Spec

Culture Vial II, Copper Addition (30°C at Atmospheric Pressure).

According to ATCC, *M. album* should be reaching turbidity within 1 week to 10 days. The culture in the first experiment took approximately 4 weeks for this to occur. Copper concentrations regulate the expression of MMO genes and copper ions are cofactors of the pMMO enzyme (Balasubramanian et al., 2010). Therefore, in this experiment, we tried to stimulate growth by increasing the copper content in the NMS media from 80 nM to 50,000 nM (as CuSO₄), as suggested in Balasubramanian et al. (2010).

Treatment and controls were prepared in 27 mL culture vials, three with regular media and three with increased copper media. The treatment and biotic controls were inoculated with 650 µL of working culture dilution and incubated for 18 days. The cultures were monitored by measuring headspace CH₄ and oxygen concentrations, and cell density using spectrophotometry, every 2 to 5 days. In addition, a DAPI (4',6-diamidino-2-phenylindole) staining method was used to monitor viable cell counts using 250 µL of media samples. This method was used only in one experiment and is described in more detail in Appendix E. The remaining 750 µL of liquid sample was used for spectrophotometric analysis.

Culture Vial III, Temperature Range (30°C, 10°C, and 1°C at Atmospheric Pressure). Since hydrate forms at low temperatures, this experiment was carried out to determine growth rates of *M. album* at temperatures that are well below the optimal temperature conditions for this culture (10°C and 1°C). Twelve 27 mL culture vials were prepared using the regular NMS media. Three vials were prepared for each temperature condition (30°C, 10°C, and 1°C) and each treatment, as well as for the biotic and abiotic controls. Three additional treatment vials were prepared for Solid Phase Extraction (SPE) to investigate changes in the dissolved organic matter produced by the cells in the media due to temperature change (described in Appendix F). The treatment and biotic control vials were inoculated with 100 µL working culture and incubated at the appropriate temperatures (30°C, 10°C, and 1°C). The vials incubated at 30°C were only cultured for 11 days after which the media became turbid. The culture vials at 10°C and 1°C were incubated

for 77 days. The cultures were monitored by measuring headspace CH₄ and oxygen concentrations and optical density during incubation.

Pressure Chamber I (1°C 39 atm). The goal of this experiment was to determine if *M. album* could be cultured in a stainless steel pressure chamber, under pressure, and at cold temperatures. The chamber, containing media with culture and a headspace of 50% CH₄ and 50% air, was held at 34 atm and 1°C for 38 days. Headspace and media samples were collected and analyzed for CH₄ and oxygen concentrations, cell density, and CH₄ stable carbon isotopes.

For all chamber experiments, liquid and gas samples were removed by washing the sample port with 1-2 mL of liquid, then removing 1-2 mL of sample liquid. Because the liquid quickly degassed, the sampling port filled with gas bubbles, making it difficult to achieve a specific liquid volume. Liquid samples were also purged of the headspaces that were collected in the sampling syringes. Decreasing pressure due to sampling loss impacted the solubility of aqueous CH₄ and further details for each pressure chamber experiment are described in Appendix G.

Pressure Chamber II (15°C at 34 atm). Since growth did not occur in the pressure chamber I experiment, the goal of this experiment was to determine if temperature or pressure was the dominant growth-limiting factor of the culture. The experiment was carried out at high pressure but not cold temperatures. The chamber, containing media with culture and a headspace of 50% CH₄ and 50% air, was held at 34 atm and 15°C for 46 days. Liquid samples were taken during this time to check the viability of the culture. This was done at day 34, when a liquid aliquot was removed from the chamber and used to inoculate culture vials that were then incubated at 30°C to see if cells were still viable.

The temperature was increased after 46 days and held at 30°C for the remainder of the experiment, because of the very little growth at the initial 15°C. Liquid and headspace samples were collected throughout the 180 days of the experiment analyzed for CH₄ and oxygen concentrations, cell density, and CH₄ stable carbon isotopes.

Pressure Chamber III (30°C to 5°C at 34 atm). The goal of this experiment was to determine if growth of the culture could be stimulated at low

temperatures by slowly ramping down the temperature. The chamber, containing media with culture and a headspace of 50% CH₄ and 50% air, was held at 34 atm and 30°C, initially. Over the first 20 days of the experiment, the temperature was lowered to 5°C over 20 days and held at 10°C for the remainder of the experiment. Liquid and headspace samples were collected throughout the 170 days of the experiment and analyzed for CH₄ and oxygen concentrations, cell density, and stable carbon isotopes of CH₄.

Pressure Chamber IV. The goal of this experiment was to form hydrate in the presence of the culture by maintaining media containing culture within the stability zone by increasing the pressure and lowering the temperature to conditions of hydrate stability (1°C and 112 atm). Media containing cells was added to the chamber as well as a headspace of 50% CH₄ and 50% air. The chamber was brought to 112 atm and 1°C. Hydrate formed overnight and a dissolution experiment was attempted via methods described in detail in Lapham et al. 2014. Briefly, once the hydrate formed, the CH₄ headspace was removed and replaced with nitrogen gas. However, this required that the pressure was released from the chamber. During this process, the hydrate dissolved rapidly and was unsuitable for further dissolution experiments.

2.3.5 Bottom Water Enrichment

Since *M. album* was a pure culture, not originally from a hydrate environment, an attempt was made to cultivate methane oxidizers from bottom water collected near a Gulf of Mexico gas hydrate site. Bottom water was collected at the GC 600 site on 6 June 2013 using a CTD Rosette Niskin bottle. 75 mL of bottom water was added to 157 mL serum vials and a 50% CH₄ and 50% oxygen headspace was prepared with vial headspaces at 1 and 2 atm (described in detail in Appendix H). The vials were then incubated at 30°C, 10°C, and 4°C and monitored using spectrophotometry and CRDS (Appendix D). Autoclaved seawater was used as the spectrophotometry blank.

2.4 Results

The culture vial and chamber experiments were monitored, in part, using GC analysis of headspace samples. In general, when growth occurred (indicated by spectrophotometry and stable isotope analysis) in the treatment vials, CH₄ and oxygen concentrations decreased. In the controls, where no growth occurred (indicated by spectrophotometry and stable isotope analysis) oxygen and CH₄ concentrations did not change. However, the measurements were highly variable (up to 10 % gas concentration). The GC and IRMS results are shown in Table 2.4. The results of GC analysis of headspace are presented in the following sections (more detail in Appendix I). However, for reasons detailed in the discussion, GC results were not useful as an indication or quantitation of culture activity.

Table 2.4. Results of experiments performed in culture vials and the pressure chamber are shown below. Methane oxidation rates were derived from the slope values of linear regressions fitted to the treatment concentrations of % CH₄. *Pressure Chamber methane oxidation rates were difficult to quantify due to methane solubility changes occurring in pressure chamber experiments.

Experiment	Methane Oxidation Rate (CH ₄ % d ⁻¹)	Δ ¹³ C-CH ₄ (‰)
Culture Vial I Passage 2	0.45	0.4
Culture Vial I Passage 3	0.76	6.4
Culture Vial III Temperature	4.64	No Data
Pressure Chamber I	No Data*	No Data
Pressure Chamber II	No Data*	4.5
Pressure Chamber III	No Data*	8.4

2.4.1 Culture Growth at Optimal Conditions

The culture was grown at 30°C and 1 atm to become familiar with growth at optimal conditions. The first passage of the culture was inspected visually and found to show increased turbidity, or cell density, after 7 days. The culture was also observed using

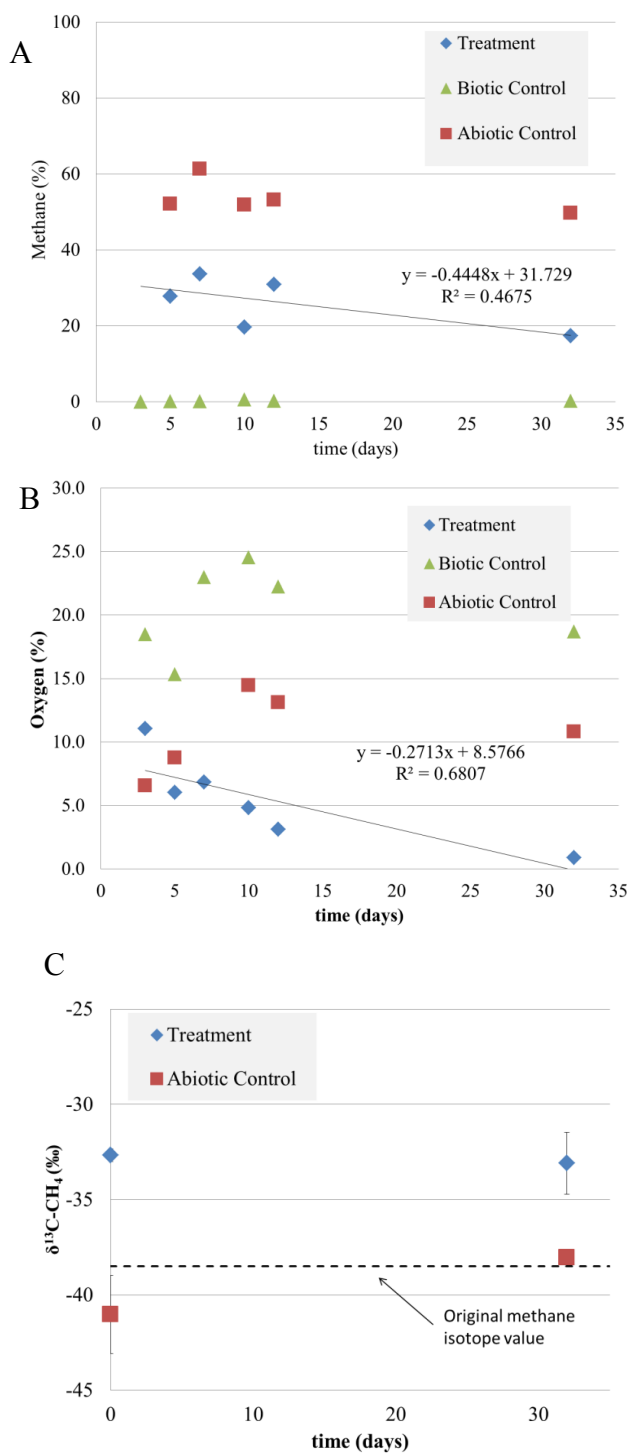


Figure 2.7. The results of the Culture Vial I experiment at optimal conditions of 30°C and 1 atm are shown. Percent CH₄ (A) and Oxygen (B) headspace measurements and stable isotope measurements of $\delta^{13}\text{C-CH}_4$ (‰) (C) are shown from the second passage. Error bars in C show standard error on duplicate measurements.

light microscopy to contain rounded rod shaped or coccobacillus cells after 13 days of inoculation. Headspace gas composition and isotope analysis was performed after 53 days and found to be 21.4% CH₄ and $-33.94 \pm 0.07 \delta^{13}\text{C-CH}_4$. In the second passage, based on the linear regression fit to the treatment condition, a methane oxidation rate of 0.45% CH₄ d⁻¹ and oxygen consumption rate of 0.27% oxygen d⁻¹ were measured (Fig 2.7a-b and Table 2.4). In addition, a 0.4‰ fractionation occurred in the $\delta^{13}\text{C-CH}_4$ values during the second passage (Fig 2.7c and Table 2.4). In the third passage, a methane oxidation rate of 0.76% CH₄ d⁻¹ and an oxygen depletion rate of 0.37% oxygen d⁻¹ were measured (Fig 2.8a-b and Table 2.4). Also, a 6.4‰ fractionation occurred in the $\delta^{13}\text{C-CH}_4$ values during the third passage (Fig 2.8c and Table 2.4).

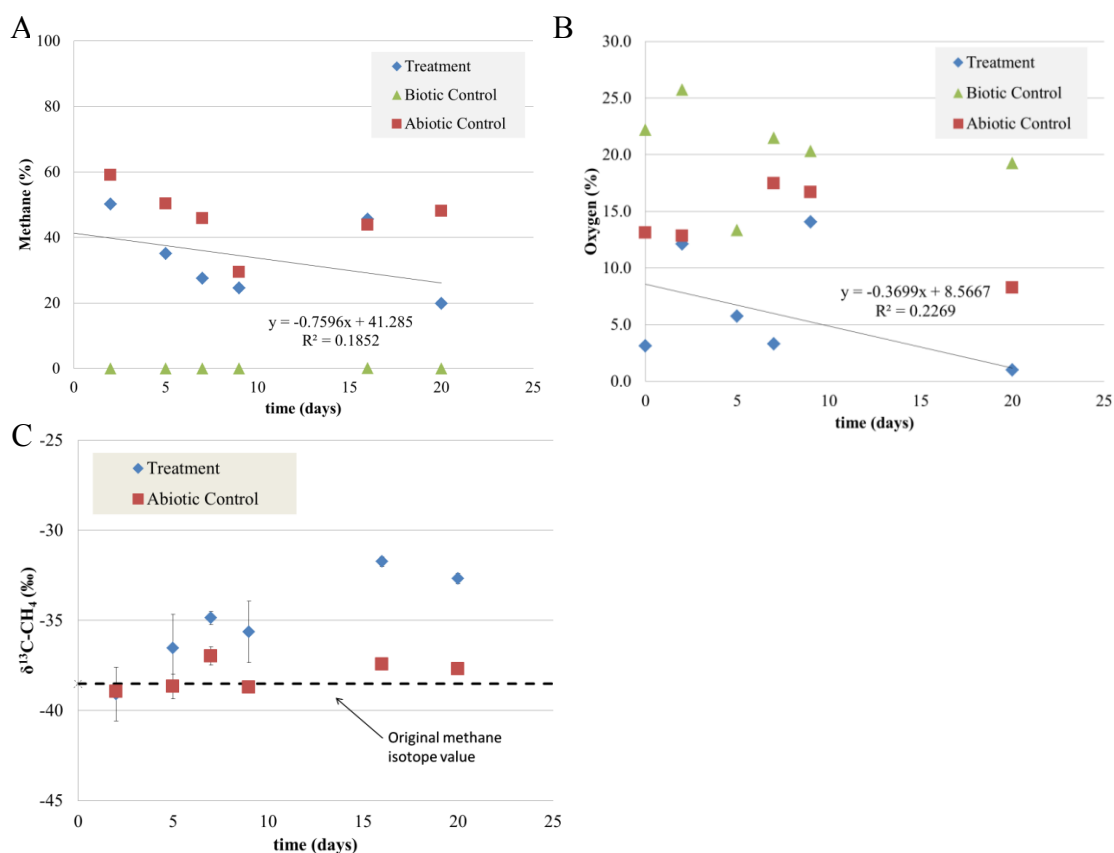


Figure 2.8. The results of the Culture Vial I experiment at optimal conditions of 30°C and 1 atm are shown. Percent CH₄ (A) and oxygen (B) headspace measurements and stable isotope measurements of $\delta^{13}\text{C-CH}_4$ (‰) (C) are shown from the third passage. Error bars in C show standard error on duplicate measurements.

2.4.2 The Addition of Copper to the Growth Media

The culture was grown at 30°C in regular media containing 80 nM copper and also in media containing 50,000 nM copper. The optical density of the media increased from 0.00 to 0.06 in the regular media treatment, whereas the high copper media treatment remained near 0.00, as well as all of the control vials (Fig 2.9). The spectrophotometry results indicated growth in the regular media, but not in the media with increased copper concentrations. Analysis of headspace CH₄ and oxygen revealed patterns that were similar in the treatment and controls despite growth or no growth (Fig 2.10-2.11).

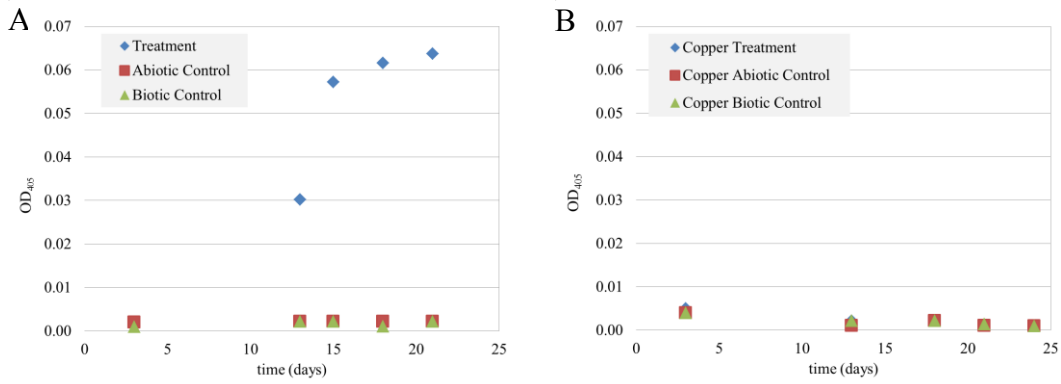


Figure 2.9. The spectrophotometry results of the Culture Vial II experiment with A) regular media and B) increased copper media at 30°C and 1 atm.

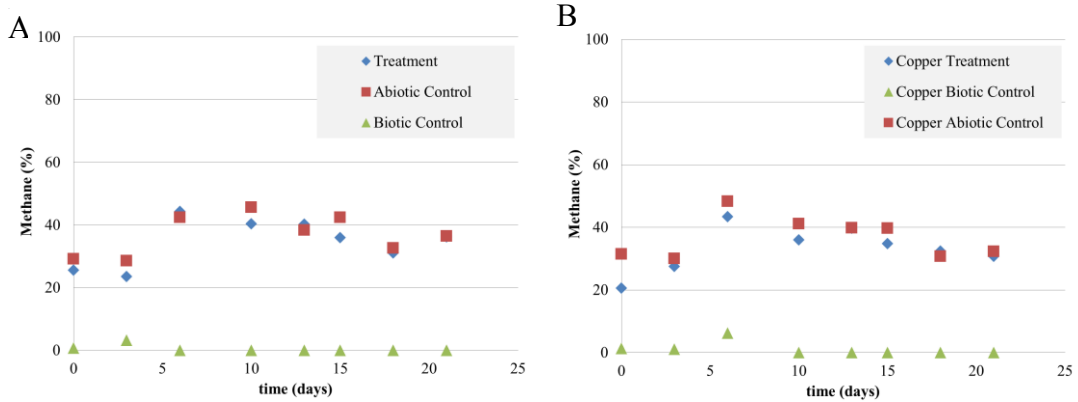


Figure 2.10. The headspace methane results from the Culture Vial II experiment with regular media and increased copper media are shown. Percent methane headspace measurements were made of culture grown in regular media (A.) and copper media (B.) at 30°C and 1 atm.

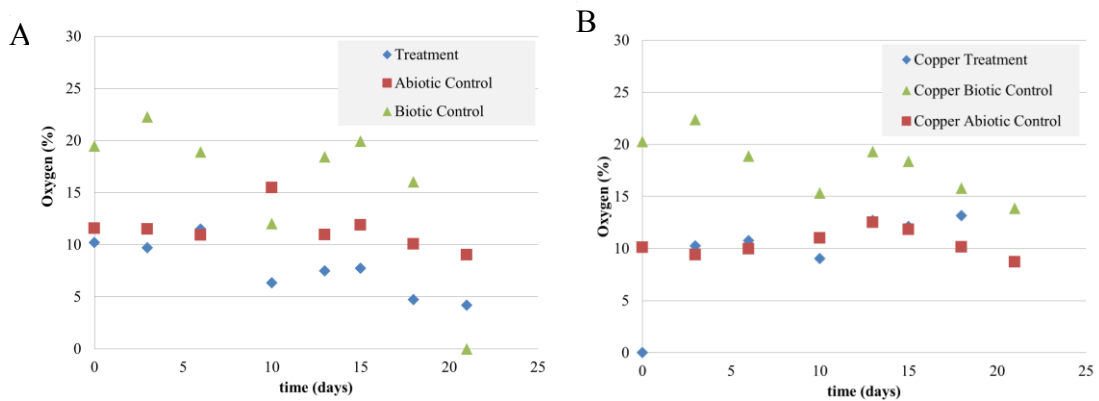
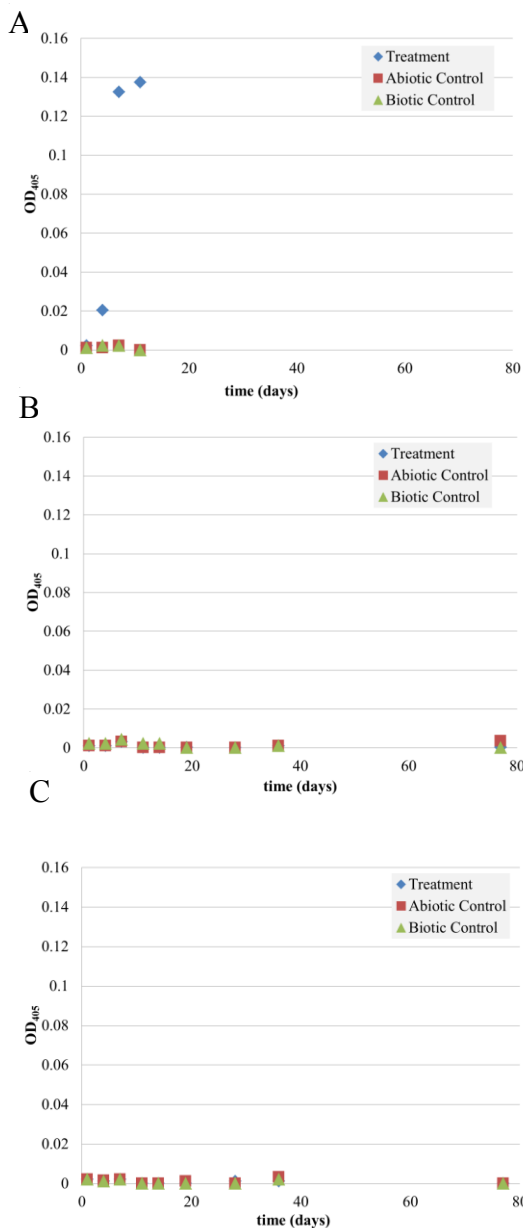


Figure 2.11. The headspace oxygen from the Culture Vial II experiment with regular media and increased copper media are shown. Percent oxygen headspace measurements were made of culture grown in regular media (A.) and copper media (B.) at 30°C and 1 atm.

2.4.3 The Impact of Cold Temperature on Culture Growth

The culture was grown at 30°C, 10°C, and 1°C to evaluate the impact cold temperatures has on the growth of the culture. Growth was observed in the 30°C treatment vials based on the optical density that increased from 0.00 to 0.14 OD₄₀₅, while the biotic and abiotic controls remained at 0.00 (Fig 2.12a). The optical density remained at 0.00 OD₄₀₅ in the 10°C and 1°C conditions in all vials (Fig 2.12b-c),



indicating no growth at colder temperatures.

Measurements of headspace gas concentrations overall did not clearly indicate growth, as CH₄ concentrations decreased and oxygen concentrations increased in the 30°C treatment vial. The 30°C treatment vial showed a decrease from 40.8 to 17.0% CH₄ over 11 days (Fig 2.13a). The abiotic control ranged from 41.5 to 31.4% CH₄ and the biotic control remained at zero (Fig 2.13a). No change in CH₄ was observed between the treatment and controls at colder temperatures (Fig 2.13b-c). Headspace oxygen increased in the 30°C treatment and control vials, and showed no change in the 10°C, and 1°C experiments (Fig 2.14). The results of the Solid Phase Extraction analysis (Described in Appendix F) showed no change due to variable temperature conditions.

Figure 2.12. The spectrophotometry results of the Culture Vial III temperature experiment are shown. Growth curve of spectrophotometry measurements at 405 nm for the experiment at 30°C (A.), 10°C (B.), and 1°C (C.) and 1 atm.

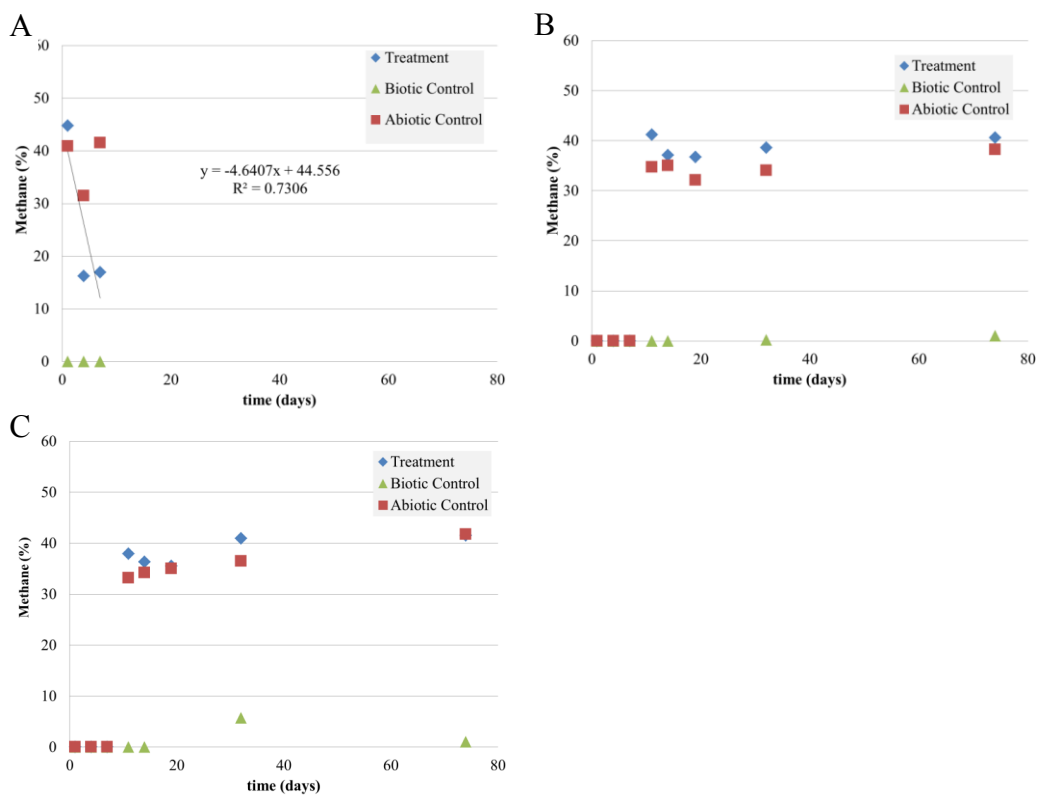


Figure 2.13. The headspace methane results of the Culture Vial III temperature experiment are shown. Percent methane headspace measurements for the experiment at 30°C (A.), 10°C (B.), and 1°C (C.) and 1 atm.

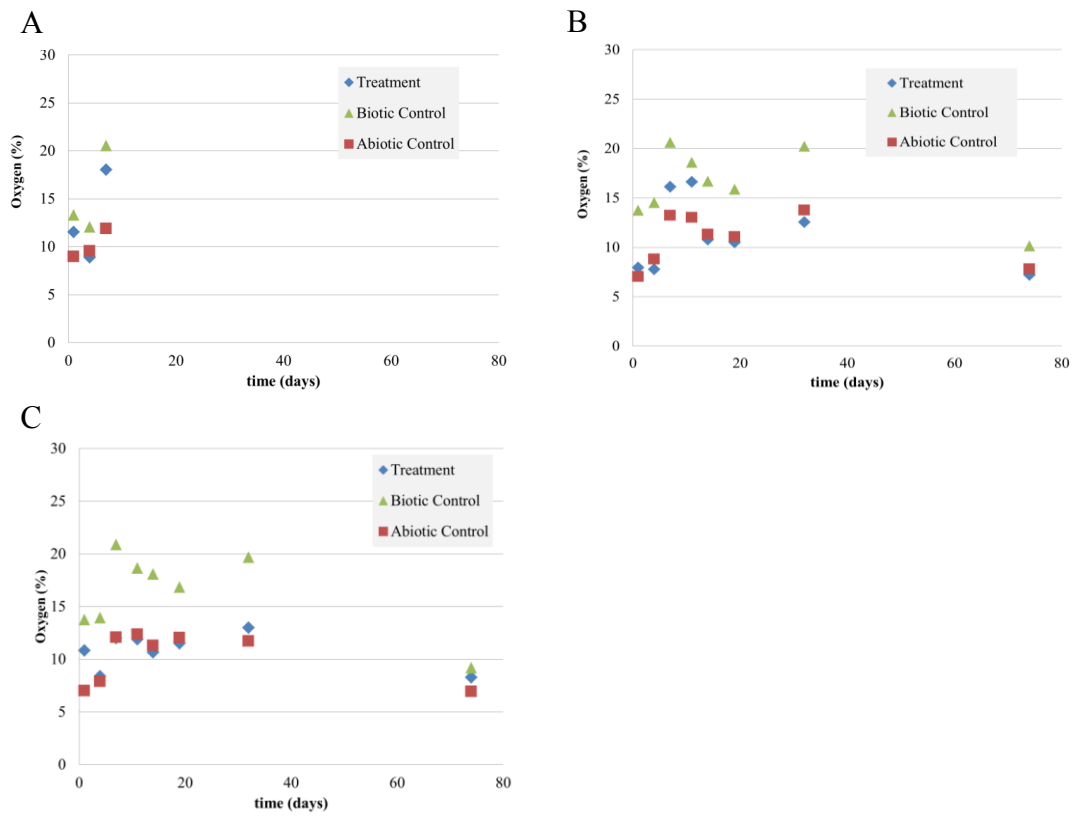


Figure 2.14. The headspace oxygen results of the Culture Vial III temperature experiment are shown. Percent oxygen headspace measurements for the experiment at 30°C (A.), 10°C (B.), and 1°C (C.) and 1 atm.

2.4.4 Pressure Chamber I: Culture Growth at High Pressure and Low Temperature

The first chamber experiment was performed at 1°C at 39 atm. The culture did not grow under these conditions, based on the optical density, which remained at

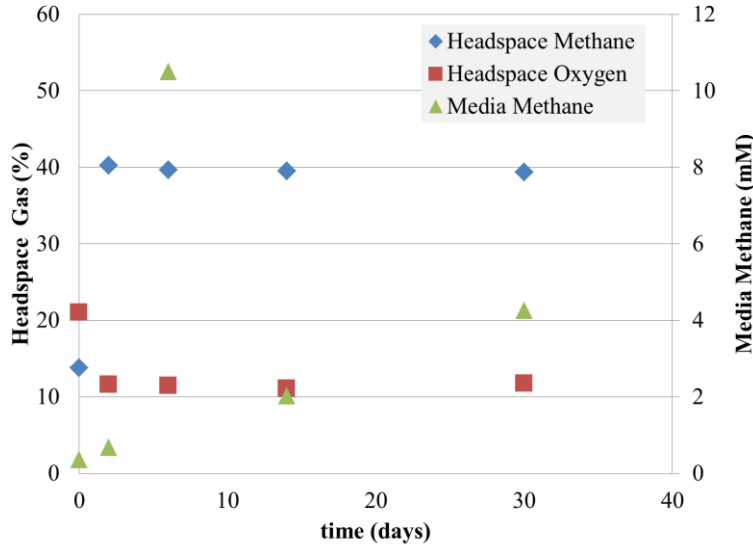


Figure 2.15. The Pressure Chamber I experiment was carried out at 1°C at 39 atm. Methane and oxygen measurements of headspace and media containing culture from the pressure chamber are shown.

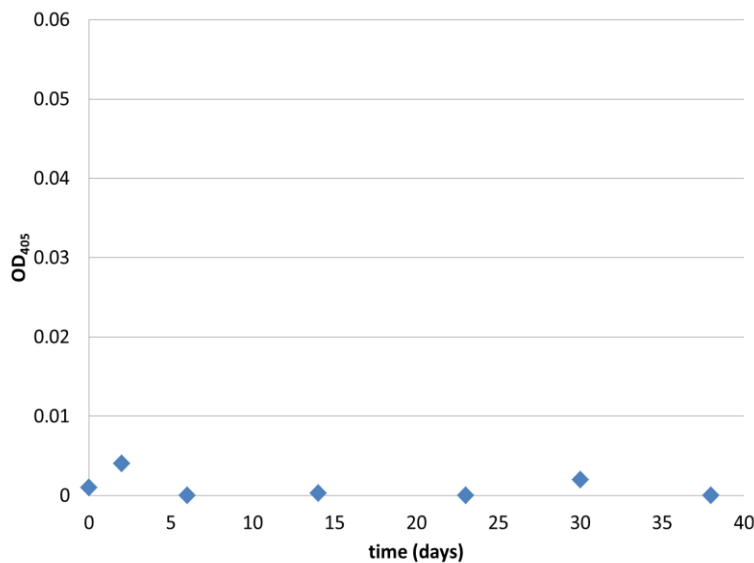


Figure 2.16. The Pressure Chamber I experiment was carried out at 1°C at 39 atm. Spectrophotometry measurements at 405 nm of media containing culture from the pressure chamber experiment I at 1°C at 39 atm.

0.00 OD₄₀₅ for the whole time series (Fig 2.16).

Headspace gas concentrations also did not change; remaining near 39.7±1.6% CH₄ and 11.5±0.5% oxygen for 30 days (Fig 2.15). Aqueous CH₄ concentrations ranged from 360 to 4,260 μM CH₄

over 30 days, probably due to methane diffusing in from the headspace (Fig 2.15). Anomalous measurements occurred on day 0, when low headspace CH₄ (13.8% CH₄) and high headspace oxygen (21.0% oxygen) were measured, and on day 7, when high CH₄ in the media (10,500 μM CH₄) was measured.

2.4.5 Pressure Chamber II: Culture Growth at High Pressure and Variable Temperature

Given the results of the Pressure Chamber I experiment, pressure chamber experiment II was intended to resolve the dominant growth-limiting factor of the culture as either pressure or temperature by measuring growth rates under high

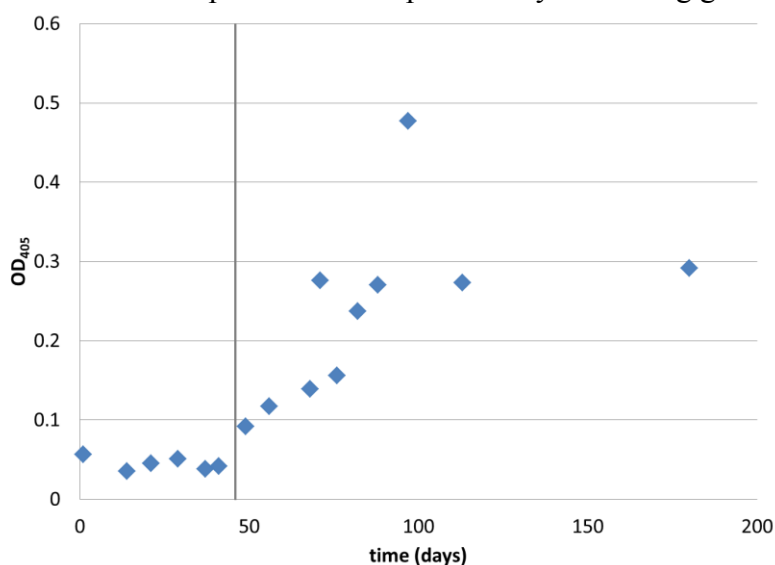


Figure 2.17. The Pressure Chamber II experiment was carried out at variable temperatures and at 34 atm. Spectrophotometry measurements at 405nm of media containing culture from the pressure chamber experiment II at 15°C at 34 atm. After 46 days, the temperature was increased to 30°C, indicated by the vertical line.

pressure at 34 atm and variable temperatures. The results indicated that growth was limited by low temperature more than high pressure.

The pressure chamber was incubated at 15°C for the first 46 days, during which the optical density measurements ranged from 0.06 to 0.04

OD₄₀₅ (Fig 2.17). A viability check on day 34 (while the chamber was still at 15°C) showed growth at 30°C (data not shown). At 46 days, the incubator temperature was increased to 30°C, to determine if the cells were still viable. Optical density increased at warm temperatures from 0.09 to a final measurement of 0.30 OD₄₀₅ (Fig 2.17).

Concentrations of aqueous CH₄ decreased in the chamber (Fig 2.18), though the impact of methane oxidation was difficult to extract from the impact of the decreasing solubility of CH₄. During the cold portion of the experiment (the first 46 days), dissolved CH₄ concentrations decreased slightly and ranged from 2.6 mM to 1.2 mM CH₄. Then dissolved CH₄ decreased from 1.0 mM to 0.7 mM CH₄ during the

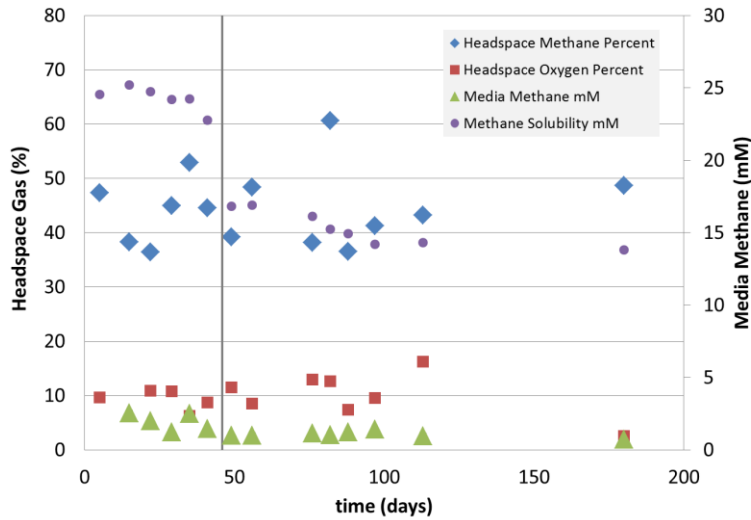


Figure 2.18. The Pressure Chamber II experiment was carried out at variable temperatures and at 34 atm. Methane and oxygen measurements of headspace gas concentrations and media methane concentrations containing culture from the pressure chamber at 15°C at 34 atm. After 46 days, the temperature was increased to 30°C, indicated by the vertical line.

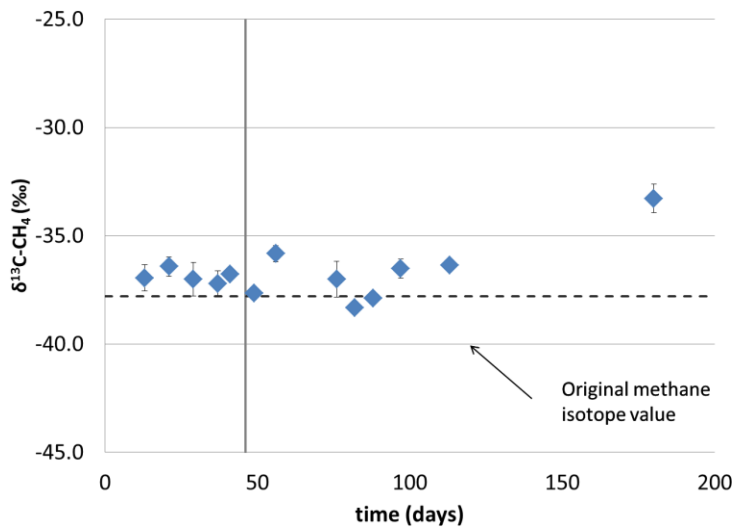


Figure 2.19. The Pressure Chamber II experiment was carried out at variable temperatures and at 34 atm. Stable isotope analysis measurements of $\delta^{13}\text{C}-\text{CH}_4$ from headspace are shown of the pressure chamber at 15°C at 34 atm. After 46 days, the temperature was increased to 30°C, indicated by the vertical line. Error bars show standard error on duplicate measurements.

warm portion of the experiment (Fig 2.18). Headspace gas concentrations remained constant at $44.3 \pm 6.9\%$ CH_4 and $9.8 \pm 3.4\%$ oxygen (Fig 2.18). CH_4 solubility was calculated (Appendix C) based on the measured partial pressure of CH_4 , temperature, pressure, and salinity (0 ppt) and ranged from 25.2-22.8 and 16.9-13.8 mM CH_4 during the first and second portions of the experiment (Fig 2.18).

Analysis of stable isotopes of CH_4 carbon showed a small enrichment of ^{13}C over the full 180 days, during which $\delta^{13}\text{C}-\text{CH}_4$ values increased by 4.5‰. For the first 46 days, the values of $\delta^{13}\text{C}-\text{CH}_4$ ranged from -36.4 to -37.2‰ at

15°C and ranged from -38.3 to -33.3‰ for the remaining 134 days of the experiment at 30°C, with a final value of -33.3‰ (Fig 2.19).

2.4.6 Pressure Chamber III: Culture Growth at High Pressure and Decreasing Temperature

With temperature determined as the growth-limiting factor, the third chamber experiment was carried out at 34 atm, and the temperature was gradually decreased

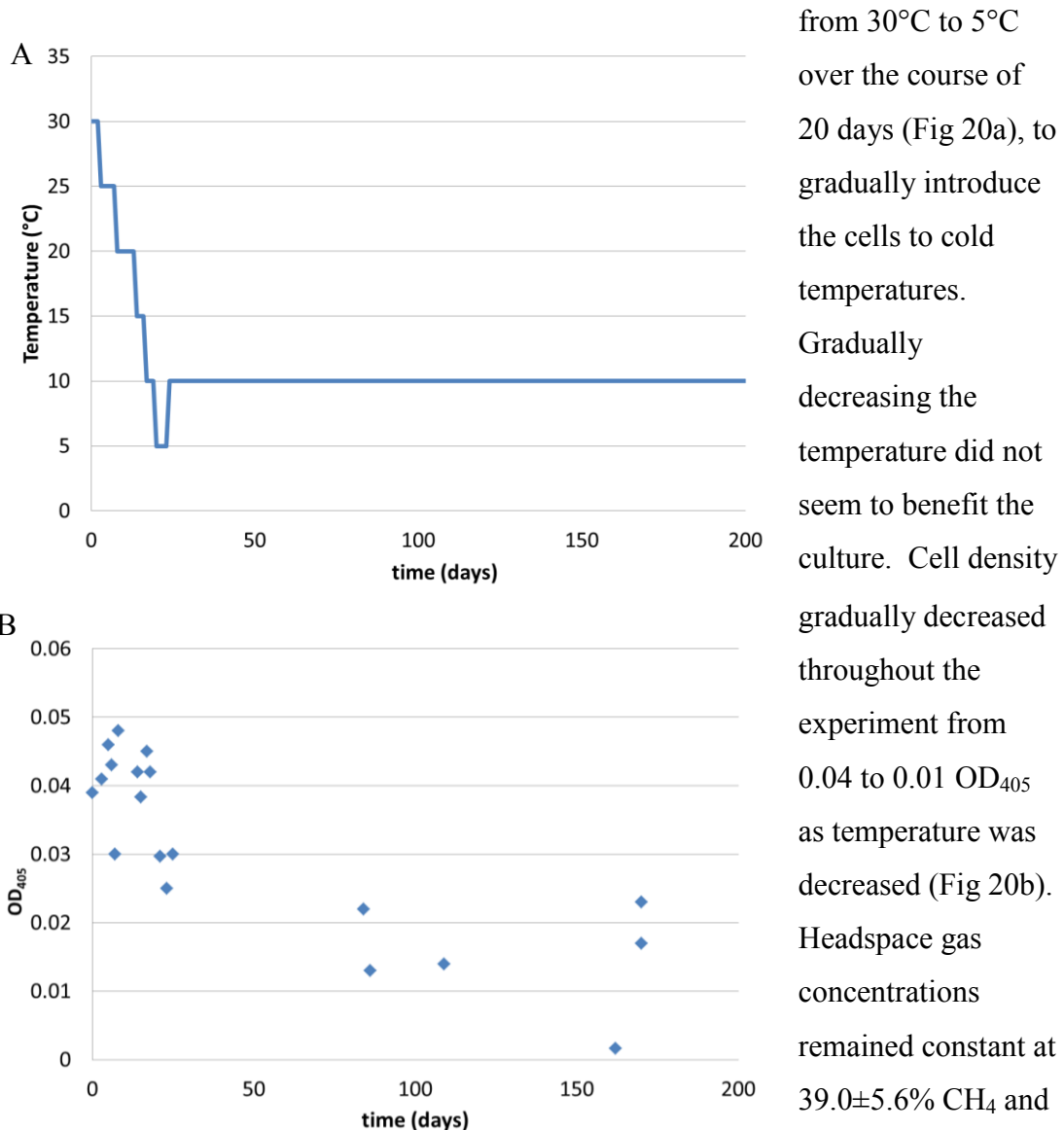


Figure 2.20. The Pressure Chamber III experiment was carried out at variable temperatures and at 34 atm. The variable temperatures over time (A) and spectrophotometry measurements at 405 nm of culture (B) are shown.

from 30°C to 5°C over the course of 20 days (Fig 20a), to gradually introduce the cells to cold temperatures. Gradually decreasing the temperature did not seem to benefit the culture. Cell density gradually decreased throughout the experiment from 0.04 to 0.01 OD₄₀₅ as temperature was decreased (Fig 20b). Headspace gas concentrations remained constant at 39.0±5.6% CH₄ and 10.2±1.9% oxygen for the duration of

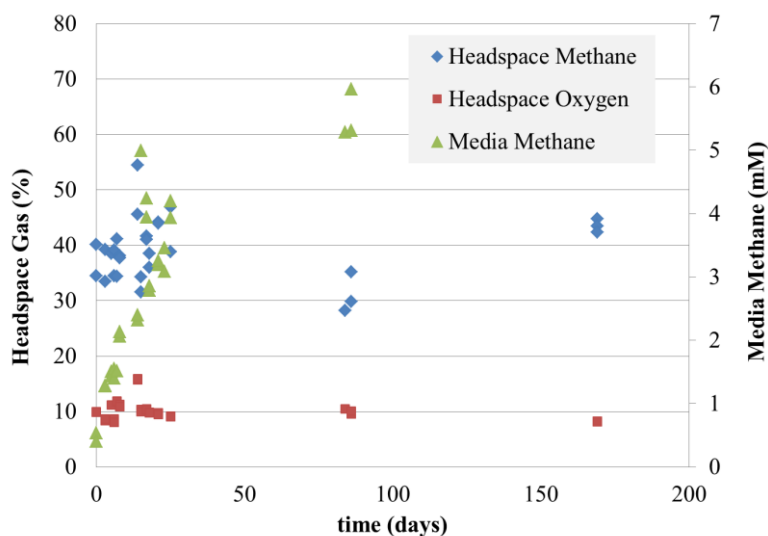


Figure 2.21. The Pressure Chamber III experiment was carried out at variable temperatures and at 34 atm. Methane measurements of headspace and media containing culture from the pressure chamber experiment are shown.

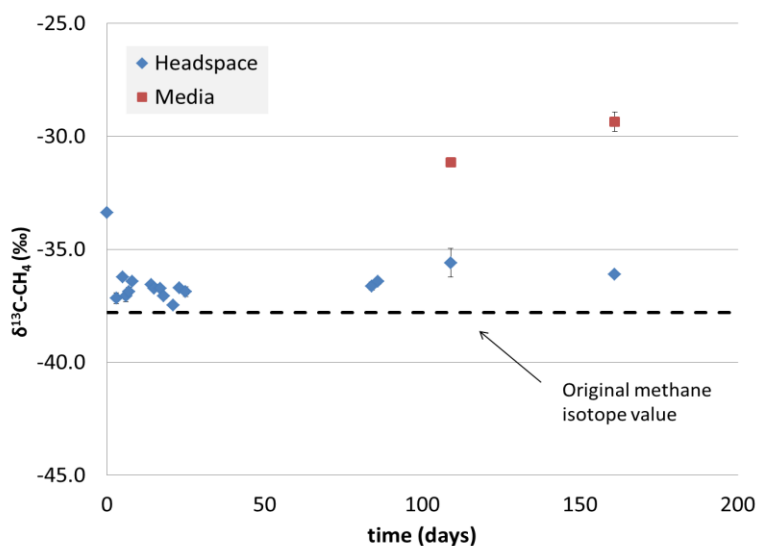


Figure 2.22. The Pressure Chamber III experiment was carried out at variable temperatures and at 34 atm. Stable isotope measurements of $\delta^{13}\text{C-CH}_4$ of headspace and media methane for pressure chamber are shown. Error bars show standard error on duplicate measurements. Analysis of media methane-carbon was conducted on the last two samples.

the experiment (Fig 2.21). Dissolved CH_4 concentrations increased from 0.4 mM to 5.3 mM (Fig 2.21). The $\delta^{13}\text{C-CH}_4$ values of the headspace ranged from -37.2 to -35.6‰, with an initial anomalous value of -33.4‰ (Fig 2.22). Two measurements of media $\delta^{13}\text{C-CH}_4$ were performed at the end of the experiment and were more enriched in ^{13}C by 8.4‰. Values increased to -29.4‰ from the original gas value of -37.8‰ used to pressurize the chamber, though initial values of media CH_4 were not measured.

2.4.7 Pressure Chamber IV: Forming Hydrate in the Presence of the Culture

Hydrate was formed in the pressure chamber containing *M. album* in NMS media. After 2 days at 112 atm and 1°C, crystals formed in the chamber at the liquid-gas interface. The appearance of the hydrate was slushy, not a solid block as has been observed in other hydrate dissolution experiments (Lapham et al., 2014). The chamber was vented and flushed over the course of 26 minutes in an attempt to remove the CH₄ from the headspace. The temperature in the chamber increased to 6°C and the crystals dissolved. The chamber was repressurized with a headspace of 50% CH₄ and 50% air to 94 atm, reforming the crystals. Insulation was added to the chamber and again the headspace was vented and flushed over the course of 14 minutes. The temperature in the chamber increased to 2°C and the crystals dissolved. The chamber was repressurized to 93 atm, reforming the crystals. After these two attempts, we determined that this hydrate was not suitable for hydrate dissolution experiments. The conditions that pressure chamber experiments I-IV were conducted at are plotted on a phase diagram of CH₄ (Fig 2.23).

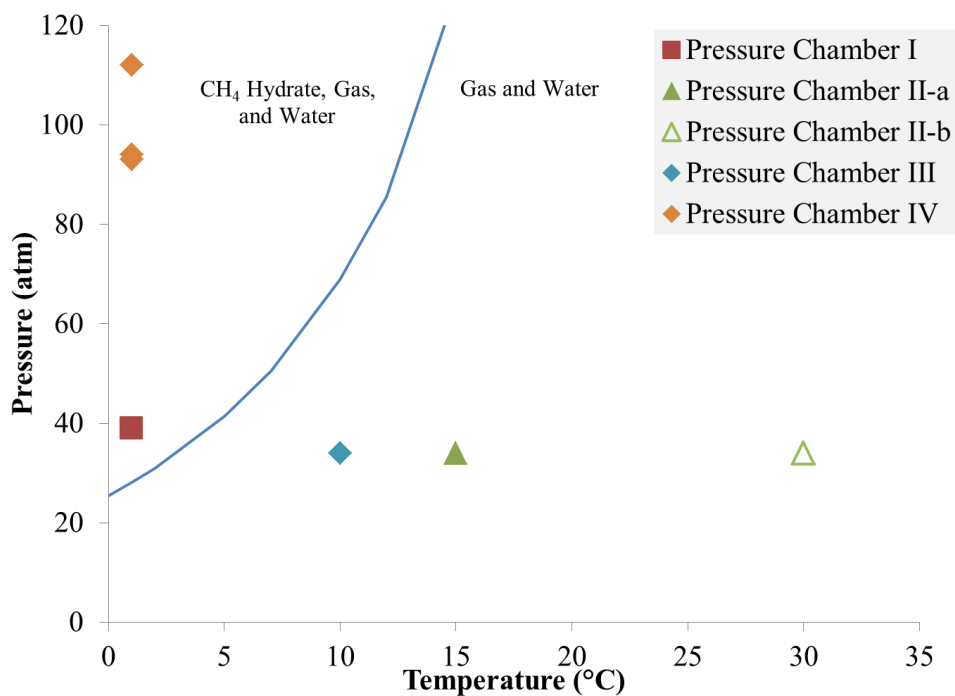


Figure 2.23. A gas hydrate phase diagram is shown. The Pressure Chamber Experiments I-IV are plotted on the diagram based on the pressure and temperature conditions at which the experiments were conducted.

2.3.8 Bottom Water Enrichment

Seawater collected from the Gulf of Mexico showed no growth in the enrichment experiment in the first 120 days, and even a year and a half after starting the experiment. Optical density remained at 0.00 over the course of 120 days (Fig 2.24). Measurements of the headspace stable isotopes of CH₄ carbon were performed

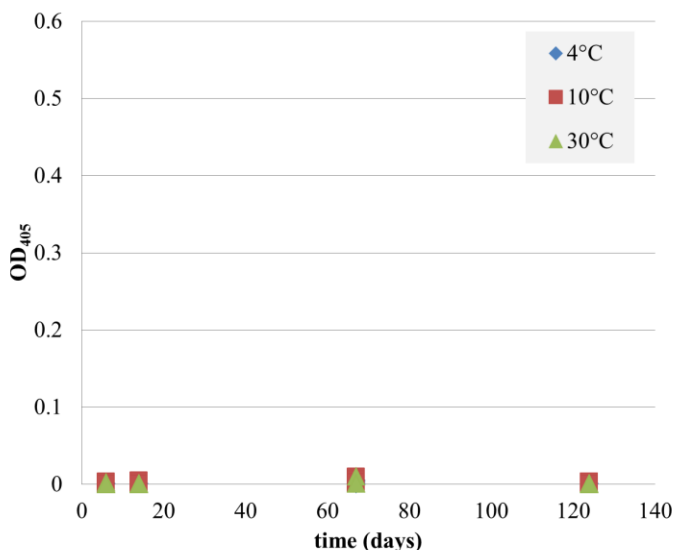


Figure 2.24. An enrichment was performed using bottom water from the Gulf of Mexico. Spectrophotometric measurements of OD₄₀₅ are shown.

523 days (a year and 5 months) after the enrichment began. Measurements from three of the 30°C vials revealed no enrichment, but a small ($1.5 \pm 0.35\text{‰}$, $2.3 \pm 0.29\text{‰}$, and $2.6 \pm 0.17\text{‰}$) depletion of ¹³C based on the measured value of the tank used to prepare the enrichment vials.

2.5 Discussion

The culture vial and pressure chamber experiments demonstrated that:

- 1) The culture does not grow at low temperatures (10°C or 1°C), but remained viable at intermediate temperatures (15°C)
- 2) High Pressure (34 atm) did not impact growth as strongly as temperature
- 3) Pressure chamber experiments also took weeks for the liquid media to equilibrate with the headspace
- 4) Hydrate formed in media containing the culture but dissolved quickly making it unsuitable for dissolution experiments
- 5) Optical density and stable isotope analysis were effectively used to monitor culture activity

- 6) Analysis of headspace gas concentrations was not an effective technique to monitor methanotrophic activity

2.6 Next Steps

Overall the results indicate that cold temperatures (at or below 15°C) were more strongly impacting the growth of the culture, than high pressures (34 atm). Hydrate formed in the presence of the organism, but was unsuitable for use in hydrate experiments. To investigate the effect of aerobic CH₄ oxidizing bacteria on gas hydrate further, the following next steps could be taken:

- 1.) An organism better adapted to cold temperatures could be used in hydrate dissolution experiments.
- 2.) The use of a surfactant could be explored to stimulate the formation of a solid block of hydrate.
- 3.) The liquid media could be equilibrated with the headspace gas during the setup of pressure chamber experiments.

2.7 Conclusion

Methane hydrate remains one of the more difficult components of the carbon cycle to quantify although it is the largest reservoir of CH₄. The experiments described in this chapter involved the pure culture *M. album* an aerobic methanotroph as a means of investigating the impact of microorganisms on gas hydrate stability. The culture grew slowly at the cold temperatures needed for hydrate formation. However, the culture was able to grow at high pressure in a stainless steel pressure, requirements for hydrate dissolution experiments. In the chamber, the dominant growth limiting factor of the culture was low temperature (below 15°C), compared to high pressure (34 atm). Headspace gas concentrations in both culture vial and pressure experiments were not effective means of monitoring growth. In pressure chamber experiments, methane oxidation was difficult to quantify based on measurements of CH₄ in the media due to interference from changes in the solubility of CH₄ due to decreasing pressure from sampling as well as intentional temperature manipulations of the chamber. Hydrate formation did occur in media containing the

culture at 112 atm and 1°C, but was unsuitable for dissolution experiments. The stability of hydrate may be impacted by the pure culture *M. album* in laboratory experiments.

More research is needed to determine the role of microorganisms and CH₄ hydrate in the carbon cycle and how it may change due to climate change. It is important to understand the factors that control the stability of CH₄ hydrate in natural settings and to further our understanding of the relationship between microbial communities and CH₄ hydrate.

Chapter 3: Methane in the Chesapeake Bay

3.1 Abstract

Global methane (CH₄) emissions from estuaries are thought to be less than 1% of the overall atmospheric sources (Middelburg et al., 2002; Reeburgh, 2007). However, due to eutrophication in estuaries, increased organic matter flux to the sediment and less efficient aerobic microbial methane oxidation may be causing hypoxia enhanced methane flux or HEMF. To address the current state of methane emissions, possibly arising from eutrophication in estuaries, CH₄ concentrations were measured. Bottom water and the sediment pore-water samples were collected continuously during the development and breakup of seasonal hypoxia in the Chesapeake Bay. OsmoSamplers were deployed on benthic landers designed to collect water approximately between 5 and 20 cm above the sediment surface and pore-water in the sediment at a depth approximately between 0 and 30 cm. Supporting measurements of concentrations of dissolved oxygen, sulfate, chloride, carbon dioxide, dissolved organic carbon, salinity, and temperature were undertaken in addition to CH₄ analysis to provide means of examining the concurrent biogeochemical conditions. CH₄ concentrations in bottom water increased from 1 μM to 40 μM in mid-July 2013 coinciding with bottom water hypoxia and anoxia as indicated by the dissolved oxygen concentrations. CH₄ concentrations decreased to levels below 1 μM when oxygen concentrations increased in the bottom water in the fall 2013. The likely source of bottom water CH₄ was the release from sediment, because pore-water concentrations of CH₄ increased from 0.03 mM to 5.5 mM CH₄, with the highest concentration measured in mid-June 2013. CH₄ may also have been formed in anoxic bottom water. To learn more about the temporal dynamics of pore-water sediment processes impacting CH₄ concentration, stable isotopic analyses of pore-water CH₄ carbon were performed. When concentrations of CH₄ increased, δ¹³C values became depleted, decreasing from -49 ‰ to -67 ‰, suggesting that microbial methanogenesis was driving the increase in CH₄ concentrations. When CH₄ concentrations decreased, the δ¹³C values became enriched, increasing from -67 ‰ to -58 ‰, suggesting microbial oxidation of methane via CO₂ reduction. Two storm-

related mixing events occurred in the Chesapeake Bay during the months of June and August. During the events CH₄ concentrations decreased in bottom water indicating a substantial loss of CH₄ possibly related to oxidation or water disturbance and a potentially large CH₄ flux from the water column to the atmosphere. By extrapolating this data over the entire Chesapeake Bay, it was calculated that between 0.05 Tg CH₄ and 0.18 Tg CH₄ was fluxed from the sediments into the water column of the Chesapeake Bay. Given these high fluxes, global estuaries experiencing hypoxia are estimated to release 7 to 23 Tg CH₄ to the atmosphere per year. From these observations it was concluded that there is a strong correlation between hypoxia and increased CH₄ flux from sediments into the water column, and possibly to the atmosphere.

3.1.1 Keywords

CH₄, stable isotopes, hypoxia, Chesapeake Bay, estuaries, sediment pore-water

3.1.2 Abbreviations

CH₄ = Methane

SO₄ = Sulfate

CO₂ = Carbon Dioxide

DO= Dissolved Oxygen

DOC= Dissolved Organic Carbon

AOM = Anaerobic Oxidation of Methane

3.2 Introduction

Estuaries are highly productive environments and are becoming increasingly eutrophic around the world due to anthropogenic nutrient additions (Diaz, 2001). Increased nutrients fuel blooms of phytoplankton that die and sink to the seafloor. The biological uptake of this fresh organic matter causes oxygen depletion through consumption. This can lead to hypoxia in the water column, which is indicated by dissolved oxygen concentrations dropping below 62.5 μM O₂ (Rabalais et al., 2009). Eutrophication has many consequences such as reduced trophic efficiency,

diversification, and deterioration of water quality as well as negative impacts on demersal fish and benthic invertebrates (Diaz and Solow, 1999; Kemp et al., 2005). Eutrophication can also have negative economic impacts on commercial and sport fisheries (Glasgow and Burkholder, 2000), tourism, and real estate (Hoagland et al., 2002). One consequence that has received little to no attention is the impact on methane (CH_4) concentrations in estuaries. In this study, it is proposed that with increasing eutrophication, CH_4 flux from estuarine systems may be enhanced. This enhanced CH_4 production could result in CH_4 flux to the water column. Once in the water column, this CH_4 could be aerobically oxidized to carbon dioxide (CO_2), further reducing oxygen as well as lowering the pH (Templeton et al., 2006; Zhu et al., 2010). If CH_4 is not fully oxidized, it could be fluxed to the atmosphere where it will contribute to the greenhouse effect. This chapter focused on understanding the fluxes of CH_4 in Chesapeake Bay sediments and bottom waters.

In the atmosphere, CH_4 generates 20 times more radiative forcing than CO_2 over 100 years (Forster et al., 2007); making it a powerful greenhouse gas. Atmospheric monitoring in the last three decades showed that CH_4 increased from 1.6 ppm to over 1.8 ppm in recent years (Nisbet et al., 2014). Because CH_4 is produced in anoxic sediments of aquatic systems (Reeburgh, 2007), effort has been devoted to determining the role aquatic systems have in CH_4 contributions that may have led to the recent increases in atmospheric CH_4 (De Angelis and Scranton, 1993; Sansone et al., 1998; Middelburg et al., 2002; Reeburgh, 2007; Zhang et al., 2014). CH_4 is produced in both freshwater and marine sediments under anoxic conditions (Reeburgh, 2007). CH_4 release from freshwater lakes was estimated to be 103 Tg $\text{CH}_4 \text{ yr}^{-1}$ (Bastviken et al., 2011). In marine systems, due to the presence of sulfate (SO_4), there is a natural biofilter for the CH_4 , where a consortium of sulfate-reducing bacteria and methanotrophs anaerobically oxidize CH_4 through sulfate-reduction (Valentine and Reeburgh, 2000; Reeburgh, 2007). As a result of this biofilter, it has been estimated that over 90% of CH_4 produced in marine sediments is oxidized anaerobically (Reeburgh, 2007). Even if CH_4 would persist past this biofilter, it would be exposed to aerobic methane oxidation in the oxygenated water columns (Reeburgh, 2007). In fact, in the deep sea, even though natural CH_4 seeps release

pure CH₄ into the water column (Westbrook et al., 2009), the CH₄ is efficiently oxidized by the microbial methane oxidation biofilter. This prevents CH₄ from being emitted to the atmosphere (McGinnis et al., 2006). Similar observations were made after the Deepwater Horizon well blowout accident, where CH₄, that was released, was oxidized aerobically in the water column preventing it from being emitted to the atmosphere (Kessler, 2011; Yvon-Lewis et al., 2011). Due to these efficient biofilter mechanisms, an estimate of CH₄ release from oceans 10 Tg CH₄ yr⁻¹ (Reeburgh, 2007), about 10 times less than emissions estimated from freshwater lakes (Bastviken et al., 2011).

Estuaries represent the connection between marine and freshwater environments, with freshwater regions possibly contributing more CH₄ to the atmosphere than more saline regions of estuaries. Estuarine contributions of CH₄ to the atmosphere were the subject of a large study in northern Europe (Middelburg et al., 2002). Surface and water column CH₄ concentrations and salinity measurements were performed in 9 European tidal estuaries, with a range of oxygen saturations and physical conditions. This study was conducted over the course of two years. Though continuous sampling was performed, the sampling events lasted days, rather than over the course of months. The aggregated data was used to calculate a global estuarine CH₄ flux of 1.1 to 3.0 Tg yr⁻¹ CH₄ (Middelburg et al., 2002). This only accounts for 0.2-0.6% of the 500 Tg yr⁻¹ CH₄ estimated to be emitted globally to the atmosphere (Reeburgh, 2007). This estimate seems surprisingly low since some estuaries (i.e. Chesapeake Bay) are known to contain CH₄ gas (i.e. bubbles) in the sediments (Hill, 1992; Hagen and Vogt, 1999; Garcia-Gil et al., 2002; Rogers et al., 2006). In addition, the microbial biofilter may be limited in estuaries, compared to oceans in two ways: 1) in the sediment, there is less SO₄ for anaerobic oxidation of methane (AOM), and 2) in the water column, estuaries are shallower and thus have an abbreviated aerobic oxidation biofilter. Furthermore, estuaries that experience eutrophication and seasonal hypoxia could have increased CH₄ production due to increased fresh organic matter input arising from eutrophication as well as less efficient abbreviated aerobic biofilters with limited oxygen in the water column. Hence, it is postulated here that estuaries are a larger potential source of atmospheric

CH₄ than current estimates imply due to higher overall and episodic fluxes of CH₄ to the atmosphere. As more and more estuaries become eutrophic and hypoxic (Diaz, 2001), this process of enhanced CH₄ flux might become more prevalent.

To investigate the importance of CH₄ flux from the sediments of a eutrophied estuary, the Hypoxia Enhanced Methane Flux or HEMF (Fig 3.1) hypothesis was tested. HEMF is a seasonally driven process that may occur in estuaries during seasonal hypoxia. In winter (Fig 3.1a), an estuary with a well-mixed and oxygenated water column receives relatively small amounts of labile autochthonous organic matter, due to colder temperatures and low light conditions. In the sediments, the organic matter is broken down from particulate organic matter to dissolved organic matter (DOM) (Burdige and Gardner, 1998). The labile portion of this DOM is then decomposed by microbial processes

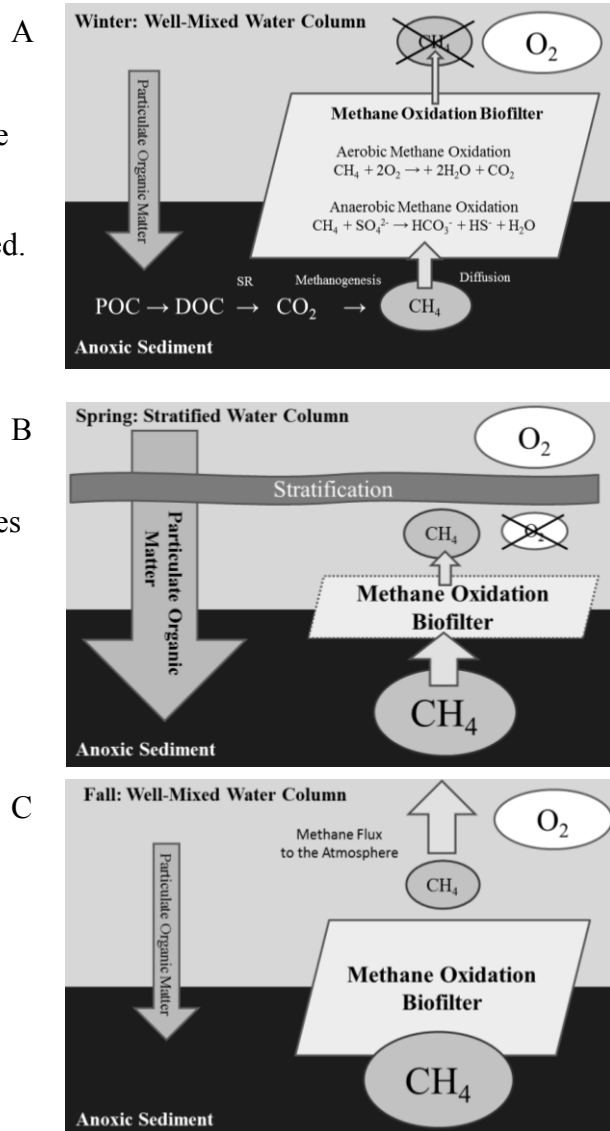


Figure 3.1. Conceptual Model of Hypoxia Enhanced Methane Flux (HEMF) A: In winter an estuary with an oxygenated water column (grey) produces CH₄ in anoxic sediments (black) via a small POC flux. CO₂ is used to produce CH₄, represented by the oval. CH₄ can be oxidized by the methane oxidation biofilter in the sediment and in the water column, represented by the parallelogram, limiting the amount of CH₄ being emitted to the atmosphere. B: HEMF develops in the spring causing increased organic matter load, represented by a large arrow, creating hypoxic conditions. Through the summer the Bay also becomes stratified. Concentrations of CH₄ in the sediment increase and escape the sediment further depleting oxygen and CH₄ accumulates below the pycnocline C: The completion of HEMF is shown with the breakup of hypoxia and stratification in the fall, the accumulated CH₄ could be mixed into the water column and possibly fluxed to the atmosphere.

that make up the biogeochemical cascade of reactions. In this cascade, the dissolved organic carbon (DOC) is remineralized to CO_2 that can be used by microorganisms to produce CH_4 in sediments as the final biogeochemical reaction (Burdige, 2006). CH_4 , that is produced in sediments via microbial methanogenesis, can diffuse upward into the sulfate-reduction zone where microorganisms consume CH_4 and SO_4 through anaerobic oxidation of methane (AOM) (Valentine and Reeburgh, 2000). When CH_4 diffuses to the water column, it is quantitatively consumed aerobically to produce CO_2 (Reeburgh, 2007). These oxidation processes would essentially limit the amount of CH_4 emitted to the atmosphere as observed in study areas such as European estuaries (Middelburg et al., 2002). However, in eutrophic systems receiving higher carbon loads (Fig 3.1b) the sediments become fully anaerobic and carbon is no longer limiting. Increased CH_4 production allows some CH_4 to diffuse through the AOM biofilter from the sediment to the water column. In the water column, the CH_4 can be oxidized aerobically, consuming oxygen. The removal of oxygen, in part by aerobic methane oxidation, may contribute to hypoxic and eventually anoxic conditions in the water column. In the Chesapeake Bay, freshwater flow generates stratification, where the less dense layer of fresh water moves above the more saline marine water (Boicourt 1992). Once the water column is stratified, bottom water equilibration with the atmosphere is limited. Nutrients from the winter and spring freshwater flow can also fuel phytoplankton blooms, which can increase oxygen demand in the bottom water below the pycnocline and lead to hypoxia. Once oxygen is consumed in the bottom water, CH_4 could then accumulate below the pycnocline throughout summer hypoxia and stratification. In the fall (Fig 3.1c), as the water column returns to a destratified and well-mixed state, the final step in the HEMF hypothesis occurs when the accumulated CH_4 could be mixed throughout the water column, where the CH_4 could be oxidized, or possibly fluxed to the atmosphere in pulses of CH_4 . These seasonal pulses of CH_4 would be difficult to capture using discrete sampling events used in previous studies (Reeburgh, 1969; Middelburg et al., 2002).

3.2.1 Testing HEMF in the Chesapeake Bay

The Chesapeake Bay is the largest estuary in the United States, spanning 11,100 km² with a length of over 300 km and an average width of 20 km. The Bay is a largely shallow embayment averaging 8 m water depth, with a deeper axial channel that reaches a maximum depth of 54 m. The channel was formed during the low sea level stand that occurred 18 ka ago when the Susquehanna River bore into the flood

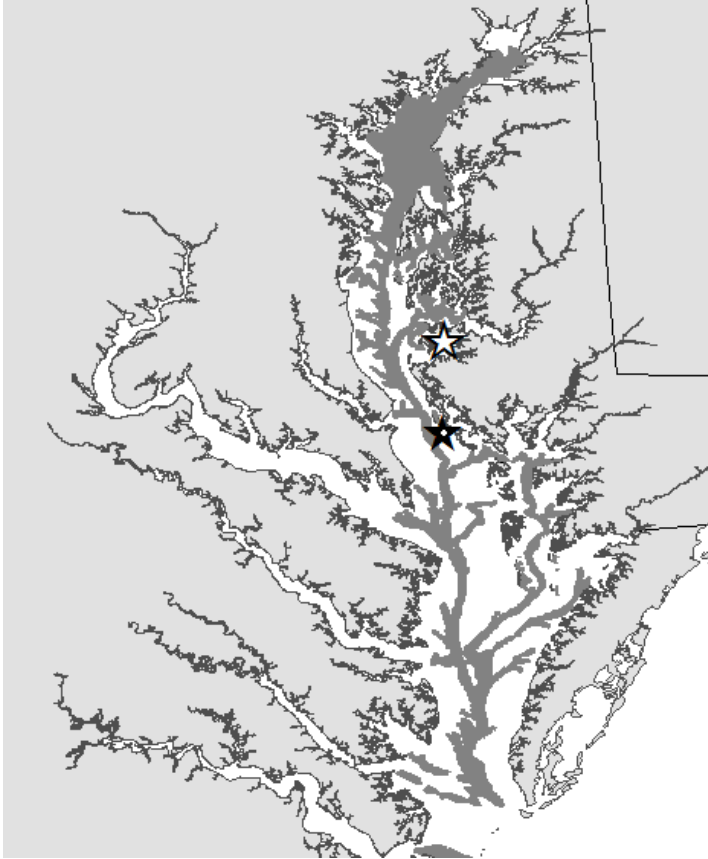


Figure 3.2. Map of Chesapeake Bay with CH₄ gas shown in grey (Hill, 1992). The benthic lander discussed in this project was deployed at a Mid-Bay sampling site indicated with a black star (38.28196N, -76.23317', water depth 30 m). The white dot, within the black star, indicates the third lander site, located 0.5 km from the site of the first and second lander that was used for temperature data in place of the data lost on the second lander. The white star indicates the location of a sediment core collected in Reeburgh (1969).

plain, forming a steep-sided channel (Colman et al., 1990). Sea level rose, filling the floodplain surrounding the channel, and forming the modern open estuary (Colman et al., 1990). In the upper bay, CH₄ concentrations exceeded solubility in shallow sediments, such that CH₄ gas bubbles formed in the sediment, and were located using acoustics across the bay above 39°N (Fig 3.2) (Hill, 1992). This CH₄ was likely produced by microbes through methanogenesis in the low salinity water, and in the absence of SO₄-driven oxidation (Hill, 1992). Below 39°N, CH₄ gas bubbles were found to be

restricted to the deep paleochannels of the Bay where low salinity sediment, rich in organic carbon, was deposited as sea level rose (Hill, 1992). Though there is most likely dissolved CH₄ in the sediment below the sulfate reduction zone across the lower bay, high concentrations of CH₄ required for bubble formation seem to be restricted to the paleochannels. Seismic techniques have shown seasonal changes in the depth of observed CH₄ gas bubbles in the Chesapeake Bay, shifting closer to the sediment surface in the summer (Hagen and Vogt, 1999). The Chesapeake Bay has experienced severe recurring deep-water hypoxia since the 1950's (Kemp et al., 2005), typically starting between April and May and ending in the fall (Testa and Kemp, 2014). Because the Chesapeake Bay contains CH₄ in shallow sediments and experiences seasonal hypoxia, the Chesapeake Bay represents an ideal study area to test the HEMF hypothesis.

The objective of this study was to test the first part of the HEMF hypothesis (Fig 3.1b) in the Chesapeake Bay by determining if CH₄ is released into the bottom water from the sediment pore-water when bottom water becomes hypoxic and quantifying the CH₄ flux by measuring bottom water and pore-water continuously over time; ideally capturing the entire hypoxic event. A novel application of OsmoSamplers (Jannasch et al., 2004) was tested during this study. OsmoSamplers are osmotically powered pumps that continuously collect sample water in small-bore tubing. One goal of this study was to validate the use of OsmoSamplers in a shallow estuary to measure CH₄ concentrations. Two OsmoSamplers were used to collect bottom water and pore-water continuously from April to October 2013 and to create a time series of CH₄ and O₂ concentrations. It was also anticipated that the data could increase understanding of the microbial processes that may be impacting methane fluxes. Therefore, SO₄ and CO₂ concentrations were also measured, because they are key components in evaluating microbial oxidation and formation of CH₄. Stable isotope analysis of CH₄ carbon was used to examine the bulk oxidative and production processes, because rates could not be measured. DOC concentrations were also quantified and yielded the foundation for a method development to perform more detailed molecular characterization of DOM in future work.

3.3 Methods

3.3.1 OsmoSampler Deployment on Landers

To obtain a time-series of CH₄ concentrations, OsmoSamplers (Jannasch et al., 2004) (Fig 3.3a) were mounted on a lander frame described in section 3.3.2 (Fig

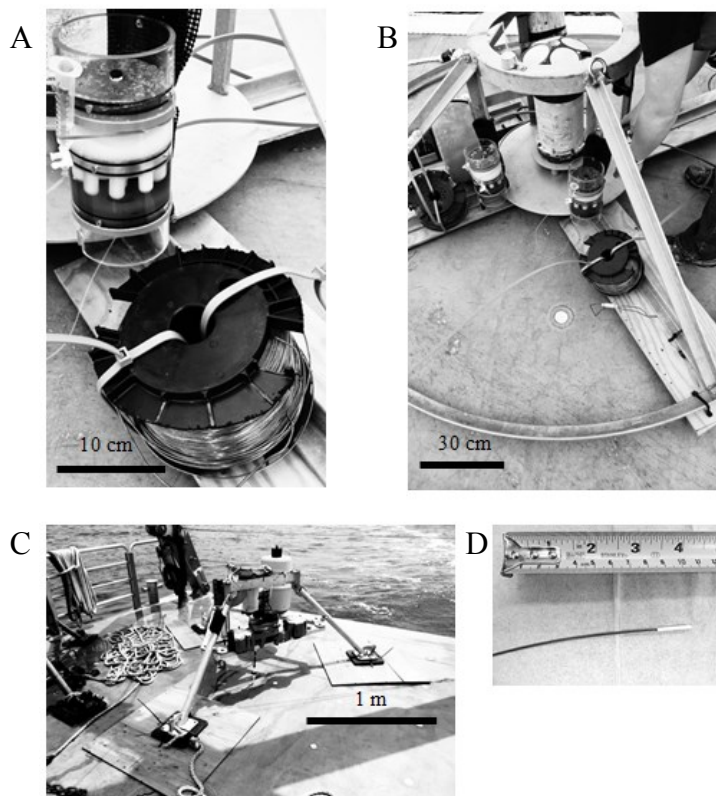


Figure 3.3. A: Osmo-pump and copper sample coil that make up the OsmoSampler. B: First Deployment Lander. C: Second Deployment Lander. D: Rhizone filter.

an osmotic pump. A sample coil, filled initially with DI water, was then connected to the DI reservoir of the pump (Fig 3.4b). During the deployment, estuarine bottom water or pore-water was slowly pumped through the sample intake of the coil, which replaced the DI water as it moved from the coil towards the DI reservoir.

The two OsmoSamplers used for this experiment, referred to as Pump A and Pump B, contained 8 osmotic membranes in each pump. Each were connected to a sample coil of 300 m of copper tubing (outer diameter of 1.6 mm and inner diameter

3.3a-c). OsmoSamplers are comprised of an osmotic pump attached to a sample coil of small bore copper tubing (Fig 3.4a-b). The osmotic pump is a cylindrical acrylic tube containing a low and a high salinity chamber separated by semi-permeable membranes (Azlet 2ML1) (Fig 3.4a). The flow generated by the difference in osmotic pressure across the membranes from the DI reservoir to the high salinity reservoir created

of 0.8 mm). Low dead volume fittings were used to connect the coils to the pumps in order to minimize mixing when the sample was collected. The other end of the copper coil, the intake, was fitted with a rhizone filter (0.2 μm) to minimize microbial activity within the tubing after sample collection. Microbial activity was also minimized because the sample was in direct contact with the copper material, which should act as an anti-microbial (Grass et al., 2011).

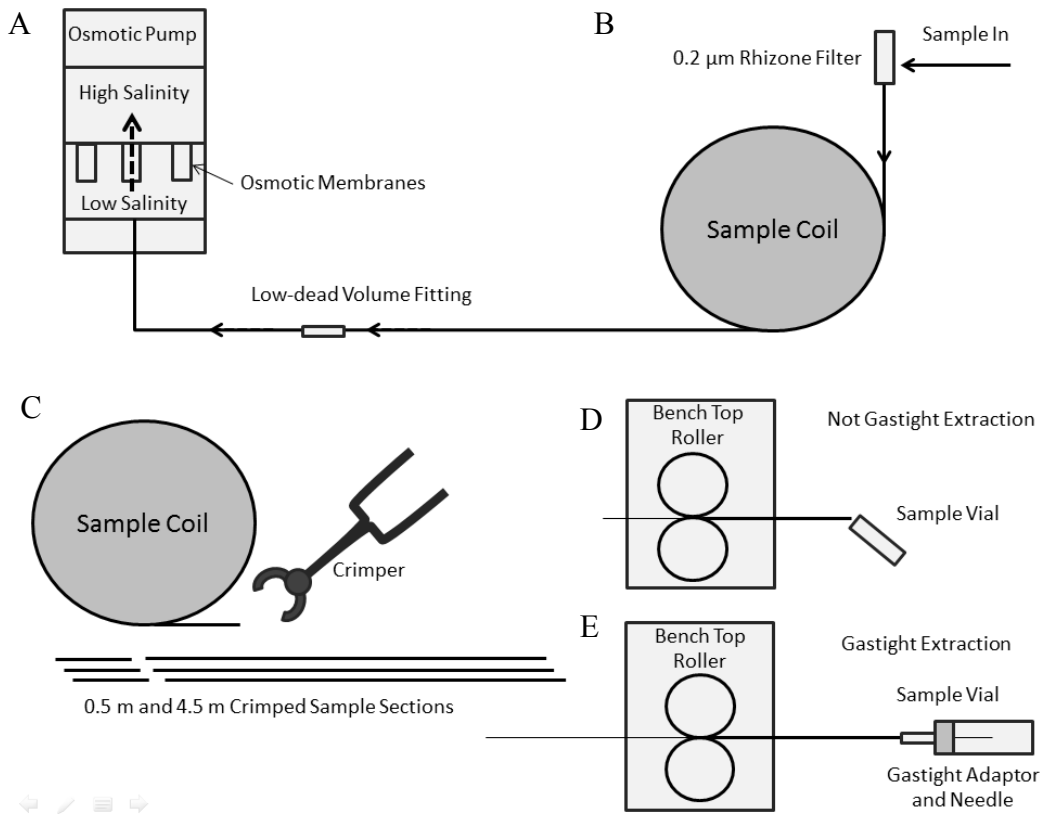


Figure 3.4. A: Osmotic Pump. B: Sample Coil. C: Coil sectioning. D: Extraction of 0.5 m samples not using gastight extraction. E: Gastight extraction of 4.5 m samples.

3.3.2 Landers

The OsmoSamplers were mounted on benthic landers (Fig 3.3b-c). The lander was composed of a metal frame that remained on the seafloor over the deployment period. Two landers were used in series; with one replacing the other upon retrieval. The first lander (referred to as “lander 1”) shown in figure 3.3b was

0.5 m high and 2 m wide with a circular base. The second lander (lander 2) shown in figure 3.3c was 1 m high and 2 m wide at the bottom with a triangular base. Both were made out of aluminum, designed at Horn Point Laboratory, and were equipped with an acoustic release, as well as conductivity, temperature, depth (CTD) and dissolved oxygen (DO) sensors. Sheets of plywood were attached using cable ties to the bottom of the landers to minimize sinking. The plywood was intended to detach upon retrieval and remain in the sediment. Two OsmoSamplers were attached to each lander using cable ties and duct tape, and the rhizone filter of each pump was then positioned on the landers to collect samples. One OsmoSampler collected sediment pore-water and one OsmoSampler collected bottom water. For the bottom water, the rhizone filter was fixed to the top of the lander so that it would remain above the seafloor and entirely in the water column. This sample set was referred to as the “bottom water sample”. For the pore-water sample, the rhizone filter was fixed near the bottom of the lander to make sure that it submerged well into the sediment and was referred to as the “pore-water sample”. Upon retrieval, the depth of the pore-water rhizone filter was then estimated based on the depth of discoloration of the lander as well as fouling organism deposition. For the first lander, we estimated the bottom water sample was within 5 cm of the sediment surface and the pore-water sample was 10-15 cm below the sediment surface. For the second lander, we estimate the bottom water sample was 10-20 cm above the sediment surface and pore-water sample was 20-30 cm below the sediment surface.

3.3.3 Lander Deployment

For the two deployments, landers were positioned at a mid-Bay site (38.28196 N, -76.23317', water depth 30 m) (Fig 3.2) within the main channel where CH₄ gas is known to exist within the upper 5 cm of sediment (Hagen and Vogt, 1999). Water samples and data were collected during two separate lander deployments, due to the requirements of other research. Lander 1 (Fig 3.3b) was deployed for 98 days from 17 April to 24 July 2013. Lander 2 (Fig 3.3c) was deployed for 97 days from 25 July to 30 October 2013. Both landers were deployed from aboard the R/V Rachel Carson, which also retrieved lander 1. Lander 2 was retrieved from aboard the R/V

Sharp. The OsmoSamplers were securely attached to the landers aboard the vessel, shortly before deployment. Once the OsmoSamplers were in place, the landers were deployed by attaching the lander frame to the A-frame of the ship, and slowly lowered in place. The vessels position and water depth were recorded at that time.

3.3.4 Lander Recovery

Landers were recovered by sending an acoustic signal to the lander which released a float. This float was then retrieved by the vessel to recover the lander. For lander 2, the acoustic release failed and the lander was located and retrieved by dredging.

Ideally, once the landers were on deck, each end of the two sample coils would be crimped immediately, in order to maintain *in situ* pressures within the coil. However, due to unforeseen circumstances, lander 1 remained on the deck until the coils could be crimped 5 hours later. Therefore, it is possible that pressure was lost during this time, and CH₄ may have degassed from the sample coils. For lander 2, the copper coils were crimped within 5 minutes of recovery. Visual inspection of the recovered landers showed that the pore-water sample coil on lander 1 became unsecured, probably upon retrieval, when the plywood disconnected from the lander supporting the coil. However, it was still attached by the copper tubing and was successfully recovered. Once the coils were removed from both landers, they were stored at 4°C prior to further processing in the lab (See Section 3.3.6). The osmotic pumps were also removed from the landers and then monitored in the lab to be evaluated by the time stamping method described in the next section.

3.3.5 OsmoSampler Time Stamp

To be able to time stamp the sample in the copper coil, the pumping rates and the tubing cross sectional area must be known. From these parameters, a time per length of tubing can be calculated to give the time stamp. The tubing cross sectional area is known (0.50 mm²). Pumping rates, however, are dependent upon *in situ* temperature. Typically, pumping rates are determined based on lab calibrations at these *in situ* temperatures. However, the bottom water temperatures of the

deployments varied by 18°C. Therefore, the pumping rates were temperature-corrected using the temperatures recorded by the CTD. For lander 1, there was no problem obtaining temperature data from the CTD. However, for lander 2, the temperature sensor malfunctioned and data could not be used. Therefore, temperature data was first extracted from a different lander 0.54 km away (Fig 3.2) and corrected for ~0.75°C difference between landers (Malcolm Scully, personal communication) before applying temperature corrections.

To determine the *in situ* pumping rate, the theoretical relationship between pumping rate and temperature, obtained from Jannasch *et al* 2004, was used according to pump-specific equations:

$$\text{Pump A: } y = 0.063x - 0.760 \quad \text{Equation 1a}$$

$$\text{Pump B: } y = 0.063x - 0.606 \quad \text{Equation 1b}$$

where y is the pumping rate (mL day^{-1}), x is the temperature ($^{\circ}\text{C}$), the slope is based on similar pump conditions to this study (number of membranes, temperature, and salinity gradient) derived from Jannasch *et al* 2004, and b is the pump-specific correction factor determined using laboratory monitoring of the pumping rates. Under controlled laboratory temperatures, at 22°C Pump A had a rate of 0.63 mL day^{-1} and Pump B had a rate of 0.72 mL day^{-1} . Once the pump-specific correction factors were determined, temperature data was used in Equations 1a and 1b to calculate temperature-corrected pumping rates (y) for each day of deployments. The temperature-corrected pumping rates ranged from 0.40 mL day^{-1} to 0.92 mL day^{-1} .

Pumping rates were then used to calculate the length of copper tubing filled with sample for each day using the following equation:

$$\text{Pumping Rate} \times \text{Length to Volume Ratio} = \text{Length per Day} \quad \text{Equation 2}$$

where pumping rate (ml day^{-1}) is multiplied by the length of tubing to sample volume ratio ($1 \text{ m} : 0.45 \text{ mL}^{-1}$) to yield length per day (m day^{-1}) of copper tubing. Sample coils were oriented such that sample section number 1 contained sample water closest

to the time of retrieval and the last sample section represented sample waters collected closest to deployment. The length per day was determined for sample section number one of each coil (coil retrieval) and subsequent lengths per day were added successively for each day of the deployment up to and including the last sample section (coil deployment) for the entire length of the sample coil. Because sample sections of tubing (See Section 3.3.6) correspond to 3-4 days of sample, the median date was assigned to each sample section.

The CTD temperature data from the beginning of the second deployment from 25 July 2013 to 21 August 2013 was missing, due to sensor malfunctioning. An average pumping rate was used for that time by dividing the sample coil length remaining (after temperature corrections for sections with temperature data) by the time remaining (without temperature data). The sample length was converted to volume using equation 2, and then the sample volume was divided by the number of days that had no temperature data. This procedure allowed assigning to each sample section date, temperature, and pumping rate, and hence the sample coils were time-stamped (Discussed further in Appendix J).

3.3.6 Sub-sampling Procedure of Coils and Analytical Methods

Once back in the lab, the copper coils were unspooled from the most recent end and crimped into alternating lengths of 50 cm and 4.5 m using a wire crimping tool (Fig 3.4c). Together, these 5 m segments resulted in one time point that was ~3-4 days in duration, at the corrected pumping rate of the OsmoSamplers (as described in Section 3.3.5). Because the pumping rates were not the same for each of the pumps, the sample coils will consequently contain different numbers of sample sections, or time points. For lander 1, 19 time points were obtained for the bottom water, and 24 for the pore-water sample (Table J.1). For lander 2, 30 time points were obtained for the bottom water sample, and 25 for the pore-water sample (Table J.2). Every other section of each sample set was used for the following analysis and the remaining samples were stored for future investigation. The 50 cm sections were tested for salinity using a handheld Extech RF20 refractometer (Fig 3.4d). Cutting was terminated when 0 ‰ salinity was observed for three samples in a row,

indicating the end of the sample liquid collected and the transition to DI water that was used to fill the coils before deployment. During sample collection in the coil and storage prior to sectioning, the sample solutes (for example CH₄) can migrate in the tubing due to diffusion and mixing, and as a result the concentrations may become more similar at narrow time intervals. Therefore, mixing and diffusion errors during sample collection and storage were calculated, similar to the approach used by Jannasch *et al* 2004 (See Appendix J). From this exercise, greater than 99% of the SO₄ and CH₄ sample was contained within the sample sections.

Sulfate/Chloride Ion Concentrations. SO₄ and chloride concentrations were measured by using the 50 cm sub-sections of each time-point. Because the 50 cm samples were not used for gas analysis, the extraction from the tubing was not gastight (Fig 3.4d). The liquid within the 50 cm sections was squeezed, using a bench top roller which essentially flattened the copper tubing and forced the liquid out (Fig 3.4d). The water samples were then collected into 1.5 mL Eppendorf tubes. A sub-sample of 100 μL was quickly removed by pipetting and combined with 10 μL of 0.1 M phosphoric acid. The acid was added to convert all possible sulfide species to sulfide gas in order to prevent contamination of SO₄ through sulfide re-oxidation. Samples were mixed well and stored at 4°C for later ion concentration analysis (described below).

The SO₄ and chloride concentrations of the sub-samples described above were analyzed using ion chromatography [IC with IonPac AG22 (4 x 50 mm) guard column, IonPac AS22 (4 x 250 mm) analytical column, and ASRS 300 (4 mm) suppressor]. An AS40 Autosampler connected to a Dionex ICS 1000 ion chromatograph was used. Sodium bicarbonate buffer was used as eluent at a flow rate of 1.2 mL min⁻¹ with a suppressor current of 50 mA. The IAPSO seawater standard produced by OSIL was used to create a ten point calibration curve from 55 to 550 mM chloride and 0.29 to 29 mM SO₄. The IC linear range for chloride was 5-500 mM and 0.29-29 mM for SO₄ ($r^2 \geq 0.998$). Samples and standards were diluted 1:135 using DI water.

Gastight Sample Extraction. CH₄ concentrations were measured on the remaining 4.5 m long copper coil sections using gastight extraction. To retrieve the

water sample, the copper coil section was squeezed using the bench top hand roller but this time, a gastight adaptor attached to a needle was connected to the end of the copper section (Fig 3.4e). The roller squeezed the sample liquid out and forced it into a 12.5 mL sample vial at the opposite end. Before squeezing, the glass vials were baked at 550°C overnight to remove residual carbon (to be able to measure dissolved organic carbon later), capped with butyl rubber septa to prevent gas exchange, and flushed with helium. Each 4.5 m copper section contained approximately 2 mL of sample liquid that was transferred to the vials, resulting in an initial overpressure of approximately 2 mL. Sample volumes were determined by subtracting empty vial weight from vials filled with sample.

Methane and Carbon Dioxide Concentrations. Once the liquid sample was transferred into the vial, the dissolved CH₄ and CO₂ equilibrated with the helium headspace after shaking the vial for two minutes and resting for at least 30 seconds. A 2 mL headspace sample was then removed and diluted with 4 mL of helium which was injected into a SRI Gas Chromatograph 8610C equipped with HayeSep D and Mol Sieve columns and a Thermal Conductivity Detector (TCD) to measure CO₂ and a Flame Ionization Detector (FID) to measure CH₄. It should be noted that the samples were not acidified, so the CO₂ concentration measured is the CO₂ (g) phase equilibrated concentration with the water.

Stable Isotope Analysis. Stable isotope ratios of CH₄ were measured on the aforementioned sample vials by adding a pressurized helium headspace. Different volumes of this over pressure were then added to helium-flushed 4.5 mL glass Exetainers® to bring the concentration to ~3,000 ppm CH₄ (the concentration at which the method is optimized for isotope analysis). Since the optimization concentration is high, only pore-water samples with sufficient concentrations of CH₄ were analyzed. The Exetainers® were mounted into the Finnigan Gas Bench II Autosampler and stable isotope ratios were measured on the CH₄ and CO₂ using a Thermo Scientific Trace Gas Pre-Concentrator coupled to a Delta V Isotope Ratio Mass Spectrometer (IRMS). Vienna Pee Dee Belemnite standard was used as well as 9,975 ppm CH₄ standard from a tank calibrated by the Florida State University Isotope-Ratio Mass Spectrometry Laboratory.

Dissolved Organic Carbon. After the gases were analyzed, the remaining water was analyzed for dissolved organic carbon (DOC) concentrations. DOC analysis was carried out at the Nutrient Analytical Services Laboratory located on the Chesapeake Biological Laboratory campus. The DOC method required 10 mL sample volume, and it was necessary to pool 5 of the 2 mL samples (Table J.1). Method blanks were run using Milli-Q water added to sample vials, and shaken for 2 minutes. The blanks were intended to test for possible DOC leaching from the sample vial septa. The DOC concentrations of the blanks were subtracted from the sample values. The 4 pooled samples and blanks were acidified using 9 N sulfuric acid to degas inorganic carbon. A high temperature combustion (680°C) method using a Shimadzu TOC analyzer was used to measure non-purge-able organic carbon. Samples were first purged of CO₂ using zero grade air (no CO₂) for 2.5 minutes. A catalyst bed of platinum coated aluminum balls was used to produce CO₂ that was measured on a non-dispersive infrared detector. The detection limit of the method used was 19.98 μM DOC. The detection limit of DOC was 4.16 μM.

3.4 Results

3.4.1 Verification of OsmoSamplers

OsmoSamplers were used for the first time to determine temporal variability of CH₄ concentrations and isotope ratios of carbon, CO₂ concentrations, SO₄ concentrations, and DOC from both bottom water and pore-water of the Chesapeake Bay estuary. Temporal aspects of the data were essential and hence, accurate time-stamps were critical. To verify the calculated and corrected time stamps (see section 3.3.5), the time stamped bottom water salinity data was compared to real-time salinity data collected using CTD sensors. Real-time salinity data was collected on the first lander for the first deployment and an appropriate nearby lander for the second deployment. Salinity from the sensors ranged from 13 ‰ and 23 ‰ over the time series (Fig 3.5). The salinity obtained from the OsmoSamplers, with a much less precise measurement (refractometer), showed a very similar pattern of salinity, but was generally 1 ‰ higher than sensor measurements ranging from 17 and 26 ‰

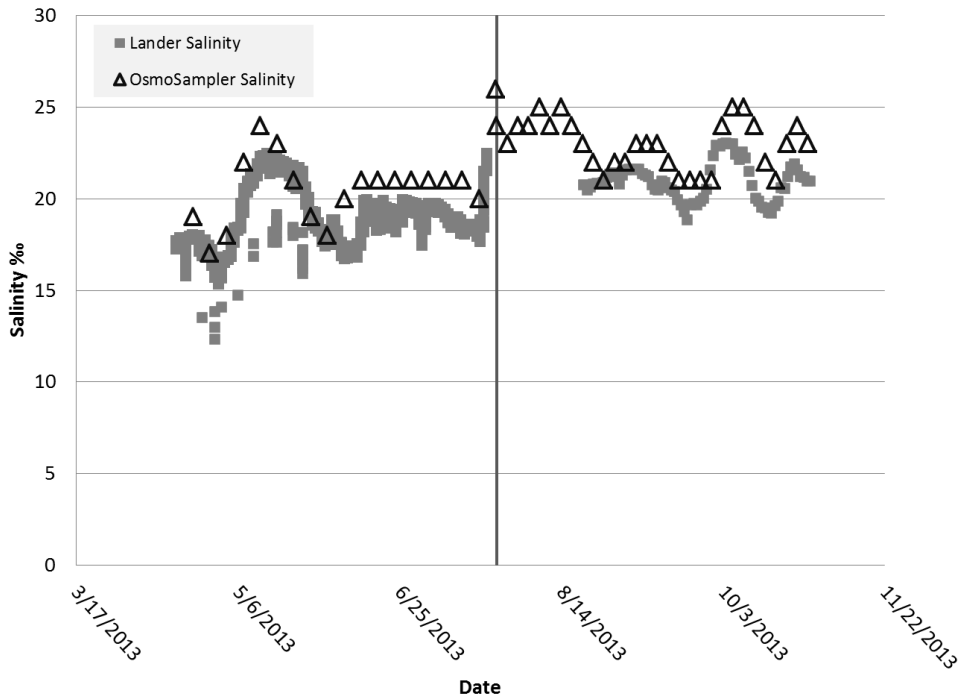


Figure 3.5. Salinity from CTD measurements as well as osmo-coil salinity measurements collected over the course of two three-month deployments, indicated by the dark line.

(Fig 3.5). This tight correlation between real-time sensor data and OsmoSampler salinity data verified the calculated time stamps.

3.4.2 Bottom Water Chemistry

Oxygen. Overall concentrations of dissolved oxygen in the bottom water showed a general trend of hypoxia from May to October 2013 (Fig 3.6). More specifically, at the beginning of the time series DO concentrations were around 109.4 $\mu\text{M O}_2$, and then decreased to 0.9 $\mu\text{M O}_2$ around 30 April 2013, increased to 156.3 $\mu\text{M O}_2$ around 8 May 2013. From 8 May 2013 concentrations gradually decreased to 0.6 $\mu\text{M O}_2$ on 6 June 2013 and remained mostly anoxic (defined as less than 63 $\mu\text{M O}_2$). Around 13 June 2013, concentrations quickly increased to 23.4 $\mu\text{M O}_2$ and returned to anoxic conditions from 23 June 2013 until the end of the first deployment. DO data is missing from the beginning of the second deployment from 25 July 2013 to 21 August 2013 due to the sensor malfunctioning. The nearby lander bottom water DO concentration was 1.6 $\mu\text{M O}_2$ on 21 August 2013, increased to 40.0 $\mu\text{M O}_2$ on 29

August 2013, and decreased quickly to 1.6 μM O_2 on 9 September 2013. DO concentrations then increased again on 17 September 2013 from 1.6 μM O_2 to 180.3 μM O_2 on 21 October 2013, and indicated the return to oxic waters.

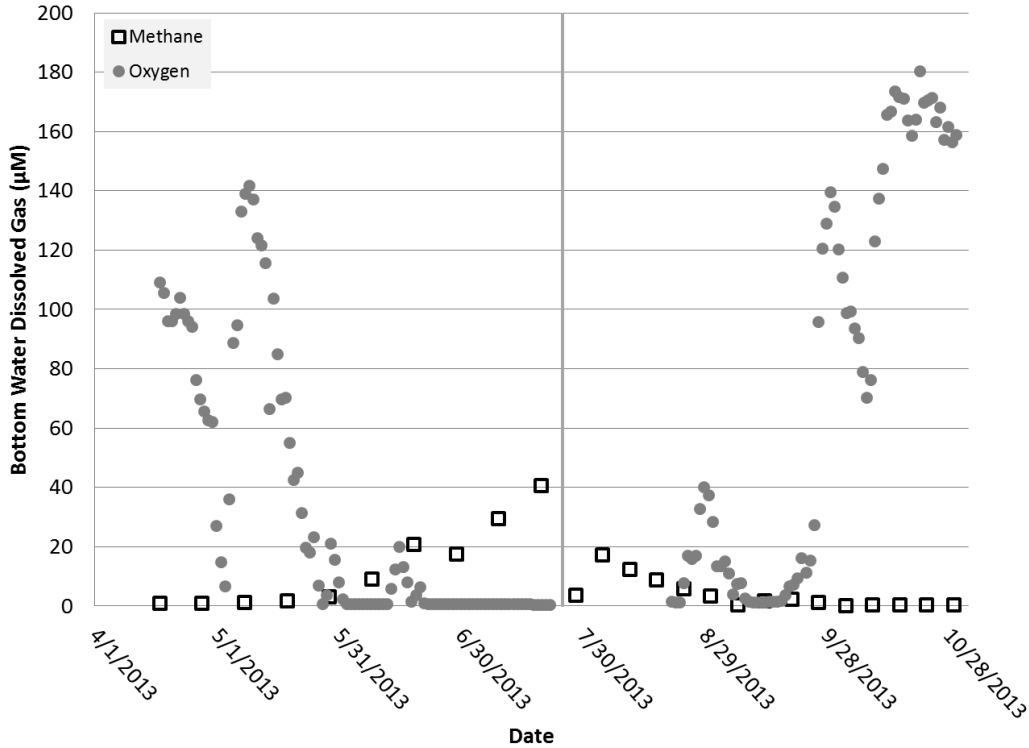


Figure 3.6. Bottom water O_2 and CH_4 concentrations collected over the course of two three-month deployments, separated by the dark line.

Methane Concentrations. The general trend was that CH_4 concentrations increased when bottom water became hypoxic and CH_4 decreased when the DO concentrations in the water increased (Fig 3.6). More specifically, on the first lander, bottom water CH_4 concentrations were around 0.1 μM at the start of the record in April, and increased gradually to 40.7 μM by 19 July 2013. There was a slight decrease of 3.0 μM on 28 June 2013, 72 days into the deployment, after which CH_4 concentrations continued to increase. For the second lander, CH_4 concentrations were initially 3.7 μM in July, which then increased to 17.3 μM by August and decreased to 0.4 μM around 9 September 2013. Low CH_4 concentrations continued after this point, remaining below 3 μM , for the rest of the time series until it was terminated in October.

3.4.3 Pore-water

Methane Concentrations. As expected, pore-water CH₄ concentrations were higher when compared to bottom water and units were presented in mM, as opposed to μM (Fig 3.7). For the first lander, pore-water CH₄ concentrations were at 0.03 mM in mid-April, peaked at 5.48 mM on 11 June 2013, and decreased slightly to 3.67 mM at the end of the first deployment on 24 July 2013. On the second lander, there was a slight increase from 0.07 mM to 0.56 mM on 5 August 2013, after which concentrations remained around 0.03 mM CH₄. Concentrations then began to rise on 9 September 2013 and reached a level of 4.7 mM on 13 October 2013 and then decreased again to 4.0 mM CH₄ at retrieval on 30 October 2013.

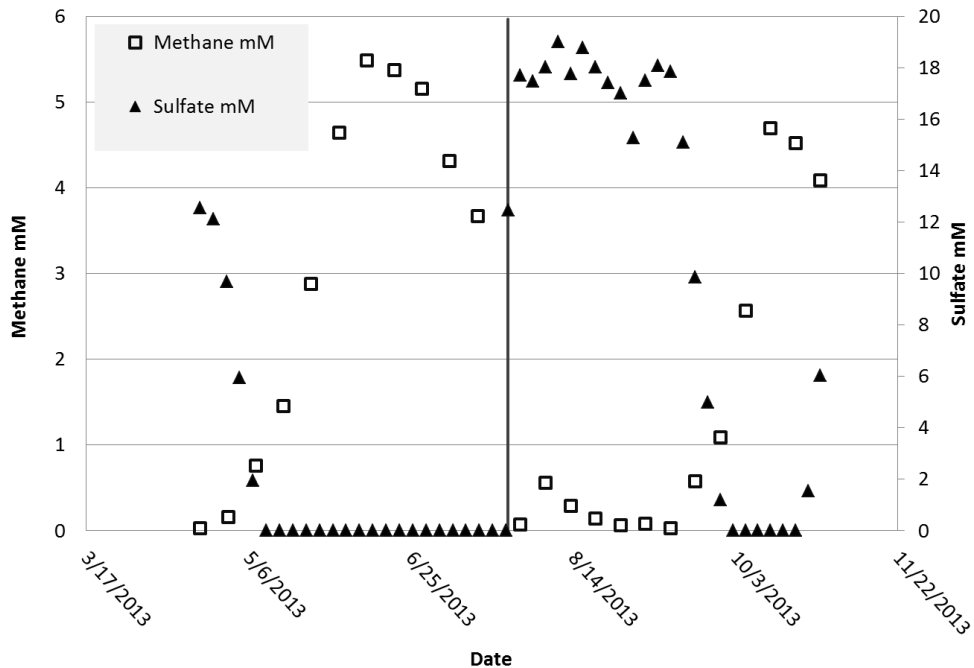


Figure 3.7. Pore-water measurements of CH₄ and SO₄ concentrations collected over the course of two three-month deployments, indicated by the dark line, are shown. The pore-water was collected from sediment depth 0 to 30 cm.

Sulfate/Chloride. Overall, concentrations of SO₄ decreased at the beginning of each deployment to levels below detection limit (0.29 mM) and remained at that level throughout most of the deployments. More specifically, pore-water SO₄ levels started at 12.54 mM on the first lander in mid-April, decreased to

below detection limit on 11 May 2013, and remained below detection limit until the end of the first lander deployment (Fig 3.7). On the second lander, SO_4 fluctuated between 15 mM and 19 mM until 1 October 2013 when SO_4 again decreased below detection limit until 22 October 2013. At the end of the deployment the SO_4 concentrations increased slightly to 6 mM.

Carbon Dioxide. During each deployment, CO_2 concentrations were low during the first part of each deployment and high during the second part of the deployment. More specifically, CO_2 concentrations in the pore-water gradually increased from 2.5 mM to 8.3 mM on 28 June 2013 then decreased to 1.1 mM by the end of the first deployment (Fig 3.8). During the second deployment, CO_2 concentrations in the pore-water remained below detection limit until 20 September 2014, then increased to 9.4 mM on 13 October 2013. The CO_2 levels then decreased to 6.2 mM at the end of the time-series.

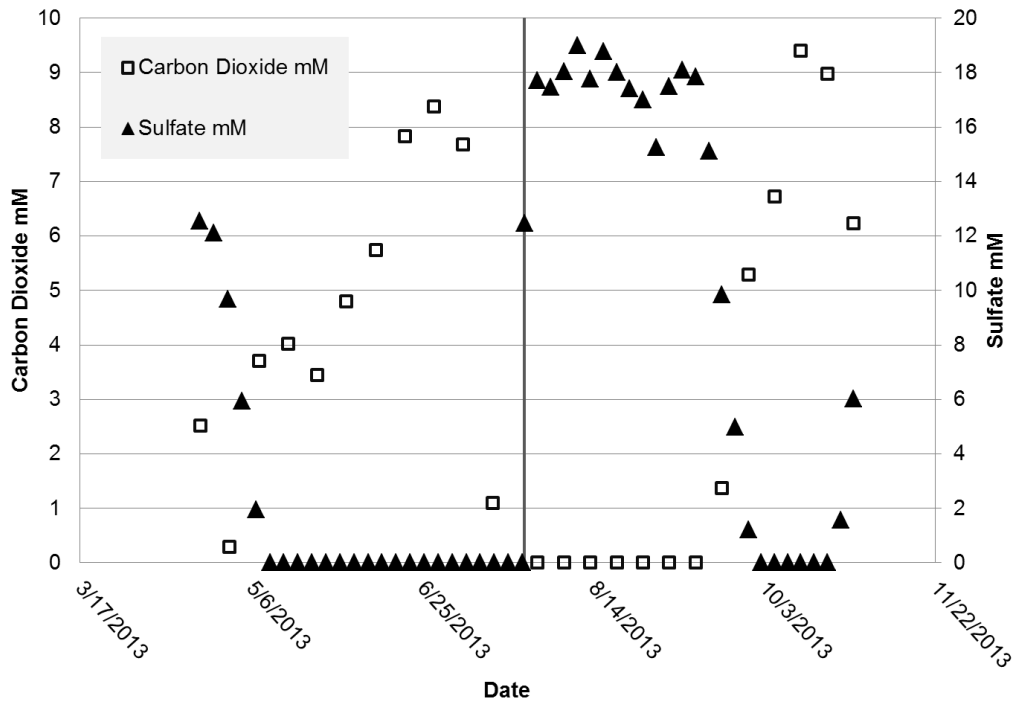


Figure 3.8. Pore-water CO_2 and SO_4 concentrations collected over the course of two three-month deployments, indicated by the dark line. The SO_4 data is from Figure 3.7. The pore-water was collected from sediment depth 0 to 30 cm.

Methane and Carbon Dioxide Stable Isotopes. Values of $\delta^{13}\text{C-CH}_4$ showed an opposite trend as CH_4 concentrations in pore-water during both deployments. The $\delta^{13}\text{C-CH}_4$ values decreased from -49 to -67 ‰ while CH_4 concentrations increased (Fig 3.9). When CH_4 concentrations began to decrease, the $\delta^{13}\text{C-CH}_4$ values began to increase from -67 to -58 ‰. This pattern was repeated during the second deployment; $\delta^{13}\text{C-CH}_4$ decreased from -56 to -65 ‰ and CH_4 concentrations increased. As CH_4 concentrations decreased, $\delta^{13}\text{C-CH}_4$ increased from -65 to -58 ‰.

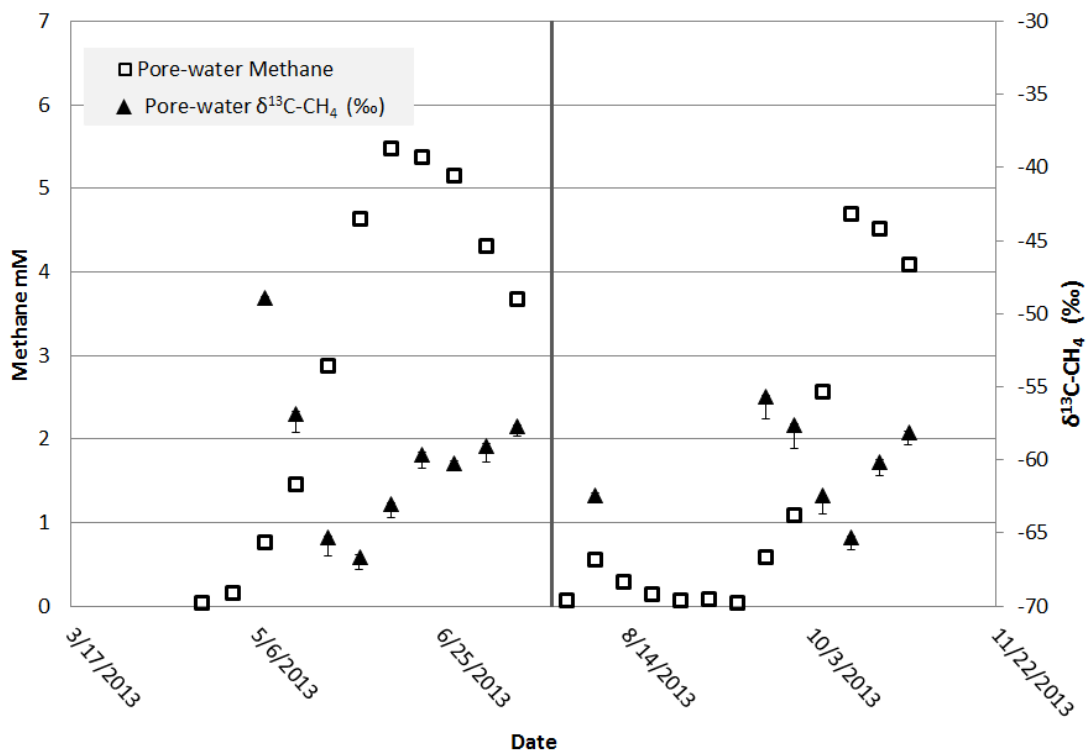


Figure 3.9. Pore-water CH_4 concentrations (mM) and $\delta^{13}\text{C-CH}_4$ (‰) values collected over the course of two three-month deployments, indicated by the dark line. The CH_4 data is from Figure 3.7.

3.4.4 Dissolved Organic Carbon

DOC concentrations were measured on pore-water and bottom water samples. In both pore-water and bottom water, when CH_4 concentrations were low, DOC concentrations were also low, with the exception of the first sample from the pore-water. DOC concentrations in the bottom water started at 0.204 mM DOC and

increased to 0.343 mM DOC, then decreased to 0.229 mM DOC (Fig 3.10a). DOC concentrations in the pore-water started at 12.052 mM DOC and decreased to 0.183 mM DOC, then increased to 5.984 mM DOC (Fig 3.10b). Method blanks were 0.075 ± 0.008 mM DOC (standard deviation, $n = 4$).

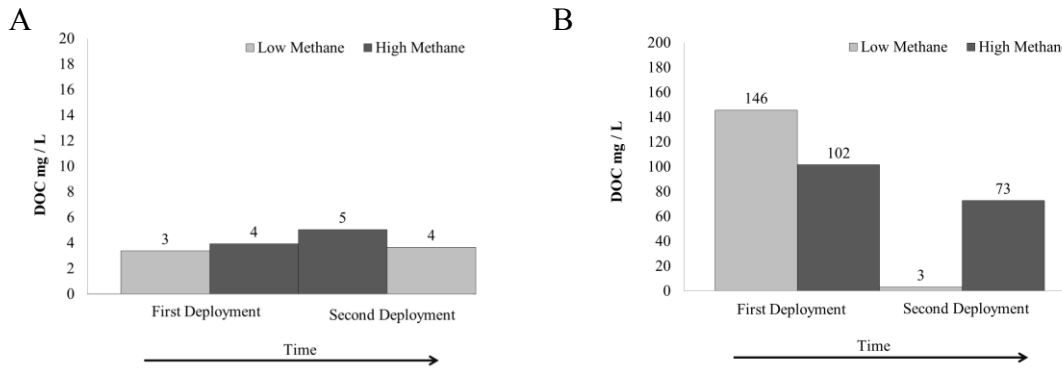


Figure 3.10. Bottom water and pore-water samples were pooled to create a sample representing high CH₄ conditions and a sample for low CH₄ conditions for each water type during each deployment, resulting in 8 samples total (Table J.1). A: Bottom water DOC (mg/L). B: Pore-water DOC (mg/L). Blanks measured were 0.9 ± 0.1 mg L⁻¹ DOC (standard deviation, $n = 4$).

3.5 Discussion

3.5.1 Proof of Concept: Using OsmoSamplers in a Shallow Water Estuary

CH₄ was measured in bottom water and pore-water of the Chesapeake Bay using a novel OsmoSampler method. One goal of this study was to determine if using OsmoSamplers are a viable method for studying CH₄ dynamics in an estuary. CH₄ has been measured in marine and estuarine systems for over four decades (Reeburgh, 1969; Hoehler et al., 1994; Reeburgh, 2007). Traditionally, these measurements come from sediment cores and samples equilibrated with a headspace, and then the methane in headspace gas is quantified by gas chromatography. The same technique was used previously in the Chesapeake Bay (Reeburgh, 1969). The samples for our study were collected under similar conditions (*i.e.* location, water column depth, time of year) though the Reeburgh method was based on sediment cores taken at three times per year accompanied with bottom water discrete sampling. In Reeburgh

(1969), CH₄ concentrations ranged from below detection limit of approximately 7 μM CH₄ in shallow sediments (10-20 cm) to 6 mM at 100 cm sediment depth. The pore-water collected in our study was restricted to the upper 30 cm of the sediment and ranged in concentration from 0.03-5.5 mM CH₄, with the highest concentration occurring in mid-June (Fig 3.6). The study (Reeburgh, 1969) also found CH₄ below detection limit in bottom water measured in November, January, and August. This may be due to less sensitive historical methods that were unable to detect low concentrations of CH₄. While these types of studies have yielded important biogeochemical information, fine-scale temporal variability is not obtained with traditional sediment sampling measurements. This highlights the importance of the continuous measurements acquired using OsmoSamplers that facilitate the capture of fluctuating CH₄ in dynamic estuarine environments.

3.5.2 Bottom Water Methane Concentrations Increase with Hypoxia

The hypothesis that CH₄ increases in bottom water related, temporally, to bottom water hypoxic conditions was tested. Time-series captured using OsmoSamplers indicated the relationship between bottom water oxygen and CH₄ and supported the first part of the proposed HEMF hypothesis (Fig 3.1b).

The mechanism that is driving the CH₄ increase in the bottom water remained unclear. Several possibilities existed. No oxygen was present in the sediments, and hence the cascade of electron acceptors available for organic matter remineralization shifted biogeochemical processes towards the sediment-water interface. This allowed CH₄ production in shallower sediments when compared to non-hypoxic conditions. The build-up of this CH₄ would then diffuse from the sediments towards the water column, and hence increase CH₄ concentrations in the bottom water. It was also possible that under anoxic conditions, the efficient aerobic methanotrophs no longer oxidize the CH₄ effectively in the surface layer of the sediment, and more CH₄ diffused out of the sediments. A third possibility was CH₄ production directly in the anoxic bottom water. More investigation is needed to decipher between these possibilities. For example, δ¹³C-CH₄ analysis of bottom water and pore-water from various sediment depths will give an understanding of what mechanisms are driving

increases in bottom water CH₄ concentration during hypoxia. Though the mechanism may still be unclear, the data collected here overall supported the concept of HEMF.

3.5.3 Temporal Observations Provided by Continuous Sampling

Methane Concentrations Decrease in Bottom Water as Oxygenated Conditions Resume. During the second lander deployment, CH₄ concentrations began to decrease in the bottom water (Fig 3.12). Two explanations for this decrease are

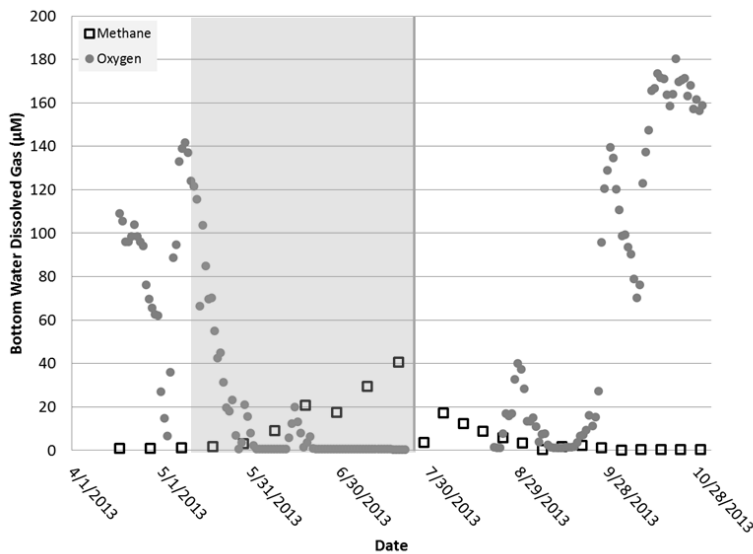


Figure 3.12. Bottom water O₂ and CH₄ concentrations are shown (Data from figure 3.6) with the increase in O₂ occurring with the decrease in CH₄ highlighted by the shaded box.

plausible: 1) increased microbial oxidation (either aerobic or anaerobic) of the available CH₄ and/or 2) the water column stratification began to breakdown, and water became well mixed. Due to missing oxygen data from 25 July 2013 to 21 August 2013, the oxygen concentration can only be

speculated to be hypoxic or anoxic. The breakdown of stratification would return the waters to oxic conditions and any methanogenesis leading to the initial increase in bottom water CH₄ (discussed in section 3.5.2), would be inhibited. If hypoxia break-up did occur, CH₄ rich bottom water mixing with surface water would lead to CH₄ fluxing to the atmosphere. The microbial and physical processes impacting water column CH₄ in estuaries could be better understood by measuring bottom water and surface water stable carbon isotopes of CH₄ as well as CH₄ concentrations and could yield valuable information in the future.

Dissolved Oxygen Concentrations Increase during “Hypoxic”

Conditions. There were several times when DO concentrations increased in bottom water for a short amount of time (10-16 days) when bottom water was mostly hypoxic. One of two events was recorded between 13-23 June 2013 (Fig 3.13). On

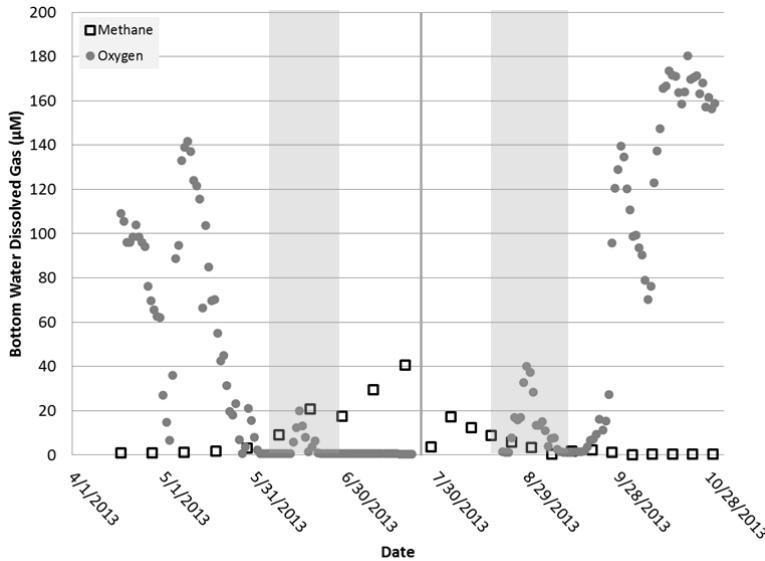


Figure 3.13. Bottom water O₂ and CH₄ concentrations are shown (Data from figure 3.6) with the wind events highlighted by the shaded boxes.

13 June 2013 a thunderstorm occurred with wind gusts up to 56 mph and waterspouts occurred in the Chesapeake Bay. During the storm event, the wind direction was from the south, maximizing water movement and effective wind speed over the Chesapeake Bay. The second mixing event,

during which DO increased, occurred between 24 August 2013 to 6 September 2013. On 22 August 2013 there was a thunderstorm with gusts up to 34 mph and winds from the south west. These mixing events most likely broke up stratification of the water column, mixing oxygenated surface water, which is low in CH₄, with bottom water, thus increasing the bottom water oxygen and decreasing bottom water CH₄. CH₄ concentrations decreased in bottom water within days following these mixing events (Fig 3.13). Thus, wind-induced mixing events were captured that could connect bottom water hypoxia to enhanced CH₄ flux from the bottom water to the atmosphere.

Such events would be difficult to capture without having continuous samplers on the seafloor, but also supported the idea of storm related enhancements of CH₄ fluxes. The hypothesis that CH₄ transported from the bottom water was directly emitted to the atmosphere during these mixing events needs to be tested with higher

resolution sampling. For the time-series, it would be possible to look more in depth at these events, because only every other sample coil length was analyzed, but that was beyond the scope of this project. These mixing events highlighted another possible mechanism for CH₄ to be emitted from shallow water estuaries to the atmosphere.

Pore-Water Sulfate Depletion and Methane Accumulation. In pore-water, SO₄ was depleted during accumulation of CH₄ and this pattern of depletion and accumulation was measured during both deployments (Fig 3.14). The pore-water CH₄ concentrations increased to 5.5 mM when SO₄ concentrations decreased. This was most likely due to the relationship between sulfate-reducing bacteria and methanogens, where sulfate-reducing bacteria out compete methanogens for substrate

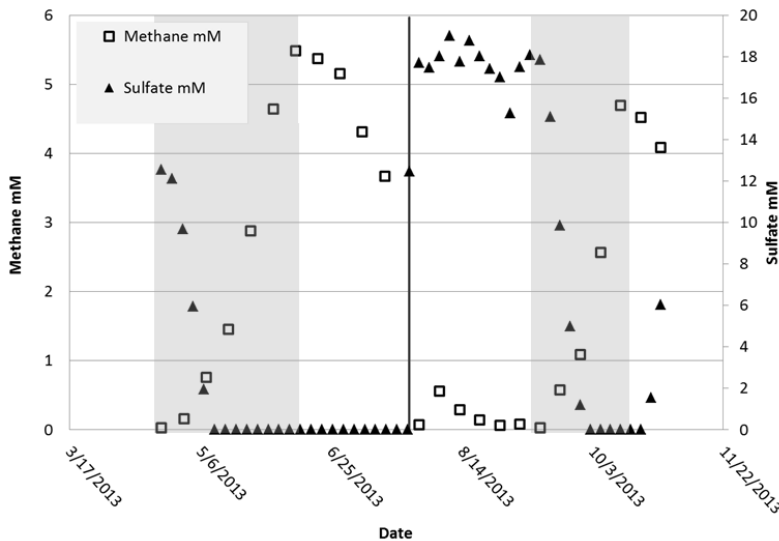


Figure 3.14. Pore-water SO₄ and CH₄ concentrations are shown (Data from figure 3.7) with the decreases in SO₄ and increases in CH₄ highlighted by the shaded boxes.

until SO₄ is depleted. The rate of SO₄ decrease was 1.0 mM day⁻¹ on the first lander and 0.9 mM day⁻¹ on the second lander. CH₄ increased at about 106 μM day⁻¹ on the first lander and 156 μM day⁻¹ on the second lander. The rate at which the transition from the sulfate-reduction to the methanogenic activity occurred was similar to previous experiments using homogenized sediment incubations (Hoehler et al., 1994). In the Hoehler experiments, the rate of SO₄ consumption was about 0.5 mM SO₄ day⁻¹ and CH₄ production was about 32 μM CH₄ day⁻¹. The study presented here measured pore-water in sediments and yielded similar, though more rapid, results to laboratory homogenized sediment experiments.

Sediment homogenization may have occurred in this study due to lander disruption that when the landers were deployed. When the lander was initially deployed, the upper layers of the sediment could have mixed with the bottom water, leading to pore-water with low concentrations of CH₄ and CO₂ as well as high concentrations of SO₄. Overtime, the sediment biogeochemistry may have reestablished itself where SO₄ was consumed and CH₄ and CO₂ was produced. This transition may be indicated when SO₄ concentrations decreased and CO₂ and CH₄ concentrations increased as each deployment progressed, possibly due to sulfate reduction, methane oxidation, and methanogenesis. During that time the lander might have been sinking. As a result the probe would also be moving into the sediment, through the biogeochemical zones, starting perhaps in bottom water, then through the sulfate-reduction zone, and into the methanogenic zone. During the second deployment, SO₄ began to decrease after a lag time of 50 days. This could be due to different lander construction (Fig 3.3 b-c), where the second lander may have taken longer to sink and submerge the pore-water rhizone because of the larger footprint (see section 3.3.2). If this happened, once the rhizone was submerged in the sediment, SO₄ would have decreased and CH₄ increased at similar rates to the first deployment.

Microbial Community Activity Observed using Methane Carbon Stable Isotopes. Isotope data were used to investigate microbial community activity and also to evaluate potential artifacts. In sediments, the $\delta^{13}\text{C-CH}_4$ was expected to be enriched in ¹³C due to methane oxidation in the sulfate-reduction zone and depleted in ¹³C in the methanogenic zone (Whiticar, 1999). If the lander were sinking further into the sediment over the course of the deployment, we would expect to see enriched and then depleted ¹³C values for the remainder of each deployment, as well as high sustained CH₄ concentrations. However, the isotopic data showed an enrichment of ¹³C at the end of each deployment as well as a decrease in concentration of CH₄ (Fig 3.15). This suggested that another process, besides the lander sinking further into the sediment, was controlling sediment CH₄ measurements. Though concentrations of pore-water CH₄ were measured, future work using probes put in place by divers or

remotely operated vehicles may be a more effective at minimizing possible artifacts due to sediment disturbance and sinking.

Stable isotope analysis of CH₄ carbon can reflect activity of microorganisms. As methanogens produce CH₄, carbon in CH₄ becomes depleted in ¹³C and conversely, as methanotrophs oxidize CH₄, carbon in CH₄ becomes enriched in ¹³C

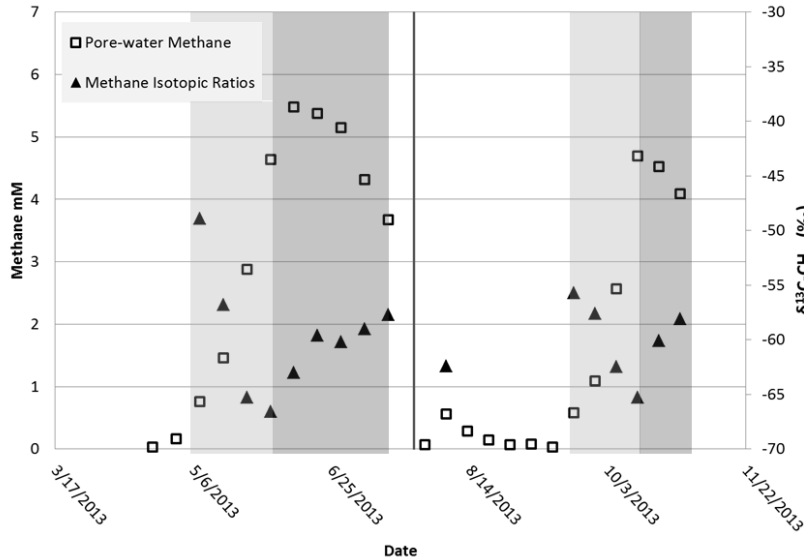


Figure 3.15. Pore-water CH₄ concentrations and stable isotopic ratios of CH₄ carbon are shown (Data from figure 3.9) with the methanogenic periods highlighted by the shaded box and the oxidation periods shown by the darker shaded box.

when CH₄ concentration decreased, there was an enrichment of ¹³C. These patterns indicated periods of methanogenesis and methane oxidation, respectively. CH₄ production is expected to occur through CO₂ reduction in marine systems which generates δ¹³C-CH₄ of -66 ‰ (Whiticar, 1999), similar to values during methanogenesis in this study (-67 ‰ and -65 ‰). The pattern of methane production and oxidation was demonstrated in the pore-water, though the extent to which oxidation limited the amount of CH₄ emitted from estuaries to the atmosphere is unclear.

Towards the end of both deployments there was a decrease in CH₄ concentrations, and it was suggested to be due to methane oxidation. However, the decrease could also be due to gas loss *in situ* and/or degassing of the sample coil upon

(Whiticar, 1999).

In both deployments, CH₄ concentrations increased to a maximum value then decreased to the end of the deployments.

During each increase in CH₄ concentration,

there was depletion of ¹³C

(Fig 3.15). Also

retrieval of the lander and before crimping. The first lander coils were crimped 5 hours after retrieval and the second lander coils within 5 minutes. There was an enrichment of $\delta^{13}\text{C}$ by 5-7 ‰ that occurred with decreasing CH_4 concentrations at the end of each deployment. Because physical degassing did not result in fractionation (Wallace et al., 2000) degassing could be ruled out. However, AOM required SO_4 , which was depleted on the first lander, though present on the second lander. Perhaps the decrease in CH_4 concentration and the corresponding enrichment ^{13}C of CH_4 could indicate the use of an alternate electron acceptor for the oxidation of CH_4 such as iron, manganese, or nitrate (Lovley and Goodwin, 1988; Hoehler et al., 1994). Future work investigating alternate electron acceptors involved in AOM could shed some light on microbial CH_4 cycling in estuarine sediments.

3.5.4 Method Development for Dissolved Organic Carbon Analysis

DOC represents the precursor in the microbial food chain to produce CO_2 and H_2 needed for CH_4 production (Burdige, 2006). Consequently, increasing DOC concentrations to sediments could lead to increased CH_4 production in estuaries. In this study, concentrations of pore-water DOC were found to be generally much higher than bottom water concentrations, as observed in previous studies (Burdige et al., 1992; Martin and McCorkle, 1993). DOC concentrations in the bottom water ranged from 0.204 mM to 0.343 mM. The highest concentration of DOC in the bottom water occurred during the lowest concentration of DOC in pore-water. This occurred during the first part of the second deployment during low pore-water CH_4 concentrations. This low pore-water DOC could indicate collection of bottom water prior to the pore-water rhizone being submerged due to sinking. Based on measurements of this study, the connection between DOC concentration and CH_4 cycling remained unclear. The unclear connection between measurements of DOC concentration and CH_4 concentration might have been due to the quality of the DOC, not the quantity. More specifically, the chemical structures of the DOC molecules and how labile or refractory the material was, governed how easily microorganisms can utilize the carbon (Hansell and Carlson, 2002) and possibly impact CH_4 cycling. In this study, DOC concentrations were determined as part of a method development

effort to characterize DOC structures using Orbitrap mass spectrometry on bottom water and pore-water samples collected using OsmoSamplers. Because the DOC blanks were large relative to bottom water DOC concentrations, the use of OsmoSamplers to collect bottom water for structural analysis may be unsuitable. Future work could evaluate the DOC for structural changes, such as the size of the molecules, possibly reflecting any microbial community activity in sediments over the course of seasonal hypoxia related to HEMF.

3.5.5 Implications of Chesapeake Bay Methane Flux

The main result of this study was that the first part of HEMF occurred; when bottom water became hypoxic and as a result CH_4 was released from sediments of the Chesapeake Bay. But where did all of this CH_4 go? The CH_4 was either oxidized in the water column or emitted to the atmosphere. If we consider CH_4 measured during the first deployment as a conservative estimate of sediment to water column CH_4 flux as a result of one season of hypoxia; how much CH_4 did this represent? The integrated CH_4 concentrations measured during the first deployment of $126 \mu\text{M}$ CH_4 and the entire Chesapeake Bay water column of 8.8×10^{13} L (8 m average depth \times $11,100 \text{ km}^2 = 8.8 \times 10^{13}$ L) were used for calculations. If we consider just sediments containing gas, comprising 30% of the Chesapeake Bay, and the water overlying the gas containing sediments (Hill, 1992) during seasonal hypoxia, 0.054 Tg CH_4 could be fluxed from the sediments to the water column. If we consider the entire Chesapeake Bay this represented 0.179 Tg CH_4 that could be fluxed from the sediments into the water column. Assuming the Chesapeake Bay has an average volume to surface area ratio, this calculation can be used to estimate a global flux. Using $1,400 \times 10^3 \text{ km}^2$ as a global estimate of estuarine surface area (Middelburg et al., 2002), the global CH_4 flux from estuarine sediments could be 6.8 Tg CH_4 (water column overlying gas) to 22.6 Tg CH_4 (Entire Chesapeake Bay water column). If this CH_4 was emitted to the atmosphere, estuaries could represent 5 % of the global sources of atmospheric CH_4 , which is as much as five times current estimates of estuarine emissions proposed by previous studies (Middelburg et al., 2002; Reeburgh, 2007).

The CH₄ could also be oxidized in the water column to CO₂ and possibly contribute to local pH change. Aerobic methane oxidizing bacteria assimilate 5-20 % of the carbon, depending on growth conditions (Templeton et al., 2006). If 100% of this CH₄ was oxidized and 80% was respired, this would represent a pCO₂ addition of 2,429 μatm. Using average Chesapeake Bay values of total alkalinity of 1,400 μmol kg⁻¹ seawater, 800 μatm pCO₂, 10 ‰ salinity, and a temperature of 20°C (Hillary Lane, personal communication), this would decrease pH by 0.6 units (CO2SYS Calculator). The calculations and parameters for the flux and pH calculation are outlined in Table 3.1. Decreases in pH can have a number of negative ecological impacts such as enhanced oyster shell dissolution (Waldbusser et al., 2011) and impaired oyster immune function (Beaven and Paynter, 1999). There is also evidence that the presence of aerobic methanotrophs and the associated cellular material produced by aerobic methane oxidizing bacteria can decrease the stability of carbonate minerals (Kawano and Hwang, 2011; Krause et al., 2014) in addition to the decreasing pH from respired CO₂. CH₄ produced through HEMF could therefore represent a significant environmental impact even if it is not emitted to the atmosphere. However, the respired pCO₂ as well as the cellular material produced through the methanotrophy would be produced over the course of the months as well as diluted throughout the pore-water and water column, it is difficult to quantify the impact methane oxidation would have on an ecosystem as a whole.

Table 3.1. Chesapeake Bay data and calculations that were used to calculate CH₄ flux and pH increase related to methanogenesis and methane oxidation.

Parameter	Value	Reference
Temporal Gradient	0-40 CH ₄ μM 98 d ⁻¹	Chapter 3.0
Integrated CH ₄	126 CH ₄ μM 98 d ⁻¹	Chapter 3.0
Chesapeake Bay Average Depth	8 m	
Chesapeake Bay Surface Area	11,100 km ²	(Smith 1992)
Chesapeake Bay Volume	$8\text{ m} \times 11,100\text{ km}^2 \times \frac{1,000,000\text{ m}^2}{1\text{ km}^2} = 8.88 \times 10^{13}\text{ L}$	Chapter 3.0
Chesapeake Bay Underlain with Shallow Gas	30% of the Area of the Bay	(Hill, 1992)
CH ₄ to the Water Column	$1.26 \times 10^{-4}\text{ M CH}_4 \times 8.88 \times 10^{13}\text{ L} \times \frac{16\text{ g C}}{\text{mol}} \times 30\% \text{ Gas} = 0.054\text{ TgCH}_4$	Chapter 3.0
Global Estuary Surface Area	$1,400 \times 10^3\text{ km}^2$	(Middelburg et al., 2002)
Total Alkalinity	1,400 μmol kg ⁻¹	Unpublished Data
pCO ₂	800 μatm	Unpublished Data
Salinity	10 ‰	Chapter 3.0
Water Temperature	20 °C	Chapter 3.0

3.6 Conclusion

Presented here is the first time-series of a 9 month record of continuous CH₄ concentrations in the bottom water and sediment pore-water of an estuary. CH₄ concentrations increased in the bottom water to as high as 20,000 times atmospheric saturation of CH₄ (~2 nM) during midsummer, the peak of hypoxic and anoxic conditions. This dataset supports the first stage of the HEMF hypothesis, in that hypoxic and anoxic conditions were correlated with increased CH₄ concentrations in bottom water. Stable isotope analyses of CH₄ carbon also revealed that rapid

microbial oxidation could prevent or modulate HEMF. However, more rapid mixing accompanying hypoxia breakup in the fall or wind-mixing events observed in this study could present a means for CH₄ accumulated in the bottom water to be rapidly transported to the surface and emitted to the atmosphere, before methane oxidation can occur in the water column. Calculations revealed that if the CH₄ remains in the bottom water, complete oxidation of the CH₄ could decrease the pH by as much as 0.6 units, representing a mechanism for detrimental impacts on estuarine ecology such as oyster shell dissolution and impaired oyster immune function (Beaven and Paynter, 1999; Waldbusser et al., 2011). If, on the other hand, this methane escapes the estuary, estuarine emissions of CH₄ could be underestimated. To determine the fate of the enhanced CH₄ flux from estuarine sediments to the water column as a result of HEMF, further research is needed to constrain these estuarine processes of methane oxidation. This project highlights that anthropogenic effects such as eutrophication and hypoxia are correlated to an enhanced CH₄ flux from estuarine bottom water to the atmosphere. Management efforts undertaken to modulate the detrimental impacts of eutrophication and hypoxia in estuarine systems could be better informed by increased understanding of methane emissions related to eutrophication in the largest estuary in the United States, the Chesapeake Bay.

Chapter 4: Conclusion

4.1 Understanding the Impacts

4.1.1 The Chesapeake Bay

Field work in the Chesapeake Bay indicated that CH₄ concentrations increase in the bottom water during seasonal hypoxia. The CH₄ that is produced annually during seasonal hypoxia is destined to be oxidized in the water column or emitted to the atmosphere. An estimated 6.8 Tg to 22.6 Tg CH₄ global flux from estuarine sediments could be occurring due to the process of HEMF. This estimate represents as much as five times current estimates of estuarine emissions proposed by previous studies (Middelburg et al., 2002; Reeburgh, 2007), and 5 % of the global sources of atmospheric CH₄.

Alternatively, the CH₄ could also be oxidized in the water column to CO₂ and possibly contribute to local pH change. Complete oxidation of the CH₄ in the bottom water was estimated to decrease pH by 0.6 units. However, the CH₄ released from the sediments occurred over 3 months, and given the buffering capacity and the retention time of the Bay, this change may be negligible. More research is needed to determine the impact of methane oxidation on estuarine pCO₂.

4.1.2 Aerobic Methane Oxidizing Bacteria

Laboratory experiments indicated that the pure culture *M. album* may be inhibiting hydrate formation, though the culture may be inappropriate for dissolution experiments. Culturing the organism at optimal conditions (30°C and 1 atm) generated a CH₄-carbon fractionation factor of 1.00274. This value was lower than previous studies, but there is also evidence that variation in isotopic fractionations can arise from temperature, different organisms, and pure culture vs. mixed cultures (Coleman et al., 1981; Kinnaman et al., 2007; Zheng et al., 2014). Because copper is a cofactor for a critical enzyme in methane oxidation, the concentration of copper was increased in the growth media. The increase in copper proved to have an inhibitory

effect on the growth of the culture. The culture was grown at a range of temperatures (30°C, 10°C, and 1°C) to determine the impact of cold temperatures on the growth of the culture. Based on measurements of optical density the culture did not grow at 10°C, and 1°C. In addition, gradually lowering the temperature in an attempt to slowly introduce the culture to low temperatures did not improve growth at low temperatures. The culture did however remained viable at high pressure and low temperature (15°C and 34 atm) and once the temperatures were increased to 30°C the culture grew rapidly.

Measurement of headspace and media CH₄ is critical in hydrate dissolution experiment design. Therefore, monitoring the growth of the culture using measurements of CH₄ is critical in hydrate dissolution experiments using culture. However, issues with CH₄ measurements were encountered in culture experiments conducted in the pressure chamber. Changes in the solubility of CH₄ that resulted from pressure and temperature manipulations of the chamber experiments impacted media CH₄ concentrations. Effects of solubility changes were difficult to extract from impacts due to the activity of the culture. Also, using a pressurized headspace of gas provides a massive supply of carbon, unique from culture vial experiments conducted at 1 atm. This supply of carbon available to the cells washes out any small consumption of CH₄ due to methane oxidation, making headspace measurements in pressure chamber experiments ineffective for monitoring culture growth.

Stable isotopic ratios of CH₄-carbon could also be used to monitor the culture activity in hydrate dissolution experiments. Headspace measurements of $\delta^{13}\text{C-CH}_4$ showed no fractionation, which may be similar to CH₄ headspace measurements that revealed no change, in that the reservoir of CH₄ is so massive, that any enrichment of ¹³C due to methane oxidation is just too small to measure. However, a fractionation was observed from the analysis of aqueous CH₄, demonstrating that measurements of aqueous $\delta^{13}\text{C-CH}_4$ are the key to monitoring methane oxidation in pressure chamber experiments.

Hydrate formed in the presence of the methane oxidizing culture was unsuitable for hydrate dissolution experiments. The hydrate formed at the liquid and gas interface as clear crystals or slush and not as a solid white block, as seen in

previous studies (Lapham et al., 2012). This could be due to low CH₄ concentrations, the lack of a surfactant, or the culture acting as an inhibitor. More development is needed to perform hydrate dissolution experiments using the pure culture *M. album*.

4.2 Next Steps

4.2.1 Validating HEMF

Research Question: Does methane increase in the bottom water when oxygen decreases during seasonal hypoxia? The results of this work found that, yes, CH₄ concentrations increased in the bottom water when oxygen decreased. For the first time, a true time series of CH₄ concentrations in an estuary was measured over the development and breakup of seasonal hypoxia. The results support the HEMF hypothesis but more work is needed to validate the process and constrain the potential to produce pH perturbations and emissions to the atmosphere. Stable isotopic analysis of the CH₄-carbon produced fascinating results of possible periods of methanogenesis and methane oxidation in the sediment. At what depth and at what time do these periods occur? What is happening in the bottom water? How are changes in solubility impacting our results? To answer these questions, future research should include the measurement of stable isotopes of CH₄-carbon in the bottom water as well as sediment pore-water at a series of known depths. This can be done by orienting multiple sample inlets (connected to multiple OsmoSamplers) along a probe that is pushed into the seafloor by a diver or a remotely operated vehicle. This would also minimize disruption due to the lander, as the probes can be inserted in the sediment away from the lander.

4.2.2 Hydrate Dissolution Experiments: A New Bug or Just Do it?

Research Question: Does the aerobic methane oxidizing bacteria *Methylomicrobium album* enhance hydrate dissolution? These results suggest that, because gas hydrate did not even form in the presence of the culture, the stability of hydrate may be impacted by the culture. However, this could also be a function of not using surfactants, as in previous hydrate dissolution experiments (Lapham et al.,

2012; Lapham et al., 2014). In order to conduct hydrate dissolution experiments, one needs solid stable hydrate first and foremost. Future work should explore the use of surfactants to produce solid hydrate. In addition, the effect of surfactants on the culture needs to be determined. Growth of *M. album* was limited at low temperatures and high pressure, though the cells remained viable. A more suitable organism could be acquired from an enrichment of bottom water or acquired from colleagues that may be more robust at low temperatures.

But is “robust” growth desirable in a gas hydrate dissolution experiments? If the methane oxidation were to reduce a measurable amount of the aqueous CH₄ during dissolution experiments, the measurement of dissolution rates would be difficult to resolve from the effects of the CH₄ oxidation. This is similar to the issue encountered in the pressure chamber experiments, when changes in solubility impacted aqueous CH₄ concentrations and disrupted measurements of methane oxidation rates. An organism, like *M. album*, that is able to withstand high pressure and remain viable, oxidizing CH₄ at low rates, without impacting dissolution rate measurements could be the perfect organism for hydrate dissolution experiments.

4.3 Conclusions

With the atmospheric activity of CH₄ as a greenhouse gas, understanding the impacts of CH₄ is critical. Both hydrate dissolution as well as HEMF represent positive feedback mechanisms for CH₄ emissions to the atmosphere, though the amount of CH₄ that reaches the atmosphere from these sources is not well understood. Eutrophication can have a range of ecological impacts that occur on a range of time scales (Kemp et al., 2005). In addition, non-linear feedback mechanisms could be difficult to predict making forecasting future estuarine emissions of CH₄ difficult, should eutrophication and hypoxia continue to spread globally.

Appendices

Appendix A: Sterilization Procedures

Preparing the Pressure Chamber

After each culture experiment, cellular debris was removed by adding deionized water and bubbling with tank air (zero CH₄) from the dip tube to create turbulence within the chamber, before it was drained. This procedure was repeated three times. The 600 mL chamber, the tubing connecting the pump to the chamber, the sampling ports, and the pump were then sterilized with a 10% bleach solution that was added to the chamber until the solution flowed from the sampling port at the top of the chamber and the solution was then drained. The lower sampling port was also opened briefly to allow bleach to flow through the liquid port. The chamber was then flushed with 6 L of autoclaved sterile water. Once the chamber was sterilized, the pump intake was covered with a sterile 50 mL centrifuge tube and parafilm. Before each use, the pump intake was again sterilized with 70% isopropanol. After sterilizing the pressure chamber, the high pressure pump was primed with sterile media and used to fill the chamber.

Preparing Culture Vials

The culture vials (27 mL and 157 mL) were sterilized using a 20 minute autoclave cycle. Since the assembled vials were autoclaved (meaning the septa and collar were attached to vial), a needle was inserted into the septa to allow gas exchange during the autoclave cycle, which heated and pressurized the vials. The needle was covered with foil during the cycle to prevent material from entering the vial through the needle. The needle and foil were removed immediately after the autoclave cycle was completed to prevent a hole from forming in the septum during cooling. With the needle removed immediately after autoclaving, the hole from the needle sealed as the septum cooled. However, during the cooling, air was observed being pulled through the hole from the needle. For this reason the vial headspace gas composition was prepared after sterilization and the septum were completely cooled and sealed.

Appendix B: Generating Seed Stock

Seed Stock

On 22 March 2013, the seed stock was prepared by thawing the original pure culture and diluting 200 μL of the pure culture with 6 mL of NMS media in 15 mL centrifuge tube (Fig 2.6a). 650 μL of this pure culture dilution was then added to 75 mL of NMS media in a 157 mL serum vial. Afterward, a 1:1 volume CH_4 to air headspace was added. This solution was incubated at 30°C for 1 week until it showed increased turbidity, which indicated a high concentration of cells. 50 mL of this turbid sample was then diluted with 50 mL of sterile glycerol in a 250 mL glass beaker and this mixture was then used as the seed stock. This seed stock was divided into 1 mL aliquots and stored at -80°C in 2 mL cryogenic vials, prior to any culture experiments (Fig 2.6c).

The aim was to expand the culture three times, to produce a large volume of turbid media, containing many cells, to be stored as aliquots of seed stock. The first dilution was performed by inoculating 150 mL of media with 100 μL of turbid media (from passage 1) in a 300 mL glass bottle with a black butyl rubber stopper. The second dilution was performed by inoculating 150 mL of media with 1 mL of turbid media (from passage 1) in a 300 mL vial with a black butyl rubber stopper. The third dilution was performed by inoculating 75 mL of media with 1 mL of turbid media (from the original culture) in a 157 mL serum vial with a blue butyl rubber stopper. The third dilution was used to produce the seed stock.

Preparing the Working Culture

A 1 mL seed stock aliquot was diluted into 5 mL of media, resulting in a 6x dilution. Then 0.5 mL of that solution was further diluted into 5 mL of media, resulting in an 11x dilution. It was again diluted to obtain the final 66x dilution. An aliquot of 1 mL of the final culture solution was then transferred to 27 mL glass culture vials (that contained 13 mL of Nitrate Minimal Salt media (Table 2.1). Afterwards, the working culture was left at atmospheric pressure and 30°C for a week to 10 days. A new working culture was prepared from the seed stock aliquots, expanded, and used at the beginning of each experiment (Fig 2.6c). Use of the organism within three passages ensured a minimal amount of

genetic drift of the working culture used in experiments from the original pure culture obtained from the culture company.

Appendix C: Calculations

Solubility of Methane

The predicted solubility of CH₄ was calculated for the pressure chamber experiments using equations 1a-b. The Bunsen solubility coefficient was first solved using the following equation, where T represents temperature in Kelvin and S represents salinity in ppt.

$$\ln\beta = -67.1962 + 99.1624 * \frac{100}{T} + 27.9015 * \ln \frac{100}{T} + S[-0.072909 + 0.041674 * \frac{100}{T} + (-0.0064603 * \left(\frac{T}{100}\right)^2)] \quad \text{Equation 1a}$$

$$\text{Solubility of CH}_4 \text{ (M)} = \beta * \text{CH}_4 \text{ (mols gas in the headspace)} \quad \text{Equation 1b}$$

Correction of Spectrophotometric Measurements

Measurements of liquid samples were corrected for the added liquid (Equation 2), where the sum of the sample volume and the original volume equals the total volume.

$$\text{Corrected OD}_{405} = \frac{\text{OD}_{405} * \text{Total Volume}}{\text{Original Volume}} \quad \text{Equation 2}$$

Correction of Culture Vial Headspace Measurements

Measurements of the gas samples were corrected for the added sampling gas (Equation 3).

$$\text{Corrected ppm} = \text{Measured ppm Sample Gas} * \frac{\text{Sample Volume} * \text{Sampling Gas ppm CH}_4}{\text{Total Volume}} \quad \text{Equation 3}$$

Appendix D: Cavity Ring Down Spectroscopy

In addition to Isotope Ratio Mass Spectrometry (IRMS) analysis, isotope analysis was performed using Cavity Ring Down spectroscopy (CRDS) with a Picarro G2201-i Analyzer equipped with a Small Sampling Isotope Module (SSIM).

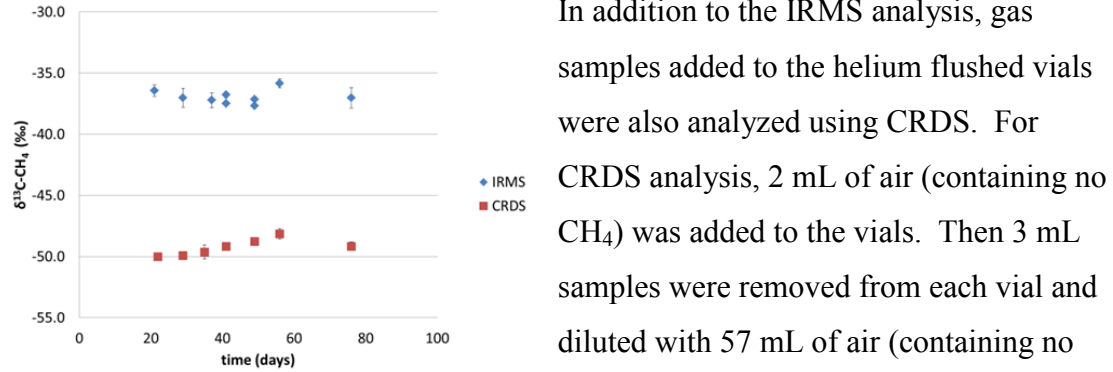


Figure D.1. Measurements of stable isotopes from Delta V Isotope Ratio Mass Spectrometer (IRMS) and Cavity Ring-Down Spectroscopy (CRDS) of $\delta^{13}\text{C-CH}_4$ for pressure chamber experiment II. Error bars show standard error on duplicate measurements.

In addition to the IRMS analysis, gas samples added to the helium flushed vials were also analyzed using CRDS. For CRDS analysis, 2 mL of air (containing no CH_4) was added to the vials. Then 3 mL samples were removed from each vial and diluted with 57 mL of air (containing no CH_4). Triplicate 20 mL samples were then analyzed using the CRDS.

A comparison of IRMS and CRDS analysis showed 15‰ difference in measurements, where CRDS analysis produced values more negative than IRMS analysis (Fig D.1).

Appendix E: DAPI Staining

DAPI (4',6-diamidino-2-phenylindole) Staining was performed on the pure culture. Two dilutions were made of cells by adding 1 mL aliquots to two 15 mL centrifuge tubes and adding 4 mL and 9 mL of deionized water to create a 5x and 10x dilutions. The dilutions were fixed by adding 100 μ L of formalin per 5 mL of liquid and incubated for 2-3 minutes. For each sample, a filter was first added to the filter tower and wetted using with deionized water. Using a vacuum, each dilution was added to the tower and filtered. The filter was transferred to a slide. One drop of DAPI stain was added to the filter and a cover slip was placed over the filter on the slide. Slides were stored at -20°C until counting. Slides were viewed at 100x using fluorescent immersion oil. Each slide was counted using 15 fields.

Appendix F: Solid Phase Extraction

Solid Phase Extraction (SPE) was performed on 13 mL liquid culture samples. The extraction resin cartridges were first activated by eluting 2 mL of methanol through each, followed by 1.5 mL acidified water. Each sample was acidified by adding 100 μ L formic acid. Each sample was then eluted through a cartridge, followed by 1.5 mL of acidified water. The cartridges were dried using nitrogen gas at 3 psi. Brown glass sample vials were first rinsed with methanol. Samples were eluted into sample vials with 4 mL of methanol. Sample vials were stored at -20°C until analysis using orbitrap mass spectrometry.

Appendix G: Chamber Experiment Details

Pressure Chamber I

The 600 mL pressure chamber was filled halfway with 300 mL of 1 part of turbid media added to 30 parts of fresh media so that the liquid level was at the viewing window of the chamber. A headspace of approximately 50% CH₄ and 50% air was added to the chamber. This was achieved by adding air until a pressure of 22 atm was reached. After 22 atm was achieved, CH₄ was added to reach a final pressure of 34 atm. The chamber was held at 1°C. Headspace and media samples were frequently collected for gas concentration and spectrophotometric measurements over 38 days.

Pressure Chamber II

After sterilization, media containing an increased density of cells was transferred into the pressure chamber. A headspace of approximately 50% CH₄ and 50% air was added. During the first headspace sampling, pressure was lost due to sampling error, resulting in a final pressure of 34 atm. However, the chamber was held at 34 atm and 15°C for 46 days. To check for cell viability, a portion of the liquid samples was used to inoculate 27 mL culture vials with 100 µL of media from the chamber (3 treatments and 1 biotic control) that were incubated at 30°C. The chamber temperature was increased to 30°C after 46 days. Temperature was increased to determine if the culture could grow at high pressure.

Headspace samples were taken in the same fashion as described for the first pressure chamber experiment, but 1 mL of gas sample was added to a helium flushed 12.5 mL vial for isotopic analysis and the remaining gas sample was used for GC analysis. Media samples were first equilibrated with 2 mL of helium by shaking for 2 minutes with a rest time of 30 seconds. The equilibrated headspace was injected into the GC to measure the dissolved CH₄ in the chamber media. The remaining media was used for spectrophotometric measurements. Liquid and headspace samples were collected throughout the 180 days of the experiment.

Pressure Chamber III

After sterilization, the chamber was filled halfway with 300 mL of 13 parts turbid media combined with 5 parts fresh media using the high pressure pump. A

headspace of 50% CH₄ and 50% air was added. The chamber was then held at 30°C for 3 days then lowered to 5 °C over the course of 20 days. Headspace and media samples were taken for gas concentration, stable isotopic analysis, and spectrophotometric measurements. Headspace samples were taken with 1 mL of gas sample added to a helium flushed 12.5 mL vial for isotopic analysis and the remaining gas sample was used for GC analysis. Media samples were first equilibrated to be used to measure the dissolved CH₄ in the chamber media. The remaining media was used for spectrophotometric measurements. Liquid and headspace samples were collected throughout the 170 days of the experiment.

Pressure Chamber IV

300 mL of media containing 2.3 parts turbid media and 1 part fresh media was transferred into the chamber to fill it halfway and a headspace of 50% CH₄ and 50% air was added. A temperature of 10°C was maintained overnight. The next day the chamber was vented and 41 atm of air and 41 atm of CH₄ were added to the chamber, which was held at 73 atm. Pressure in the chamber was increased to 112 atm and the temperature was lowered to 1°C. Methane hydrate was formed in the pressure vessel after 2 days. The chamber was vented and flushed over the course of 26 minutes in an attempt to remove the CH₄ from the headspace. The temperature in the chamber increased to 6°C and the hydrate dissolved. The chamber was repressurized with a headspace of 50% CH₄ and 50% air and 94 atm. Insulation was added to the chamber and again the headspace was vented and flushed over the course of 14 minutes. The temperature in the chamber increased to 2°C and the hydrate dissolved. The chamber was repressurized to 93 atm. The experiment was stopped due to difficulty maintaining hydrate for dissolution experimentation.

The dissolution experiment design was based on methods from Lapham et al. 2014, where a solid block of CH₄ hydrate was formed in the chamber. After formation the hydrate was surrounded with CH₄-free liquid and the dissolution experiment was initiated. Because the hydrate could not be stabilized in order to set up the experiment, dissolution rates could not be measured.

Appendix H: Bottom Water Enrichment

The water was collected and stored in a 4L cubitainer at 4°C until back at the lab. 75 mL of bottom water was added to sterile 157 mL glass culture vials that were fitted with autoclaved blue septa and collars. With the stoppers in place, the vial volume was 157 mL. With 75 mL of liquid added there was a headspace of 82 mL in the vials. To achieve a 50% CH₄ headspace, syringes containing 82 mL of 100% CH₄ were equilibrated with the vial headspaces (containing 100% lab air). Vial headspaces were generated at 1 and 2 atm. Vials were prepared by removing the excess 82 mL of the equilibrated gas from the vials that contained 1 atm headspace gas and pressurizing the vials with the excess 82 mL vials that contained 2 atm headspace gas. Triplicate vials of each pressure condition (6 total) were then incubated at 30°C, 10°C, and 4°C for 90 days. Sampling occurred every week for the first month and then once a month for the following two months. Liquid samples were taken by equilibrating 1 mL of autoclaved bottom water with each vial and removing a 1 mL sample and measuring optical density at 405 nm.

Appendix I: Culture Vial Headspace Analysis

Culture Vial I

Passage 1: Headspace gas composition and isotope analysis was performed after 53 days and found to be 21.4% CH₄ and $-33.94 \pm 0.07 \delta^{13}\text{C-CH}_4$.

Passage 2: In the second passage, CH₄ concentrations decreased from 27.7 to 17.4%, though the initial measurement was lost. This represents a change in CH₄ concentrations over time of at least 10.3% over 32 days (Fig 2.8a). CH₄ concentrations in the biotic control ranged from 0.0 to 0.2 % and CH₄ concentrations ranged from 61.3 to 49.7% in the abiotic control, over the course of the experiment. Growth of the culture was also monitored via stable carbon isotopes of the CH₄ (Fig 2.8b). In the beginning of the experiment, $\delta^{13}\text{C-CH}_4$ values were -32.7‰ (treatment) and -41.0‰ (abiotic control). After 32 days, values were similar for the treatment (-33.1‰) and slightly heavier for the abiotic control (-38.0‰). Stable isotopes were not measured for the biotic control because methane concentrations were too low. A methane oxidation rate of 0.45 %CH₄ d⁻¹ and $\Delta^{13}\text{C-CH}_4$ of 0.4 ‰ were measured during the second passage (Table 2.4).

Passage 3: In the third passage at optimal conditions, headspace CH₄ concentrations decreased from 50.2 to 19.9% over 20 days (Fig 2.9a). CH₄ concentrations in the biotic control ranged from 0.0-0.1% and CH₄ concentrations ranged from 59.1-29.3% in the abiotic control. Also $\delta^{13}\text{C-CH}_4$ values were measured at -39.1‰ (treatment) and -38.9‰ (abiotic control) and were measured at -32.7‰ (treatment) and -37.7‰ (abiotic control) after 20 days of growth (Fig 2.9b). Stable isotopes were not measured for the biotic control because methane concentrations were too low. A methane oxidation rate of 0.76 %CH₄ d⁻¹ and $\Delta^{13}\text{C-CH}_4$ of 6.4 ‰ were measured during the third passage (Table 2.4).

Culture Vial II

Copper Addition: The headspace CH₄ ranged from 20.6 to 48.3% in the regular and copper media treatments and the abiotic controls, initially around 30%, then increasing to over 40% CH₄, and then decreasing back to around 30% (Fig 2.11). The biotic control headspace CH₄ ranged from below detection to 6.0% (Fig 2.11). Analysis of headspace CH₄ concentrations in the treatment and abiotic control culture

vials revealed a pattern, where CH₄ decreased and then increased, that does not seem to indicate growth, but is very unclear. This was most likely due to operator error and the development of a new method used after the first two time points.

Appendix J: Chesapeake Bay Supplemental

Diffusion Calculations

The first deployment pore-water coil was crimped on 9 September 2013, 56 days after retrieval and 154 days after deployment. The first deployment bottom water coil was crimped on 11 November 2013, 110 days after retrieval and 208 days after deployment. The second deployment pore-water coil was crimped on 13 November 2013, 14 days after retrieval and 111 days after deployment. The second deployment bottom water coil was crimped on 15 November 2013, 16 days after retrieval and 113 days after deployment. Over the sampling periods the *in situ* temperatures ranged from 7 °C to 25 °C and salinity from 13 ‰ to 23 ‰. After retrieval the coils were stored at 2 °C until crimping. Diffusion was calculated using maximum values of 208 days at 25 °C and 13 ‰ salinity to obtain a “worst case scenario” diffusion coefficient. Diffusion coefficients, D , were calculated under these conditions for CH_4 and SO_4 to be $1.684 \times 10^{-5} \text{ cm}^2 \text{ day}^{-1}$ for CH_4 and $1.041 \times 10^{-5} \text{ cm}^2 \text{ day}^{-1}$ for SO_4 (Chemical Oceanography 1975). Because flow-induced dispersion is reduced in sub-millimeter tubing (Taylor, 1953), we calculated effective diffusion coefficients, k . Given the tubing inner radius, $r = .04 \text{ cm}$, and the velocity, $v = 0.72 \text{ mL day}^{-1} = 0.00185 \text{ cm s}^{-1}$, the effective diffusion coefficients were calculated using equation 1.

$$k = \frac{r^2 v^2}{48D} \quad \text{Equation 1}$$

To account for the additive effects of fluid flow and diffusion along the tubing, the sums of these two effects were calculated using equation 2.

$$k' = k + D \quad \text{Equation 2}$$

A dispersion gradient was calculated using k' for the period of 208 days and equation 3 (Jannasch et al., 2004).

$$C(x, t) = \frac{C_0}{2} \operatorname{erf} \frac{x}{2\sqrt{D't}} \quad \text{Equation 3}$$

The dispersion gradients for CH₄ and sulfate are shown in Figure J.1, where the CH₄ and the SO₄ sample had an initial relative concentration of 1 to the left of the tube length zero and a relative concentration of zero to the right. Due to dispersion from diffusion as well as fluid flow, these concentrations will mix along the axis of the tubing both to the right and to the left. In the case of the 50 cm sections used for SO₄ analysis, at least 82% of the sample will be contained within that section. However, SO₄ sample sections are located in between 4.5 m sections used for CH₄

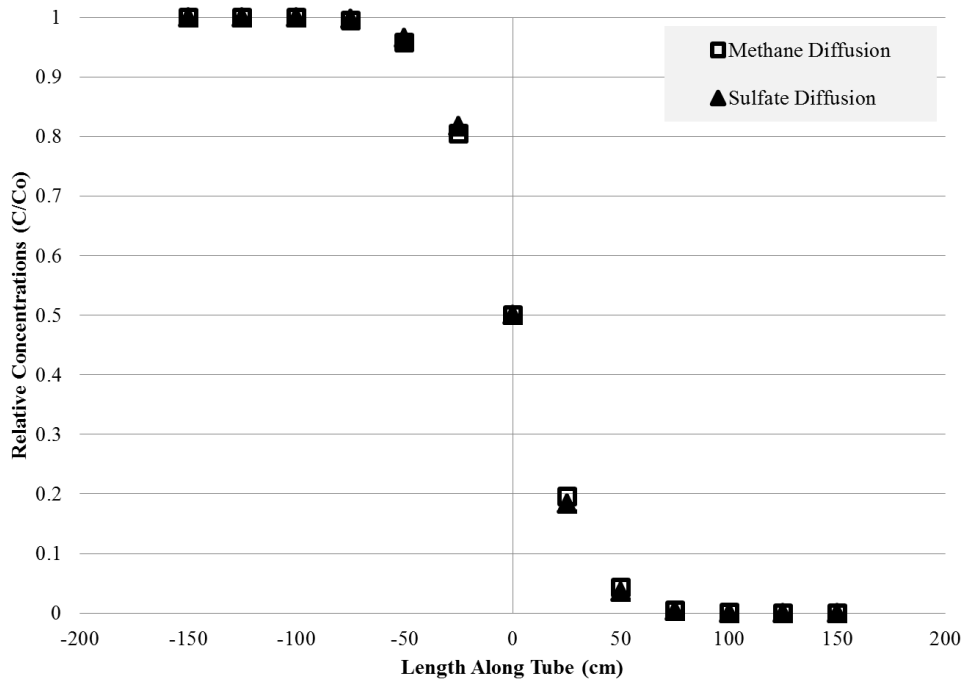


Figure J.1. Dispersion gradients for methane and sulfate along the copper sample tubing axis.

analysis. Each SO₄ sample could contain up to 18% of sulfate from nearby sample collected at close to the same time (within a day) and are separated from the next sample by 4.5 m. When we consider the SO₄ sections as 4.5 m sections, greater than 99% of the sample is contained in these 4.5 m sections that separate the 50 cm SO₄ sections. For the 4.5 m sections used for CH₄ analysis, greater than 99% of the sample will be contained within the sample section.

Table J.1. Chesapeake Bay OsmoSampler general sampling Data.

Deployment	First Deployment		Second Deployment	
Date of Deployment	17 April to 24 July		25 July to October 30	
Days of Deployment	98		97	
Pump	Pump A	Pump B	Pump A	Pump B
Sample	Bottom Water	Pore-water	Pore-Water	Bottom Water
Crimping Date	11 November 2013	9 September 2013	13 November 2013	15 November 2013
Number of Samples	19	24	25	30
OLW DOC Samples Pooled	19, 17, 15, 13, 11	9, 7, 5, 3, 1	27, 25, 23, 21, 19, 17	15, 13, 11, 9, 7, 5, 3, 1
PW DOC Samples Pooled	23, 21, 19, 17, 15, 13	11, 9, 7, 5, 3	25, 23, 21, 19, 17, 15	13, 11, 9, 7, 5, 3, 1

Table J.2 Chesapeake Bay OsmoSampler Pore-water Data.

OsmoSampler Pore-water Data						
Sample	Date	OsmoSampler Salinity	mM Methane	mM Carbon Dioxide	$\delta^{13}\text{C-CH}_4$	Sulfate mM
24	4/17/2013	18	-	-	-	12.54
23	4/21/2013	18	0.03	2.51	ND	12.12
22	4/25/2013	17	-	-	-	9.69
21	4/29/2013	17	0.16	0.30	ND	5.94
20	5/4/2013	18	-	-	-	1.96
19	5/8/2013	19	0.76	3.71	-48.9	0.00
18	5/12/2013	20	-	-	-	0.00
17	5/16/2013	20	1.45	4.02	-56.8	0.00
16	5/21/2013	20	-	-	-	0.00
15	5/25/2013	20	2.87	3.44	-65.3	0.00
14	5/29/2013	20	-	-	-	0.00
13	6/2/2013	20	4.63	4.80	-66.6	0.00
12	6/7/2013	21	-	-	-	0.00
11	6/11/2013	20	5.48	5.74	-63.0	0.00
10	6/15/2013	20	-	-	-	0.00
9	6/20/2013	20	5.37	7.84	-59.6	0.00
8	6/24/2013	20	-	-	-	0.00
7	6/28/2013	21	5.15	8.38	-60.2	0.00
6	7/2/2013	20	-	-	-	0.00
5	7/7/2013	20	4.31	7.68	-59.0	0.00
4	7/11/2013	21	-	-	-	0.00
3	7/15/2013	21	3.67	1.10	-57.7	0.00
2	7/19/2013	21	-	-	-	0.00
1	7/24/2013	21	ND	ND	ND	0.00
26	7/25/2013	16	-	-	-	12.46
25	7/28/2013	24	0.05	0.00	ND	17.71
24	8/1/2013	22	-	-	-	17.45
23	8/5/2013	23	0.38	0.00	-62.4	18.03
22	8/9/2013	25	-	-	-	19.00
21	8/13/2013	23	0.20	0.00	ND	17.76
20	8/17/2013	24	-	-	-	18.78
19	8/20/2013	23	0.10	0.00	ND	18.02
18	8/24/2013	22	-	-	-	17.40
17	8/28/2013	22	0.04	0.00	ND	17.00
16	9/1/2013	22	-	-	-	15.26

15	9/5/2013	23	0.05	0.00	ND	17.50
14	9/9/2013	23	-	-	-	18.09
13	9/13/2013	23	0.02	0.00	ND	17.84
12	9/16/2013	23	-	-	-	15.11
11	9/20/2013	23	0.39	1.37	-55.7	9.85
10	9/24/2013	23	-	-	-	4.98
9	9/28/2013	22	0.74	5.29	-57.6	1.20
8	10/2/2013	23	-	-	-	0.00
7	10/6/2013	23	1.75	6.72	-62.5	0.00
6	10/9/2013	23	-	-	-	0.00
5	10/13/2013	23	3.20	9.41	-65.3	0.00
4	10/17/2013	23	-	-	-	0.00
3	10/21/2013	22	3.08	8.98	-60.1	0.00
2	10/25/2013	24	-	-	-	1.56
1	10/29/2013	24	2.78	6.24	-58.1	6.02

Table J.3 Chesapeake Bay OsmoSampler bottom water Data.

OsmoSampler Bottom Water Data				
Sample	Date	OsmoSampler Salinity ppt	mM Methane	mM Sulfate
19	4/17/2013	19	0.91	14.60
18	4/22/2013	17	-	13.83
17	4/27/2013	18	0.96	14.75
16	5/2/2013	22	-	17.44
15	5/7/2013	24	1.11	17.80
14	5/13/2013	23	-	17.71
13	5/18/2013	21	1.86	16.18
12	5/23/2013	19	-	14.30
11	5/28/2013	18	3.18	13.72
10	6/2/2013	20	-	14.80
9	6/8/2013	21	9.19	15.95
8	6/13/2013	21	-	15.93
7	6/18/2013	21	20.66	16.08
6	6/23/2013	21	-	15.85
5	6/28/2013	21	17.46	15.69
4	7/4/2013	21	-	15.35
3	7/9/2013	21	29.49	14.96
2	7/14/2013	20	-	14.91
1	7/19/2013	26	40.71	17.66
27	8/3/2013	24	17.11	18.05
26	8/7/2013	25	-	19.14
25	8/10/2013	24	12.15	18.33
24	8/13/2013	25	-	18.65
23	8/17/2013	24	8.54	18.23
22	8/20/2013	23	-	17.26
21	8/23/2013	22	5.69	18.43
20	8/27/2013	21	-	18.74
19	8/30/2013	22	3.10	19.00
18	9/2/2013	22	-	18.99
17	9/6/2013	23	0.42	19.49
16	9/9/2013	23	-	19.59
15	9/12/2013	23	1.70	19.31
14	9/16/2013	22	-	18.80
13	9/19/2013	21	2.43	18.47

12	9/22/2013	21	-	17.94
11	9/26/2013	21	1.29	17.68
10	9/29/2013	21	-	18.01
9	10/2/2013	24	0.26	20.05
8	10/6/2013	25	-	20.73
7	10/9/2013	25	-0.02	20.52
6	10/12/2013	24	-	19.79
5	10/16/2013	22	-0.02	18.30
4	10/19/2013	21	-	16.98
3	10/22/2013	23	0.01	18.70
2	10/26/2013	24	-	18.34
1	10/29/2013	23	0.00	17.47

Table J.4

Sensor data measurements were averaged for each day. Data collected during part of the second deployment (25 July 2013 to 21 August 2013) was from a nearby lander. The full dataset is located on the lab server (L:\CB osmo deployments).

Sensor Bottom Water Data			
Date	DO μM	Temperature	Salinity ppt
4/17/2013	109.00	6.95	17.47
4/18/2013	105.51	6.89	17.74
4/19/2013	96.00	6.93	17.66
4/20/2013	96.10	7.31	17.02
4/21/2013	98.61	7.33	17.85
4/22/2013	103.81	7.93	17.92
4/23/2013	98.52	8.26	17.85
4/24/2013	96.10	8.82	17.74
4/25/2013	94.06	9.17	17.12
4/26/2013	76.19	9.35	17.47
4/27/2013	69.74	9.56	17.24
4/28/2013	65.74	9.91	16.90
4/29/2013	62.63	10.37	16.28
4/30/2013	62.06	10.79	15.60
5/1/2013	27.16	10.39	16.51
5/2/2013	14.71	10.43	16.71
5/3/2013	6.69	10.84	16.79
5/4/2013	35.99	12.14	17.44
5/5/2013	88.68	13.44	18.16
5/6/2013	94.81	13.69	18.39
5/7/2013	132.93	14.14	19.41
5/8/2013	138.87	14.29	20.15
5/9/2013	141.67	14.35	20.77
5/10/2013	137.20	14.34	21.09
5/11/2013	123.97	14.35	21.22
5/12/2013	121.61	14.39	21.54
5/13/2013	115.60	14.60	22.21
5/14/2013	66.34	14.77	22.30
5/15/2013	103.77	14.86	22.15
5/16/2013	85.03	14.84	21.70

5/17/2013	69.70	14.88	22.05
5/18/2013	70.14	14.97	22.09
5/19/2013	55.06	14.90	21.83
5/20/2013	42.56	14.95	21.94
5/21/2013	45.08	14.95	21.78
5/22/2013	31.35	14.97	21.66
5/23/2013	19.75	14.93	21.31
5/24/2013	18.11	14.92	21.24
5/25/2013	23.29	15.28	21.61
5/26/2013	6.84	15.71	20.67
5/27/2013	0.60	15.95	20.16
5/28/2013	3.77	16.16	19.64
5/29/2013	20.96	16.23	19.08
5/30/2013	15.61	16.16	18.82
5/31/2013	8.14	16.25	18.37
6/1/2013	2.36	16.33	17.98
6/2/2013	0.65	16.36	17.71
6/3/2013	0.61	16.34	17.55
6/4/2013	0.61	16.35	18.49
6/5/2013	0.61	16.54	18.47
6/6/2013	0.61	16.72	18.01
6/7/2013	0.60	17.15	17.22
6/8/2013	0.60	17.28	16.83
6/9/2013	0.61	17.07	17.19
6/10/2013	0.60	17.19	17.35
6/11/2013	0.60	17.47	17.02
6/12/2013	0.60	17.45	17.33
6/13/2013	5.96	18.44	18.32
6/14/2013	12.28	19.29	18.91
6/15/2013	19.98	20.40	19.74
6/16/2013	13.19	20.45	19.35
6/17/2013	8.11	20.47	19.17
6/18/2013	1.41	20.63	18.80
6/19/2013	3.69	20.97	19.27
6/20/2013	6.26	21.43	19.52
6/21/2013	0.87	21.40	19.14
6/22/2013	0.55	21.47	19.10
6/23/2013	0.55	21.46	19.04
6/24/2013	0.55	21.50	18.86
6/25/2013	0.54	21.58	19.20
6/26/2013	0.54	21.63	19.58

6/27/2013	0.54	21.67	19.74
6/28/2013	0.54	21.70	19.56
6/29/2013	0.54	21.74	19.61
6/30/2013	0.54	21.72	19.44
7/1/2013	0.54	21.68	19.12
7/2/2013	0.54	21.60	18.25
7/3/2013	0.54	21.71	19.39
7/4/2013	0.54	21.77	19.56
7/5/2013	0.54	21.77	19.47
7/6/2013	0.55	21.80	19.52
7/7/2013	0.54	21.81	19.41
7/8/2013	0.55	21.83	19.37
7/9/2013	0.54	21.89	19.22
7/10/2013	0.54	21.97	19.02
7/11/2013	0.55	22.09	18.72
7/12/2013	0.54	22.13	18.84
7/13/2013	0.54	22.29	18.92
7/14/2013	0.54	22.79	18.52
7/15/2013	0.54	22.99	18.31
7/16/2013	0.54	22.99	18.41
7/17/2013	0.53	23.07	18.51
7/18/2013	0.53	23.60	18.33
7/19/2013	0.52	24.04	18.18
7/20/2013	0.52	24.33	18.35
7/21/2013	0.50	25.40	20.90
7/22/2013	0.50	25.37	19.45
Second Deployment			
8/21/2013	1.49	25.05	25.05
8/22/2013	1.34	25.05	25.05
8/23/2013	1.33	25.03	25.03
8/24/2013	7.67	25.03	25.03
8/25/2013	17.04	24.97	24.97
8/26/2013	15.91	24.93	24.93
8/27/2013	16.98	24.88	24.88
8/28/2013	32.68	24.79	24.79
8/29/2013	39.97	24.75	24.75
8/30/2013	37.35	24.71	24.71
8/31/2013	28.26	24.72	24.72
9/1/2013	13.45	24.75	24.75
9/2/2013	13.55	24.68	24.68
9/3/2013	14.94	24.66	24.66

9/4/2013	11.02	24.64	24.64
9/5/2013	4.02	24.62	24.62
9/6/2013	7.43	24.62	24.62
9/7/2013	7.64	24.62	24.62
9/8/2013	2.46	24.64	24.64
9/9/2013	1.47	24.66	24.66
9/10/2013	1.31	24.66	24.66
9/11/2013	1.27	24.68	24.68
9/12/2013	1.27	24.68	24.68
9/13/2013	1.28	24.68	24.68
9/14/2013	1.41	24.72	24.72
9/15/2013	1.57	24.77	24.77
9/16/2013	1.56	24.73	24.73
9/17/2013	1.78	24.81	24.81
9/18/2013	3.65	24.89	24.89
9/19/2013	6.77	24.74	24.74
9/20/2013	7.19	24.62	24.62
9/21/2013	9.37	24.44	24.44
9/22/2013	16.06	24.26	24.26
9/23/2013	11.30	24.61	24.61
9/24/2013	15.46	24.62	24.62
9/25/2013	27.42	24.43	24.43
9/26/2013	95.86	23.60	23.60
9/27/2013	120.51	23.35	23.35
9/28/2013	128.91	23.10	23.10
9/29/2013	139.49	22.60	22.60
9/30/2013	134.72	22.44	22.44
10/1/2013	120.24	22.45	22.45
10/2/2013	110.84	22.44	22.44
10/3/2013	98.65	22.43	22.43
10/4/2013	99.28	22.41	22.41
10/5/2013	93.74	22.36	22.36
10/6/2013	90.22	22.29	22.29
10/7/2013	78.97	22.26	22.26
10/8/2013	70.34	22.21	22.21
10/9/2013	76.20	22.01	22.01
10/10/2013	122.84	21.61	21.61
10/11/2013	137.46	21.46	21.46
10/12/2013	147.54	21.27	21.27
10/13/2013	165.62	21.03	21.03
10/14/2013	166.78	20.93	20.93

10/15/2013	173.61	20.75	20.75
10/16/2013	171.52	20.67	20.67
10/17/2013	171.08	20.56	20.56
10/18/2013	163.78	20.55	20.55
10/19/2013	158.59	20.61	20.61
10/20/2013	163.94	20.46	20.46
10/21/2013	180.22	20.23	20.23
10/22/2013	169.63	20.23	20.23
10/23/2013	170.63	20.12	20.12
10/24/2013	171.43	19.95	19.95
10/25/2013	163.16	19.89	19.89
10/26/2013	168.01	19.51	19.51
10/27/2013	157.10	19.54	19.54
10/28/2013	161.52	19.31	19.31
10/29/2013	156.49	19.19	19.19
10/30/2013	158.80	19.10	19.10

Bibliography

- Allen D. T., Torres V. M., Thomas J., Sullivan D. W., Harrison M., Hendler A., Herndon S. C., Kolb C. E., Fraser M. P., Hill A. D., Lamb B. K., Miskimins J., Sawyer R. F. and Seinfeld J. H. (2013) Measurements of methane emissions at natural gas production sites in the United States. *Proc. Natl. Acad. Sci. U. S. A.* **110**, 17768–17773.
- De Angelis M. A. and Scranton M. I. (1993) Fate of methane in the Hudson River and estuary. *Global Biogeochem. Cycles* **7**, 509–523.
- Anisimov O. A. (2007) Potential feedback of thawing permafrost to the global climate system through methane emission. *Environ. Res. Lett.* **2**.
- Balasubramanian R., Smith S. M., Rawat S., Yatsunyk L. A., Stemmler T. L. and Rosenzweig A. C. (2010) Oxidation of methane by a biological dicopper centre. *Nature* **465**, 115–119.
- Bastviken D., Tranvik L. J., Downing J. A., Crill P. M. and Enrich-Prast A. (2011) Freshwater methane emissions offset the continental carbon sink. *Science* **331**, 50.
- Beal E. J., House C. H. and Orphan V. J. (2009) Manganese- and iron-dependent marine methane oxidation. *Science* **325**, 184–187.
- Beaven A. E. and Paynter K. T. (1999) Acidification of the phagosome in *Crassostrea virginica* hemocytes following engulfment of zymosan. *Biol. Bull.* **196**, 26–33.
- Boetius A., Ravensschlag K., Schubert C. J., Rickert D., Widdel F., Gieseke A., Amann R., Jørgensen B. B., Witte U. and Pfannkuche O. (2000) A marine microbial consortium apparently mediating anaerobic oxidation of methane. *Nature* **407**, 623–626.
- Bousquet P., Ringeval B., Pison I., Dlugokencky E. J., Brunke E.-G., Carouge C., Chevallier F., Fortems-Cheiney A., Frankenberg C., Hauglustaine D. a., Krummel P. B., Langenfelds R. L., Ramonet M., Schmidt M., Steele L. P., Szopa S., Yver C., Viovy N. and Ciais P. (2011) Source attribution of the changes in atmospheric methane for 2006–2008. *Atmos. Chem. Phys.* **11**, 3689–3700.
- Bowman J. P., Sly L. I. and Stackebrandt E. (1995) The Phylogenetic Position Of The Family Methylococcaceae (VOL 45, PG 184, 1995). *Int. J. Syst. Bacteriol.* **45**, 185–185.

- Brewer P., Paull G. C., Peltzer E. T., Ussler W., Rehder G. and Friederich G. (2002) Measurements of the fate of gas hydrates during transit through the ocean water column. *Geophys. Res. Lett.* **29**, 1–4.
- Burdige D. J. (2006) *Geochemistry of Marine Sediments*. 1st ed., Princeton University Press, Princeton, NJ.
- Burdige D. J., Alperin M. J., Homstead J. and Martens C. S. (1992) The Role of Benthic Fluxes of Dissolved Organic Carbon in Oceanic and Sedimentary Carbon Cycling. *Geophys. Res. Lett.* **19**, 1851.
- Burdige D. J. and Gardner K. G. (1998) Molecular weight distribution of dissolved organic carbon in marine sediment pore waters. *Mar. Chem.* **62**, 45–64.
- Cao M., Gregson K. and Marshall S. (1998) Global methane emission from wetlands and its sensitivity to climate change. *Atmos. Environ.* **32**, 3293–3299.
- Cicerone R. J. and Oremland R. S. (1988) Biogeochemical Aspects of Atmospheric Methane. *Global Biogeochem. Cycles* **2**, 299–327.
- Coleman D. D., Risatti J. B. and Schoell M. (1981) Fractionation of carbon and hydrogen isotopes by methane-oxidizing bacteria. *Geochim. Cosmochim. Acta* **45**, 1033–1037.
- Colman S. M., Halka J. P., Hobbs C. H., Mixon R. B. and Foster D. S. (1990) Ancient channels of the Susquehanna River beneath Chesapeake Bay and the Delmarva Peninsula. *Geol. Soc. Am. Bull.* **102**, 1268–1279.
- Craig H. and Chou C. C. (1982) Methane: The record in polar ice cores. *Geophys. Res. Lett.* **9**, 1221–1224.
- Crespo-Medina M., Meile C. D., Hunter K. S., Diercks A.-R., Asper V. L., Orphan V. J., Tavormina P. L., Nigro L. M., Battles J. J., Chanton J. P., Shiller A. M., Joung D.-J., Amon R. M. W., Bracco A., Montoya J. P., Villareal T. A., Wood A. M. and Joye S. B. (2014) The rise and fall of methanotrophy following a deepwater oil-well blowout. *Nat. Geosci.* **7**, 423–427.
- Dedysh S. N. and Dunfield P. F. (2011) Facultative and obligate methanotrophs: How to identify and differentiate Them. *Methods Enzymol.* **495**, 31–44.
- Diaz R. J. (2001) Overview of hypoxia around the world. *J. Environ. Qual.* **30**, 275–81.
- Diaz R. J. and Solow A. (1999) *Ecological and Economic Consequences of Hypoxia.*, Silver Spring, Maryland.

- Dlugokencky E. J. (2003) Atmospheric methane levels off: Temporary pause or a new steady-state? *Geophys. Res. Lett.* **30**.
- Dlugokencky E. J., Steele L. P., Lang P. M. and Masarie K. A. (1994) The Growth Rate and Distribution of Atmospheric Methane. *J. Geophys. Res. - Atmos.* **99**, 17021–17043.
- Duan Z. and Mao S. (2006) A thermodynamic model for calculating methane solubility, density and gas phase composition of methane-bearing aqueous fluids from 273 to 523 K and from 1 to 2000 bar. *Geochim. Cosmochim. Acta* **70**, 3369–3386.
- Faure G. and Mensing T. M. (2009) *Isotopes: Principles and Applications*. 3rd ed., John Wiley and Sons, Inc., Hoboken, NJ.
- Forster P. V., Ramaswamy P., Bernsten A., T. Betts R., Fahey D. W., Haywood J., Lean J., Lowe D. C., Myhre G., Nganga J., Prinn R., Raga G., Schulz M. and Van Dorland R. (2007) Changes in Atmospheric Constituents and in Radiative Forcing. In *Climate Change 2007: The Physical Science Basis. Contribution of Working Group I to the Fourth Assessment Report of the Intergovernmental Panel on Climate Change* (eds. S. Solomon, D. Qin, M. Manning, Z. Chen, M. Marquis, K. B. Averyt, M. Tignor, and H. L. Miller). Cambridge University Press, Cambridge, United Kingdom and New York, NY, USA.
- Froelich P. N., Klinkhammer G. P., Bender M. L., Luedtke N. A., Heath G. R., Cullen D., Dauphin P., Hammond D., Hartman B. and Maynard V. (1979) Early oxidation of organic matter in pelagic sediments of the eastern equatorial Atlantic: suboxic diagenesis. *Geochim. Cosmochim. Acta* **43**, 1075–1090.
- Fung I. (1991) Three-dimensional model synthesis of the global methane cycle. *J. Geophys. Res.* **96**, 13,033–13,065.
- Garcia-Gil S., Vilas F. and Garcia-Garcia A. (2002) Shallow gas features in incised-valley fills (Ria de Vigo, NW Spain): A case study. In *Continental Shelf Research* pp. 2303–2315.
- Glasgow H. B. and Burkholder J. M. (2000) Water Quality Trends And Management Implications From A Five-Year Study Of A Eutrophic Estuary. *Ecol. Appl.* **10**, 1024–1046.
- Grass G., Rensing C. and Solioz M. (2011) Metallic copper as an antimicrobial surface. *Appl. Environ. Microbiol.* **77**, 1541–1547.
- Hagen R. A. and Vogt P. R. (1999) Seasonal Variability of Shallow Biogenic Gas in the Chesapeake Bay. *Mar. Geol.* **158**, 75–88.

- Hansell D. A. and Carlson C. A. (2002) Biogeochemistry of Marine Dissolved Organic Matter. In (eds. D. A. Hansell and C. A. Carlson). Academic Press, San Diego, California.
- Hansen J. E. and Sato M. (2001) Trends of measured climate forcing agents. *Proc. Natl. Acad. Sci. U. S. A.* **98**, 14778–14783.
- Hanson R. S. and Hanson T. E. (1996) Methanotrophic bacteria. *Microbiol. Rev.* **60**, 439–471.
- Hill J. M. (1992) Distribution of Shallow Gas on Bulk Estuary Sediment Properties. *Cont. Shelf Res.* **12**, 1219–1229.
- Hoagland P., Anderson D. M., Kaoru Y. and White A. W. (2002) The economic effects of harmful algal blooms in the United States: Estimates, assessment issues, and information needs. *Estuaries* **25**, 819–837.
- Hoehler T. M., Alperin M. J., Albert D. B. and Martens C. S. (1994) Field and laboratory studies of methane oxidation in an anoxic marine sediment: Evidence for a methanogen-sulfate reducer consortium. *Global Biogeochem. Cycles* **8**, 451–463.
- Hoehler T. M., Alperin M. J., Albert D. B. and Martens C. S. (1998) Thermodynamic control on hydrogen concentrations in anoxic sediments. **62**, 1745–1756.
- Inagaki F., Tsunogai U., Suzuki M., Kosaka A., Machiyama H., Takai K., Nunoura T., Nealson K. H. and Horikoshi K. (2004) Characterization of C1-metabolizing prokaryotic communities in methane seep habitats at the Kuroshima Knoll, southern Ryukyu Arc, by analyzing *pmoA*, *mmoX*, *mxoF*, *mcrA*, and 16S rRNA genes. *Appl. Environ. Microbiol.* **70**, 7445–7455.
- Jannasch H. W., Wheat C. G., Plant J., Kastner M. and Stakes D. (2004) Continuous chemical monitoring with osmotically pumped water samplers: OsmoSampler design and applications. *Limnol. Oceanogr. Methods* **2**, 102–113.
- Karion A., Sweeney C., Petron G., Frost G., Michael Hardesty R., Kofler J., Miller B. R., Newberger T., Wolter S., Banta R., Brewer A., Dlugokencky E., Lang P., Montzka S. A., Schnell R., Tans P., Trainer M., Zamora R. and Conley S. (2013) Methane emissions estimate from airborne measurements over a western United States natural gas field. *Geophys. Res. Lett.* **40**, 4393–4397.
- Kawano M. and Hwang J. (2011) Roles of microbial acidic polysaccharides in precipitation rate and polymorph of calcium carbonate minerals. *Appl. Clay Sci.* **51**, 484–490.

- Kemp W., Boynton W., Adolf J., Boesch D., Boicourt W., Brush G., Cornwell J., Fisher T., Glibert P., Hagy J., Harding L., Houde E., Kimmel D., Miller W., Newell R., Roman M., Smith E. and Stevenson J. (2005) Eutrophication of Chesapeake Bay: historical trends and ecological interactions. *Mar. Ecol. Prog. Ser.* **303**, 1–29.
- Kessler J. D. (2011) A Persistent Oxygen Anomaly Reveals the Fate of Spilled Methane in the Deep Gulf of Mexico John D. Kessler ,. *Science (80-.)*. **312**.
- Kinnaman F. S., Valentine D. L. and Tyler S. C. (2007) Carbon and hydrogen isotope fractionation associated with the aerobic microbial oxidation of methane, ethane, propane and butane. *Geochim. Cosmochim. Acta* **71**, 271–283.
- Kirschke S., Bousquet P., Ciais P., Saunois M., Canadell J. G., Dlugokencky E. J., Bergamaschi P., Bergmann D., Blake D. R., Bruhwiler L., Cameron-Smith P., Castaldi S., Chevallier F., Feng L., Fraser A., Heimann M., Hodson E. L., Houweling S., Josse B., Fraser P. J., Krummel P. B., Lamarque J.-F., Langenfelds R. L., Le Quércé C., Naik V., O’Doherty S., Palmer P. I., Pison I., Plummer D., Poulter B., Prinn R. G., Rigby M., Ringeval B., Santini M., Schmidt M., Shindell D. T., Simpson I. J., Spahni R., Steele L. P., Strode S. a., Sudo K., Szopa S., van der Werf G. R., Voulgarakis A., van Weele M., Weiss R. F., Williams J. E. and Zeng G. (2013) Three decades of global methane sources and sinks. *Nat. Geosci.* **6**, 813–823.
- Krause S., Aloisi G., Engel A., Liebetrau V. and Treude T. (2014) Enhanced Calcite Dissolution in the Presence of the Aerobic Methanotroph *Methylosinus trichosporium*. *Geomicrobiol. J.* **31**, 325–337.
- Kvenvolden K. A. (1988) Methane hydrate — A major reservoir of carbon in the shallow geosphere? *Chem. Geol.* **71**, 41–51.
- Lanoil B. D., Sassen R., La Duc M. T., Sweet S. T. and Nealson K. H. (2001) Bacteria and Archaea Physically Associated with Gulf of Mexico Gas Hydrates. *Appl. Environ. Microbiol.* **67**, 5143–5153.
- Lapham L. L., Chanton J. P., Chapman R. and Martens C. S. (2010) Methane under-saturated fluids in deep-sea sediments: Implications for gas hydrate stability and rates of dissolution. *Earth Planet. Sci. Lett.* **298**, 275–285.
- Lapham L. L., Wilson R. M. and Chanton J. P. (2012) Pressurized laboratory experiments show no stable carbon isotope fractionation of methane during gas hydrate dissolution and dissociation. *Rapid Commun. Mass Spectrom.* **26**, 32–36.
- Lapham L. L., Wilson R. M., MacDonald I. R. and Chanton J. P. (2014) Gas hydrate dissolution rates quantified with laboratory and seafloor experiments. *Geochim. Cosmochim. Acta* **125**, 492–503.

- Lovley D. R. and Goodwin S. (1988) Hydrogen concentrations as an indicator of the predominant terminal electron-accepting reactions in aquatic sediments. *Geochim. Cosmochim. Acta* **52**, 2993–3003.
- Lovley D. R. and Klug M. J. (1986) Model for the distribution of sulfate reduction and methanogenesis in freshwater sediments. *Geochim. Cosmochim. Acta* **50**, 11–18.
- Martin W. R. and McCorkle D. C. (1993) Dissolved organic carbon concentrations in marine pore waters determined by high-temperature oxidation. *Limnol. Oceanogr.* **38**, 1464–1479.
- Maslin M., Owen M., Betts R., Day S., Dunkley Jones T. and Ridgwell A. (2010) Gas hydrates: past and future geohazard? *Philos Trans A Math Phys Eng Sci* **368**, 2369–2393.
- McGinnis D. F., Greinert J., Artemov Y., Beaubien S. E. and West A. (2006) Fate of rising methane bubbles in stratified waters: How much methane reaches the atmosphere? *J. Geophys. Res. C Ocean.* **111**.
- Middelburg J., Nieuwenhuize J., Iversen N., Hogh N., de Wilde H., Helder W., Seifert R. and Christof O. (2002) Methane distribution in European tidal estuaries. *Biogeochemistry* **59**, 95–119.
- Milkov A. V. (2004) Global estimates of hydrate-bound gas in marine sediments: How much is really out there? *Earth-Science Rev.* **66**, 183–197.
- Mitchell J. F. B. (1989) The “Greenhouse” effect and climate change. *Rev. Geophys.* **27**, 115–139.
- Nisbet E. G., Dlugokencky E. J. and Bousquet P. (2014) Atmospheric science. Methane on the rise--again. *Science* **343**, 493–495.
- Orcutt B. N., Boetius A., Lugo S. K., MacDonald I. R., Samarkin V. A. and Joye S. B. (2004) Life at the edge of methane ice: microbial cycling of carbon and sulfur in Gulf of Mexico gas hydrates. *Chem. Geol.* **205**, 239–251.
- Rabalais N. N., Turner R. E., Diaz R. J. and Justic D. (2009) Global change and eutrophication of coastal waters. *ICES J. Mar. Sci.* **66**, 1528–1537.
- Raghoebarsing A. A., Pol A., van de Pas-Schoonen K. T., Smolders A. J. P., Ettwig K. F., Rijpstra W. I. C., Schouten S., Damsté J. S. S., Op den Camp H. J. M., Jetten M. S. M. and Strous M. (2006) A microbial consortium couples anaerobic methane oxidation to denitrification. *Nature* **440**, 918–921.

- Reeburgh W. S. (1969) Observations of gases in Chesapeake Bay sediments. *Limnol. Oceanogr.* **14**, 368–375.
- Reeburgh W. S. (2007) Oceanic methane biogeochemistry. *Chem. Rev.* **107**, 486–513.
- Rehder G., Kirby S. H., Durham W. B., Stern L. A., Peltzer E. T., Pinkston J. and Brewer P. G. (2004) Dissolution rates of pure methane hydrate and carbon-dioxide hydrate in undersaturated seawater at 1000-m depth. *Geochim. Cosmochim. Acta* **68**, 285–292.
- Reshetnikov A. I., Paramonova N. N. and Shashkov A. A. (2000) An evaluation of historical methane emissions from the Soviet gas industry. *J. Geophys. Res.* **105**, 3517–3529.
- Rogers J. N., Kelley J. T., Belknap D. F., Gontz A. and Barnhardt W. A. (2006) Shallow-water pockmark formation in temperate estuaries: A consideration of origins in the western gulf of Maine with special focus on Belfast Bay. *Mar. Geol.* **225**, 45–62.
- Rogers R., Zhang G., Dearman J. and Woods C. (2007) Investigations into surfactant/gas hydrate relationship. *J. Pet. Sci. Eng.* **56**, 82–88.
- Sansone F. J., Rust T. M. and Smith S. V. (1998) Methane Distribution and Cycling in Tomales Bay, California. *Estuaries* **21**, 66.
- Sassen R., Joye S., Sweet S. T., Defreitas D. A., Milkov A. V. and MacDonald I. R. (1999) Thermogenic gas hydrates and hydrocarbon gases in complex chemosynthetic communities, Gulf of Mexico continental slope. *Org. Geochem.* **30**, 485–497.
- Sloan D. and Koh C. A. (2007) *Clathrate hydrates of natural gases*. 3rd ed., CRC Press, Boca Raton, FL.
- Stumm W. and Morgan J. J. (1996) *Aquatic Chemistry: Chemical Equilibria and Rates in Natural Waters*. 3rd ed., John Wiley & Sons, Inc., New York.
- Sugimoto A. and Wada E. (1995) Hydrogen isotopic composition of bacterial methane: CO₂/H₂ reduction and acetate fermentation. *Geochim. Cosmochim. Acta* **59**, 1329–1337.
- Taylor G. I. (1953) Dispersion of soluble matter in solvent flowing through a tube.
- Templeton A. S., Chu K. H., Alvarez-Cohen L. and Conrad M. E. (2006) Variable carbon isotope fractionation expressed by aerobic CH₄-oxidizing bacteria. *Geochim. Cosmochim. Acta* **70**, 1739–1752.

- Testa J. M. and Kemp W. M. (2014) Spatial and Temporal Patterns of Winter – Spring Oxygen Depletion in Chesapeake Bay Bottom Water.
- Valentine D. L. and Reeburgh W. S. (2000) New perspectives on anaerobic methane oxidation. *Environ. Microbiol.* **2**, 477–484.
- Waldbusser G. G., Steenson R. A. and Green M. A. (2011) Oyster Shell Dissolution Rates in Estuarine Waters: Effects of pH and Shell Legacy. *J. Shellfish Res.* **30**, 659–669.
- Wallace P. J., Dickens G. R., Paull C. K. and Ussler III W. (2000) Effects of core retrieval and degassing on the carbon isotope composition of methane in gas hydrate- and free gas-bearing sediments from the Blake Ridge. In *Proceedings of the Ocean Drilling Program, Scientific Results, Vol. 164*
- Westbrook G. K., Thatcher K. E., Rohling E. J., Piotrowski A. M., P?like H., Osborne A. H., Nisbet E. G., Minshull T. A., Lanoisell?? M., James R. H., H??hnerbach V., Green D., Fisher R. E., Crocker A. J., Chabert A., Bolton C., Beszczynska-M??ller A., Berndt C. and Aquilina A. (2009) Escape of methane gas from the seabed along the West Spitsbergen continental margin. *Geophys. Res. Lett.* **36**.
- Whiticar M. J. (1999) Carbon and hydrogen isotope systematics of bacterial formation and oxidation of methane. *Chem. Geol.* **161**, 291–314.
- Whiting G. J. and Chanton J. P. (1993) Primary production control of methane emission from wetlands. *Nature* **364**, 794–795.
- Whittenbury R., Phillips K. C. and Wilkinson J. F. (1970) Enrichment, isolation and some properties of methane-utilizing bacteria. *J. Gen. Microbiol.* **61**, 205–218.
- Yvon-Lewis S. a., Hu L. and Kessler J. (2011) Methane flux to the atmosphere from the Deepwater Horizon oil disaster. *Geophys. Res. Lett.* **38**, n/a–n/a.
- Zhang G. L., Zhang J., Liu S. M., Ren J. L. and Zhao Y. C. (2014) Methane in the Changjiang (Yangtze River) Estuary and its adjacent marine area : riverine input , sediment fluxes release and atmospheric. **91**, 71–84.
- Zhang Y. and Xu Z. (2003) Kinetics of convective crystal dissolution and melting, with applications to methane hydrate dissolution and dissociation in seawater. *Earth Planet. Sci. Lett.* **213**, 133–148.
- Zheng Y., Huang R., Wang B. Z., Bodelier P. L. E. and Jia Z. J. (2014) Competitive interactions between methane- and ammonia-oxidizing bacteria modulate carbon and nitrogen cycling in paddy soil. *Biogeosciences* **11**, 3353–3368.

Zhu C., Talbot H. M., Wagner T., Pan J. M. and Pancost R. D. (2010) Intense aerobic methane oxidation in the Yangtze Estuary: A record from 35-aminobacteriohopanepolyols in surface sediments. *Org. Geochem.* **41**, 1056–1059.